2015

Predictive Methods for End of Life Prognosis in Composites

Vamsee Vadlamudi
University of South Carolina - Columbia

Recommended Citation

Vadlamudi, V.(2015). *Predictive Methods for End of Life Prognosis in Composites.* (Master's thesis). Retrieved from http://scholarcommons.sc.edu/etd/3145

Predictive Methods for End of Life Prognosis in Composites

by

Vamsee Vadlamudi

Bachelor of Engineering
Osmania University, 2010

Submitted in Partial Fulfillment of the Requirements

For the Degree of Master of Science in

Mechanical Engineering

College of Engineering and Computing

University of South Carolina

2015

Accepted by:

Kenneth L. Reifsnider, Director of Thesis

Prasun K. Majumdar, Reader

Lacy Ford, Vice Provost and Dean of Graduate Studies

ACKNOWLEDGEMENTS

I would like to thank Dr. Kenneth Reifsnider, my research advisor, for his invaluable advice, guidance, and support that made this work possible. His encouraging words and positive way of thinking motivated me throughout my master's program. It has been enjoyable, challenging and above all an educational experience working with him.

I would also like to thank the other members of my advisory committee. I am grateful to Dr. Majumdar for his help and support in academic activities. His enthusiasm and dedication towards the scientific research has been an inspiration to my research.

I really appreciate the help of my colleagues, Jon-Michael Adkins, Jeffrey Baker, Fazle Rabbi, Rassel Raihan and Faisal Haider during my research work.

ABSTRACT

The long-term properties of continuous fiber reinforced composite materials are increasingly important as applications in airplanes, cars, and other safety critical structures are growing rapidly. The mechanical, electrical, and thermal properties of composite materials are altered by the initiation and accumulation of discrete fracture events whose distribution and eventual interaction defines the limits of design, such as strength and life. There is a correlation that exists between the long term behavior of those materials under combined mechanical, thermal, and electrical fields, and the functional properties and characteristics of the composite materials that requires a fundamental understanding of the material state changes caused by deformation and damage accumulation. While a strong foundation of understanding has been established for damage initiation and accumulation during the life of composite materials and structures, an understanding of the nature and details that define fracture path development at the end of life has not been established. This present research reports a multiphysics study of that progression, which is focused on measured and predicted changes in through-thickness electric/dielectric response of polymer based composites. Experimental data are compared to simulations of micro-defect interactions and changes in electrical and mechanical properties. Applications of the concepts to prognosis of behavior are discussed.

Also, we model a composite microstructure and analyze the material behavior using Finite Element Analysis (FEA) and subsequently perform conformal dielectric studies on the deformed microstructure by multiphysics simulation to relate this study to experimental data and simulations done using the electrical analogue method. We discuss two different models related to this, discuss results and postulate future work

TABLE OF CONTENTS

LIST OF TABLES

LIST OF FIGURES

CHAPTER 1 INTRODUCTION

The long-term properties of continuous fiber reinforced composite materials are increasingly important as applications in airplanes, cars, and other safety critical structures are growing rapidly. Aerospace industries are more inclined to use these multifunctional composites to reduce the weight to achieve fuel efficiency, and also for energy storage and structural stability.

The mechanical, electrical, and thermal properties of composite materials are altered by the initiation and accumulation of discrete fracture events whose distribution and eventual interaction defines the limits of design, such as strength and life. Unlike metallic materials, engineered materials (e.g. composites) are designed to develop distributed damage consisting of various types of defects and even multiple breaks in the same reinforcing fiber. Generally, creation of a single microscopic crack does not individually affect the strength or life of composite materials. Therefore, the primary interest is not in single local events but in the evolution process of multiple events that have a collective global effect. A recent review article has emphasized the need for understanding such nonlinearity due to damage accumulation, stating that "any analysis of fatigue damage evolution that accounts for the irreversibility driving the damage progression has the potential to predict fatigue life with minimum resort to empiricism."[1]

In the present work, we use the calculated response of an analogue material to a vector electric field that passes through the thickness of the composite to study defect development, growth, coalescence, and fracture path development in a heterogeneous material to represent material degradation (progressive damage and fracture path development) under repeated or long-term continuous loading during the life of that material. We simulate the dielectric response to an alternating current (AC) excitation of a test element of the material, for the undamaged and fracture-path case, which are then compared to laboratory experiments. As shown in Figure 1.1, for the undamaged case, for a material such as a glass-reinforced epoxy composite, the AC response is purely capacitive (no DC conduction), and (for linear materials, over a wide range of the response) the absolute value of the impedance (the square root of the sum of the squares of the real and imaginary components) is an essentially linear function of frequency with downward slope, i.e., inversely proportional to the AC frequency (like a parallel plate capacitor). When a fracture path has developed in the element, by definition, there will be a continuous voided path from one physical face to the other. Let us postulate that air with some hydration or simply diffused moisture (or other gas or fluid with some ionic content) enters that voided space. If that diffused material is conductive, and the path is continuous, then the idealized response (magnitude of the impedance) will not depend on the frequency of excitation (at least to first order) as shown in Figure 1.1.

Our physical observations will focus on continuous fiber reinforced structural composite materials, typically laminated with multiaxial ply orientations or with woven fiber architectures, subjected to quasi-static or cyclic loading until fracture. The literature is replete with discussions of the micro-cracking, debonding, delamination, and fiber fracture events that develop during such loadings.[2-4] Examples of the damage patterns that are observed are shown in Figures 1.2 and 1.3 which show matrix cracks and some fiber fractures, transverse to the principal load axis, through the laminate thickness.

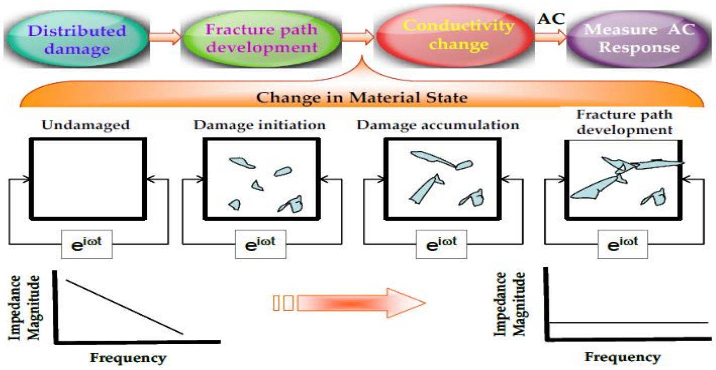

Figure 1.1 Framework created in previous work [1] that connects material state change to dielectric response

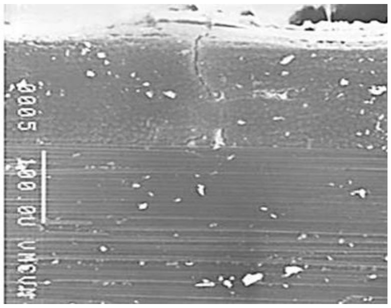

Figure 1.2 Through-thickness crack pattern development (white lines) in a multiaxial laminate subjected to fatigue loading [2-4].

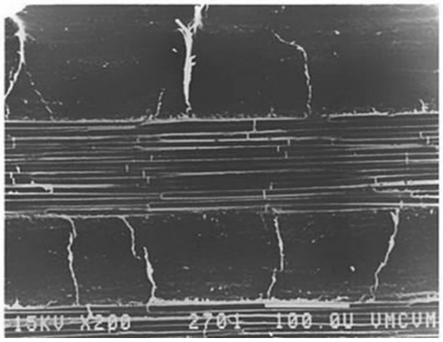

Figure 1.3 Surface crack initiation (top center) in a laminate under quasi-static tensile loading [2-4].

The literature says that “if a group of physical concepts or quantities are related to each other in a certain matter, as by equations of a certain form, and another group of concepts or quantities are interrelated in a similar manner, then an analogy may be said to exist between the concepts of the one group and those of other group.”[5]Under combined applied field conditions, materials degrade progressively. To evaluate such material state changes there are many tools and methods but most of them do not give a direct and quantitative assessment of the damage state.

Composite materials by nature are heterogeneous dielectric material systems. When degradation happens in the material system, it develops a combination of material state and morphology changes. Broadband Dielectric Spectroscopy (BbDS) is a robust tool to extract the material-level information, including the morphology changes caused by micro-detect generation and the orientation of those defects. Composite materials should be designed in such a way that they can cope with their applied environments; to achieve this, it is necessary to engineer the material system from the nano- and micro- scale by controlling the shape, size, properties and interfaces of those systems. The local material states of high performance composite structures change during their service period. In order to achieve a prognosis of the composite durability, structural integrity, damage tolerance, and fracture toughness, we must take into consideration the appropriate balance equations, defect growth relationships, and constitutive equations with specified material property variations. Local changes in the material state also have significant effects on the prognosis of the future behavior of a composite material system.

CHAPTER 2 LITERATURE REVIEW

2.1 Progressive Failure in Composite Materials

Damage in composite materials under various loading conditions have been studied and published in engineering journals since the late 1970s [6]. Various stages of degradation from micro cracking to fiber fracture are described below

2.1.1 Microcracking

Microcracking is the basic damage mode in composite materials which initiates changes to the material mechanical properties [7-14]. Fiber matrix debonding and initiation of matrix microcracks is shown in Figure 2.1 [8]. After the initial development microcracks grow through the ply thickness and width parallel to the fiber direction. Distributed amounts of microcracks have small or no effect, rather their local stress fields typically interact and can change the global stiffness considerably causing local stress redistributions. Experimental data shows that changes in stiffness are not uniform throughout the life of a material element; initially and near the onset of fracture, the change is substantial [8-13].

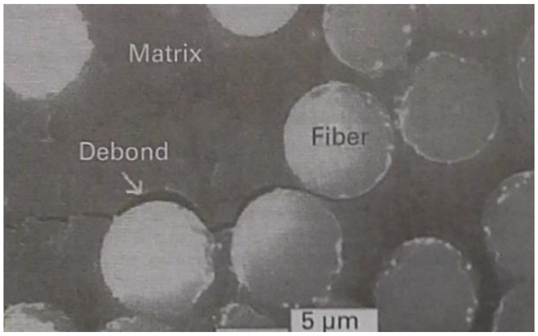

Figure 2.1 Matrix crack initiation from fiber/matrix debonding. [8]

2.1.2 Delamination

Difference in deformation patterns in response to the local loads and stiffness changes at local regions of composites may initiate delamination as shown in Figure 2.2. Most delamination is initiated by microcracking [14]. This delamination can influence changes in the laminate strength, which is not seen in the case of microcracking, and the end result of stress redistribution associated with delamination may lead to fracture [15].

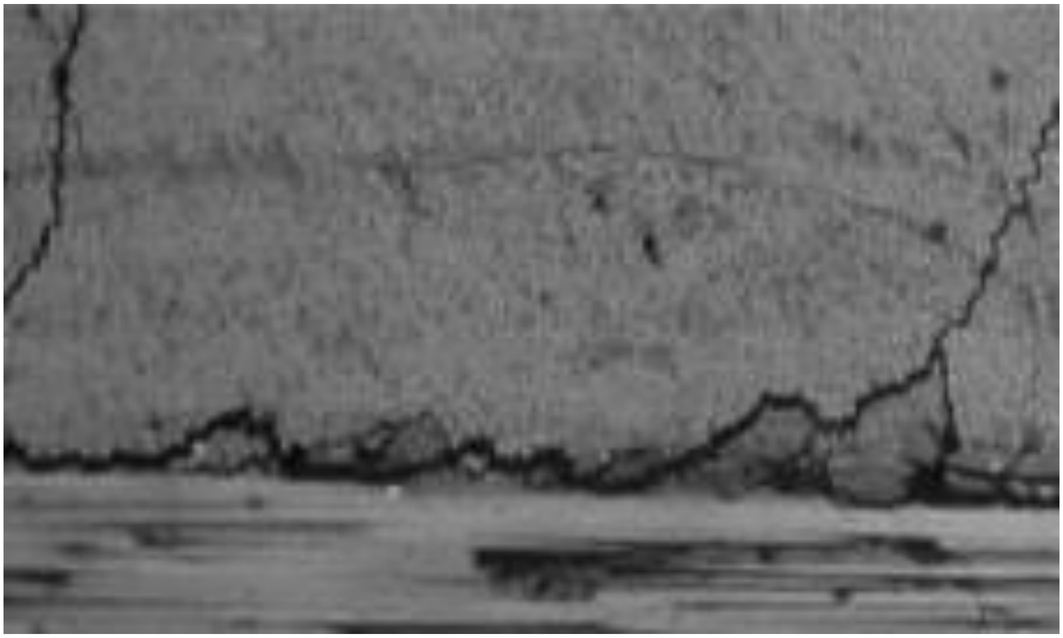

Figure 2.2 Interlaminar delamination crack formed due to joining of two adjacent matrix cracks in a fiber reinforced composite laminate [8]

2.1.3 Fiber Fracture:

Fiber fracture is a failure mode difficult to detect and studied less completely than any of the other damage modes in structural composites. Fiber fracture is highly coupled to damage in fiber and matrix materials as shown in Figure 2.3 [8].

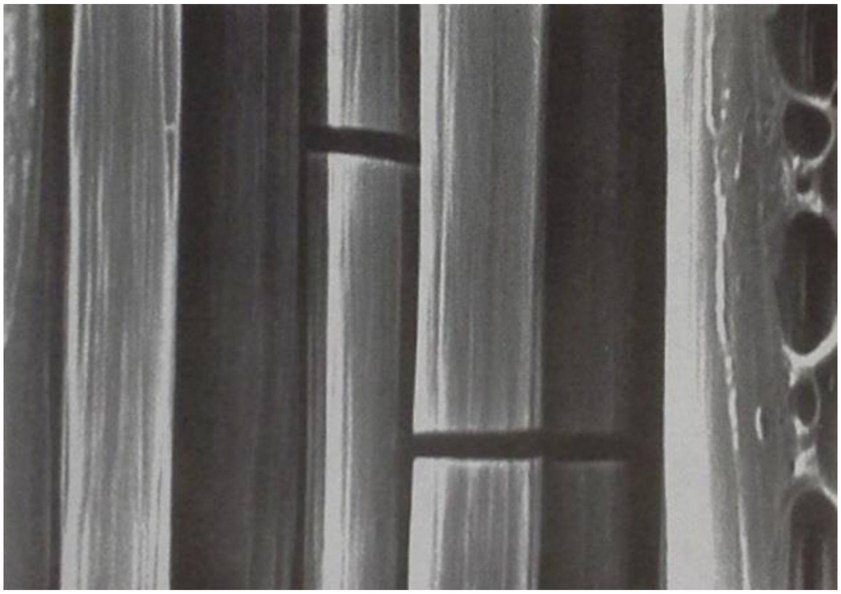

Figure 2.3 Fiber fractures in carbon-epoxy composite [8].

2.2 Fracture Path Development

Damage initiation in plies with different orientations occurs at different load levels for quasi-static loading and at different rates for cyclic loading, according to well-understood ply-level strength concepts [16]. A defining feature of this early degradation is a decelerating damage rate; in the case of fatigue loading at a constant load level, the microcracking of the individual plies that develop damage reaches a steady state with a characteristic crack spacing. A sample of such behavior is shown in Figure 2.4. Matrix cracks develop early in the plies that form cracks at the given load level, and reach a stable number and spacing that depends on their relative stiffness in the laminate and on their position through the thickness. The registration of those cracks along the length of the specimen is nominally random, but in the later stages of life (or highest load levels in a tensile test), the cracks in different plies “seek each other” to try to complete their path through the thickness (as shown in Figure 1.2). Fiber fractures align with matrix cracks in some cases, as is shown in the center of Figure 1.2. When this coupling creates a continuous crack through the thickness, a potential "fracture plane" is formed, although it should be remembered that since the matrix cracks run parallel to the fiber directions in each ply, a coincident plane of cracking (through the thickness) in one position (like the edge of the specimen shown in Figure 1.2) will not be coincident (in the same way) at some other position across the section width.

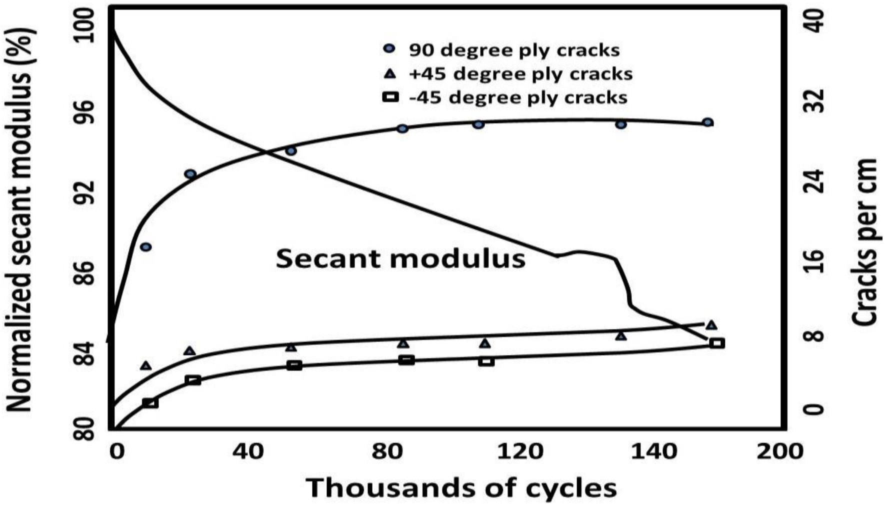

Figure 2.4. Crack development in off-axis plies and corresponding change in secant stiffness as a function of cyclic load cycles.

When a fracture plane forms through the thickness and across the width of the specimen, specimen rupture occurs at the global level. That is a crack coupling process, not represented by the data in Figure 2.4.

We know remarkably little about that end-of-life coupling process or how it forms the fracture plane. The first question is how to measure something that is sensitive to the damage details in that phase of the life, and how to interpret such measurements in such a way that we can use those interpretive models to extract a "warning" of impending failure.

Fazzino et al. have suggested that dielectric response (measured through the thickness of a laminate, and interpreted with standard dielectric spectroscopy methods) can provide a multi-physics method of relating the changes in material state (reflected in changes in AC impedance) to the micro details of damage development, and further, found that such a method was particularly sensitive to the coupling events at the end of life [17] and Figure 1.1. However, how the specific changes they observed were related to the details of the coupling of microcracks and the formation of a fracture plane were not determined. The present thesis is an attempt to contribute to that interpretation.

Various models have been established to simulate dielectric response of heterogeneous materials such as effective medium theories, bounding methods, percolation theory, random walks, hopping model, Fourier expansion, finite difference time domain methods (FDTD), Monte Carlo techniques, RC network methods, and so on [18]. In the present work we use an RC network analogue model as an approximation to a composite material (e.g. Matrix capacitive nature modeled as capacitors, fibers as conductors or insulators modeled as resistors).

CHAPTER 3 END OF LIFE PREDICTION BY ELECTRICAL ANALOGUE METHOD

3.1 Methodology

In the present case we draw an analogy between how a fracture pattern is generated because of a series of local stress interactions that result in a global fracture path, and local electric current changes when resistive elements are shorted in the analogue network shown below. We consider a Representative Volume Element (RVE) of a laminate section (through the thickness) in which we assume that vertical elements represent constituent material of one type (e.g., fibers) and the horizontal elements represent a second constituent type (e.g. the matrix) as shown in Figure 3.1.

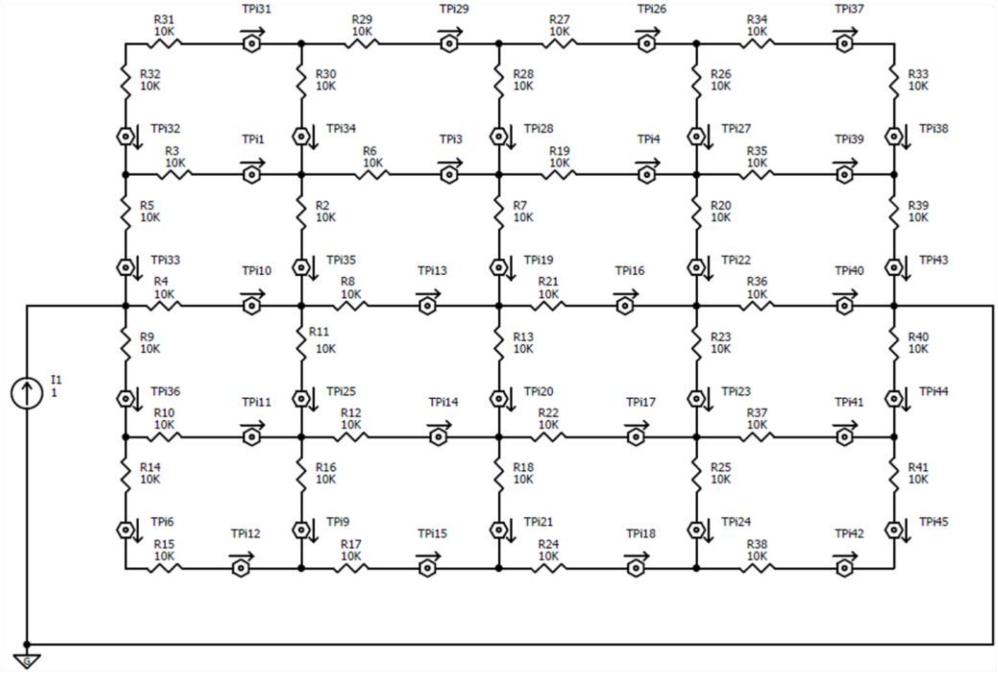

Figure 3.1 Analogue model comprising of constituent elements (Matrix and Fiber) for Simplicity

For simplicity in the current discussion, we initially start with equal electrical resistance values for fiber and matrix segments. The scope of this methodology is not limited to constituents of the laminate; the elements in the circuit could represent different layers of a laminate, or combinations of different materials (ex. metal and composite), or different orientations in a laminate, etc. By varying the magnitude of the electrical properties of the elements in the circuit we can simulate similar local mechanical or electrical property variations.

A current equal to 1 Ampere is chosen as the power source, applied across two opposing surface points. Distribution of that current source was selected as an analog of how a composite material behaves locally, i.e., during loading when matrix cracking starts and local material elements are no longer able to bear the load, the local material micro-damage will redistribute the load to the adjacent elements. Similar behavior can be observed in the case of a current source circuit; when we short any element (to simulate the local failure of a matrix or fiber element), in order to maintain equilibrium the current is redistributed in a manner that is similar to the mechanical phenomenon of local stress redistribution in composites. It also suggests the subsequent direction of “micro-crack” formation. We assess those indications to study the path of simulated crack growth through the thickness of our analytical “sample”.

After shorting an element to simulate local crack formation, we re-analyze the circuit and determine the current at each element in the circuit; we then consider the element that has the highest subsequent difference in current to be the next micro-crack location, which is an analogy to a local stress increase in a composite. The subsequent crack may or may not be adjacent to the last crack location. This cycle is repeated until fracture occurs i.e., to the condition where all the fractured/shorted elements create a continuous path of least resistance through which current flows. That path simulates the fracture path in the mechanical specimen, and changes in material state variables such as compliance to the global applied field can be predicted and observed during the process.

3.2 Demonstration of the Method

We start with an initial random shorting of an element and then carry on, determining how the circuit behaves as discussed above. Ideally in a “real” composite under mechanical loading, first ply failure (or an equivalent statistical concept) can be applied to determine which element fails first. The initial current readings of all the elements in the present model have been tabulated under the “Before shorting” column in Table 3.1. In this case R22 is randomly selected and initially shorted. After shorting R22, the analysis is repeated and the current readings in all remaining elements are noted and tabulated in the “After shorting” column in Table 3.1. Then the difference in the current at each local ‘ammeter’ is noted and the element with the highest increase in current during the last step is identified for shorting next. That particular element is highlighted in Table 3.1. The Value highlighted in red had the greatest increase in current, which illustrates that the current flows through the path of least resistance, and since R22 has already been shorted, R23 is the element that has the next highest increase in current (R23 has been highlighted in green in Table 3.1). This cycle of local shorting to simulate sequential microcracking is repeated until a fracture path is formed, i.e., current passes only through the continuous shorted path of least resistance, as shown in Table 3.2.

Table 3.1: Values of current at different elements in the circuit before and after shorting

Element	Ammeter Associated	Value(|I| amps)		Difference (amps)
		Before Shorting	After Shorting	
R2	TPi35	0.06818	0.05532	-0.01286
R3	TPi1	0.18182	0.17755	-0.00427
R4	TPi10	0.40909	0.40857	-0.00052
R5	TPi33	0.29545	0.28634	-0.00911
R6	TPi3	0.20454	0.19284	-0.0117
R7	TPi19	0	0.016608	0.016608
R8	TPi13	0.27272	0.26477	-0.00795
R9	TPi36	0.29545	0.30508	0.00963
R10	TPi11	0.18182	0.19197	0.01015
R11	TPi25	0.068181	0.08848	0.020299
R12	TPi14	0.20454	0.24618	0.04164
R13	TPi20	0	0.069892	0.069892
R14	TPi6	0.11363	0.11312	-0.00051
R15	TPi12	0.11363	0.11312	-0.00051
R16	TPi9	0.045454	0.034267	-0.01119
R17	TPi15	0.15909	0.14738	-0.01171
R18	TPi21	0	0.064529	0.064529
R19	TPi4	0.20454	0.18021	-0.02433
R20	TPi22	0.068181	0.047882	-0.0203
R21	TPi16	0.27272	0.21148	-0.06124
R22	TPi17	0.20454	0.3806	0.17606
R23	TPi23	0.06818	0.14159	0.073409
R24	TPi18	0.15909	0.082854	-0.07624
R25	TPi24	0.04545	0.18325	-0.02713
R26	TPi27	0.04545	0.039341	0.00611
R27	TPi26	0.15909	0.14485	-0.01424
R28	TPi28	0	0.003979	0.003979
R29	TPi29	0.15909	0.14882	-0.01027
R30	TPi34	0.04545	0.04003	-0.00542
R31	TPi31	0.11363	0.10879	-0.00484
R32	TPi32	0.11363	0.10879	-0.00484
R33	TPi38	0.11363	0.1055	-0.00813
R34	TPi37	0.11363	0.1055	-0.00813
R35	TPi39	0.18182	0.17167	-0.01015
R36	TPi40	0.40909	0.40095	-0.00814
R37	TPi41	0.18182	0.22068	0.03886
R38	TPi42	0.11363	0.10118	-0.01245
R39	TPi43	0.29545	0.27717	-0.01828
R40	TPi44	0.29545	0.32186	0.02641
R41	TPi45	0.11363	0.10118	-0.01245

Table 3.2: Tabulated values of current readings through elements that are a path of least resistance.

Element	Ammeter Associated	Value(|I| amps)
R2	TPi35	0
R3	TPi1	0
R4	TPi10	1
R5	TPi33	0
R6	TPi3	0
R7	TPi19	0
R8	TPi13	0
R9	TPi36	0
R10	TPi11	0
R11	TPi25	1
R12	TPi14	0
R13	TPi20	0
R14	TPi6	0
R15	TPi12	0
R16	TPi9	1
R17	TPi15	1
R18	TPi21	0
R19	TPi4	0
R20	TPi22	1
R21	TPi16	0
R22	TPi17	0
R23	TPi23	1
R24	TPi18	1
R25	TPi24	1
R26	TPi27	0
R27	TPi26	0
R28	TPi28	0
R29	TPi29	0
R30	TPi34	0
R31	TPi31	0
R32	TPi32	0
R33	TPi38	0
R34	TPi37	0
R35	TPi39	1
R36	TPi40	0
R37	TPi41	0
R38	TPi42	0
R39	TPi43	1
R40	TPi44	0
R41	TPi45	0

The predicted fracture path is highlighted in Figure 3.2. It was observed that some elements although shorted at some step of the path development, are not a part of the final contiguous ‘fracture path.’ Those elements are highlighted in Figure 3.2. This is an analogue of the physical behavior in composites in which a local failure is due to local crack interaction and accumulation, and not due to individual crack initiation, propagation, or growth. The staggered final fracture path in Figure 3.2 has a similar character to the through-thickness patterns in Figure’s 1.2 and 1.3.

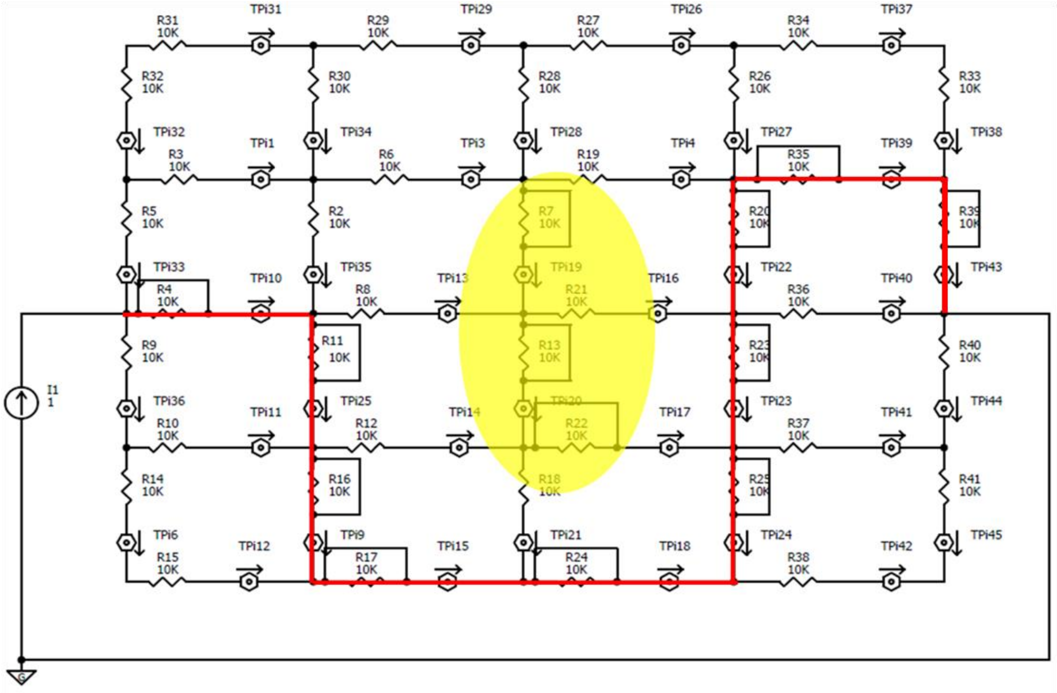

Figure 3.2 Analogue model with highlighted fracture path and showing the presence of damage accumulation

3.3 Compliance Concepts

During the simulation analysis, after shorting of each element, the effective resistance of the circuit is calculated and a comparison between Effective Resistance ‘R’ and No. of Cracks ‘N’ is obtained; values for one set of simulations are tabulated in Table 3.3. From the plot of such data shown in Figure 3.3, it is observed that as the circuit/material accumulation proceeds towards failure its effective resistance reduces (compliance increases) and at the fracture point it reaches 0 (or infinite compliance). In the above plot the highlighted parts of the curve mark a significantly larger change in the effective resistance of the model. This change is brought about when two local ‘cracks’ interact and a tertiary bridging crack or a “fracture plane growth” has occurred. In terms of the physical phenomenon, this change could be attributed to fiber failure, or crack opening, or delamination as observed in Chou’s work [19] and a similar behavior was observed in a multiphysics model, constructed by Dr. Rassel Raihan [20].

Table 3.3 Table showing variation of effective Resistance ‘R’ with No of cracks ‘N’

No. of Cracks ‘N’	Effective Resistance ‘R’ Ohms(Homogeneous)
0	13636
1	12858
2	12430
3	11885
4	11723
5	11580
6	10299
7	7071.1
8	7049.1
9	6941.3
10	6457.5
11	5862.6
12	4792.1
13	0.01

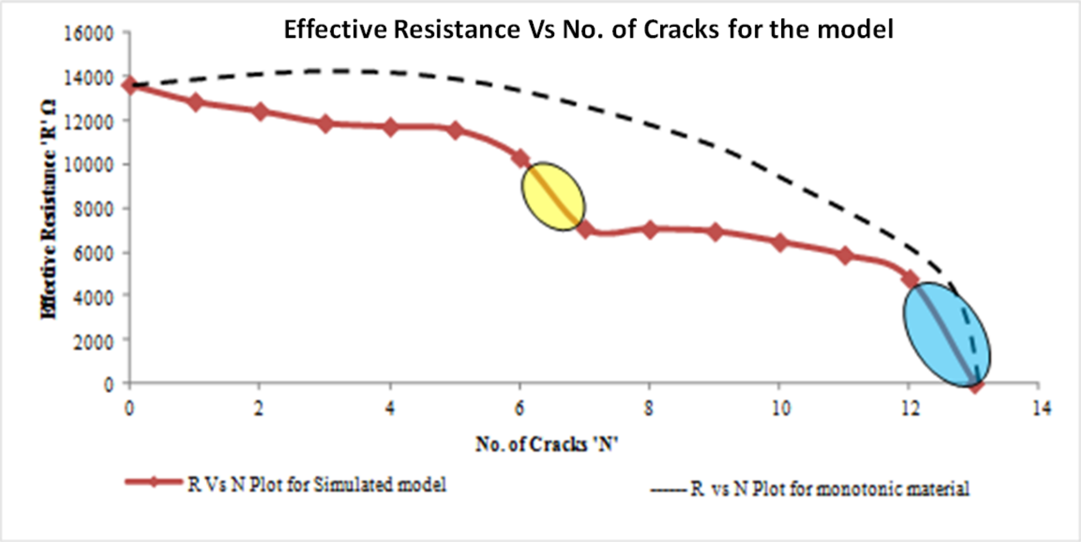

Figure 3.3 Plot to show the variation of electrical compliance (Eff. Resistance ‘R’) with No. of Cracks ‘N’ for simulated (analogue) and monotonic model.

3.4 Non-Linearity (Damage Accumulation vs. Damage Growth)

Damage accumulation is fundamentally different from crack propagation. If the present analysis is representative of that accumulation process, “simple” crack propagation should not be a preferred result.

To test that premise, we shorted an element along the plane of symmetry between our two contact points and started the analysis. If the model were to exhibit only linear crack growth behavior, than the current would take the horizontal path of least resistance, i.e., the fracture path should be a straight line as shown in Figure 3.4, but the predicted path with the present analysis method was completely different as shown in Figure 3.5, which gives evidence that this model can exhibit the non-linear phenomenon of damage accumulation and fracture path formation observed in fibrous composites (e.g., Figure’s 1.2 & 1.3).

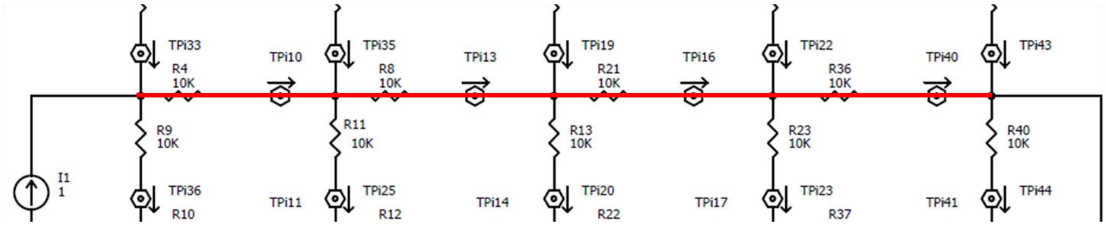

Figure 3.4 Expected Path of Fracture

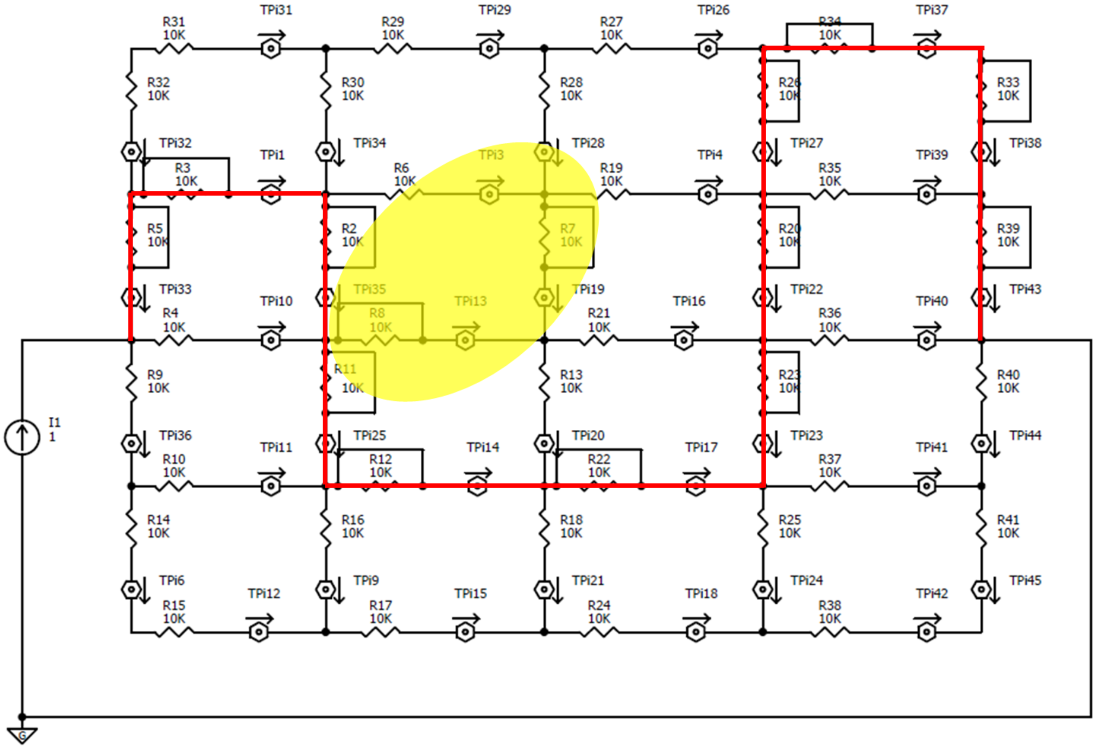

Figure 3.5 Predicted fracture path

3.5 Dielectric Response

3.5.1 Introduction of Anisotropy into the model

Up to this point the present model was constituted with horizontal and vertical elements with equal initial magnitudes of resistance. In order to introduce anisotropy, a capacitance in parallel with the resistive element is added to the horizontal elements (in this case, the “matrix”) since a polymer matrix, for example, is known to exhibit a capacitive response. Figure 3.6 shows the resulting circuit.

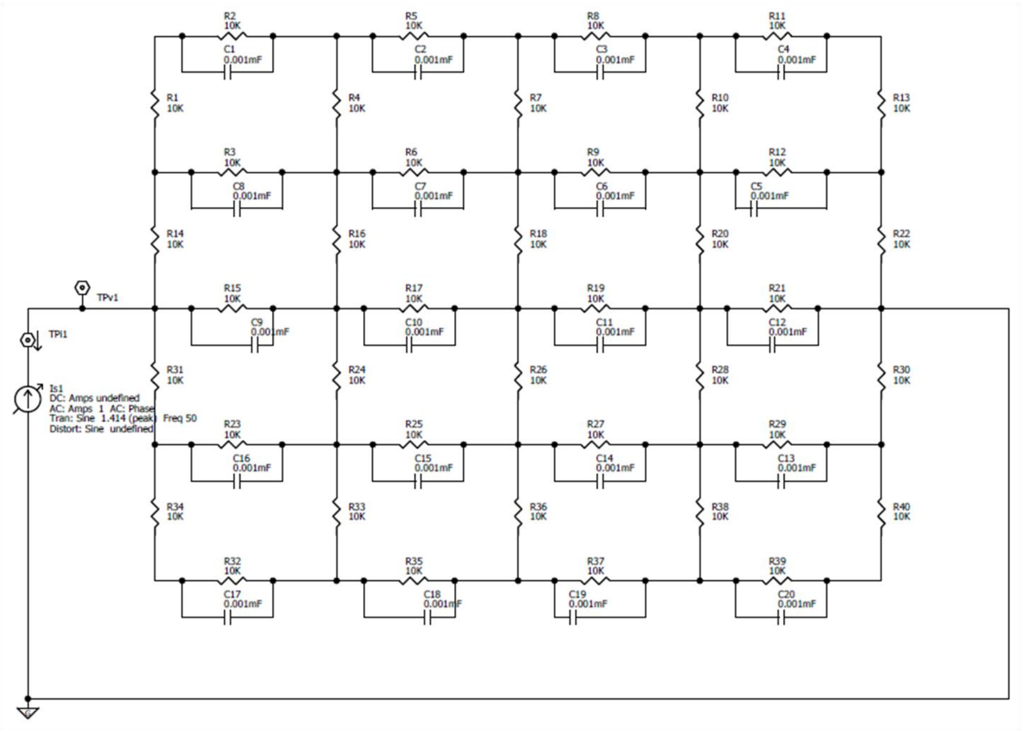

Figure 3.6 Anisotropic model in initial state with all of the elements intact

3.5.2 Randle’s Circuit

In Electro-Chemical Impedance Spectroscopy (EIS) analysis, a Randle’s circuit is widely used to represent the dielectric Impedance of material elements. Impedance is the magnitude of the total complex resistance encountered when a current flows through a system, which is most often interpreted as a circuit made of resistors, capacitors, or inductors, or any combination of these.[18] In our AC analysis, when we short a particular element, an additional resistance has been added in series to the capacitance and the main resistance is shorted in order to simulate the damage that has occurred because of the applied “load” and local “micro-fracture.”

3.5.3 Initial Stage

In the initial stage under a no-load condition in the composite, i.e., without shorting any elements as shown in Figure 3.6, the dielectric response of the anisotropic model to an AC current was analyzed and the response was found to be equivalent to an insulator between two plates, as shown in Figure 3.7 and observed in Figure 1.1.

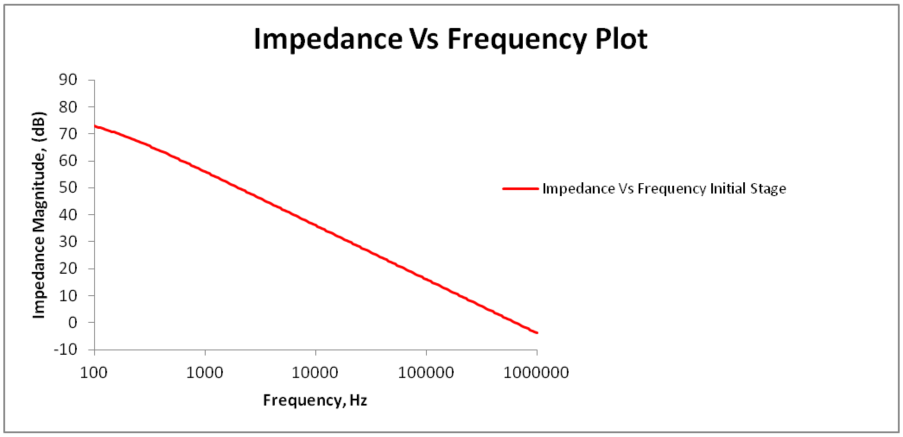

Figure 3.7 Dielectric Response of the model in the initial state similar to an Insulator.

3.5.4 Final Stage

During analysis of the fracture path development, the fractured elements were replaced by a Randle’s circuit as shown in Figure 3.8 and the dielectric response was analyzed. It was observed that the response becomes more similar to a conductor as shown in Figure 3.9, and observed in Figure 1.1.

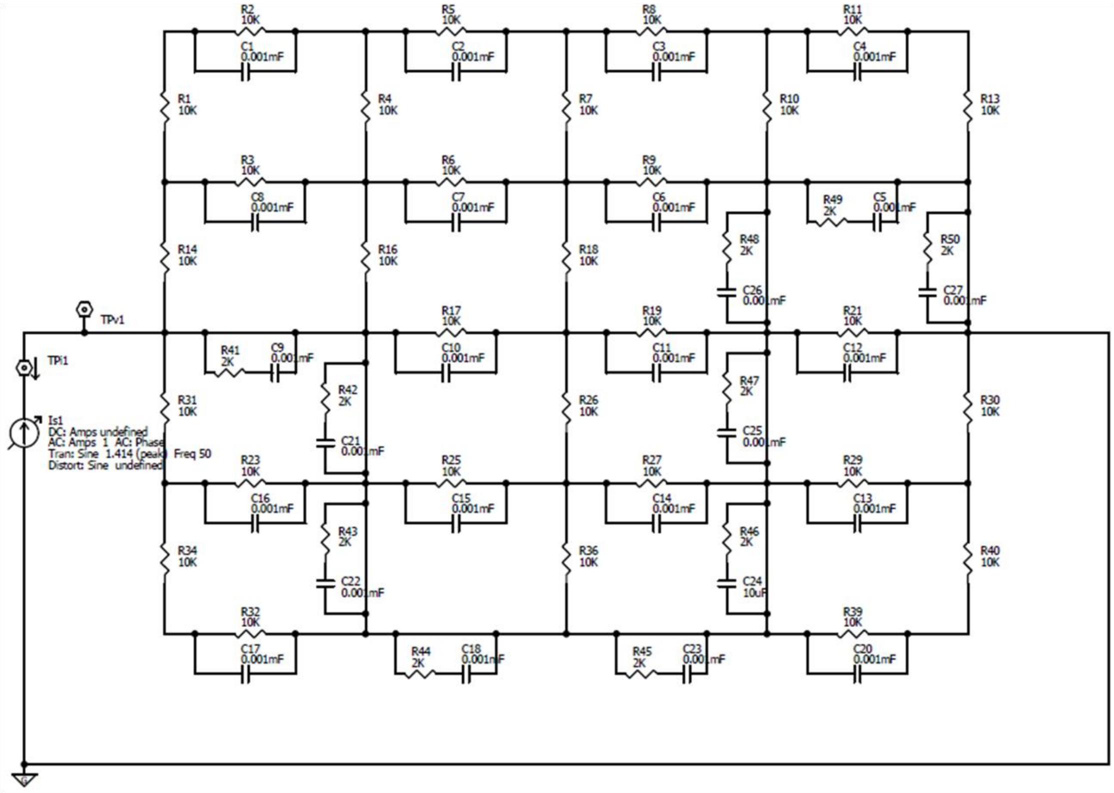

Figure 3.8 Model with randle's circuit elements along fractured path.

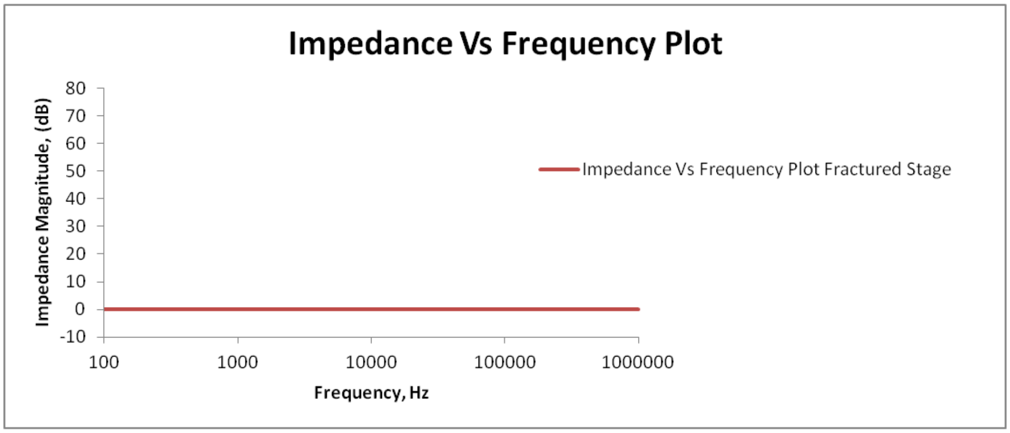

Figure 3.9 Response of the fractured model similar to a conductor.

3.5.5 Dielectric Response at different stages of life

Based on previous work, to validate the results obtained at different life fractions of bend-fatigue life, as shown in Figure 3.10, the results of our model were divided into four different stages. Response at each stage is shown in Figure 3.11. The predicted behavior closely approximates the observations in Figure 1.1 that motivated this work.

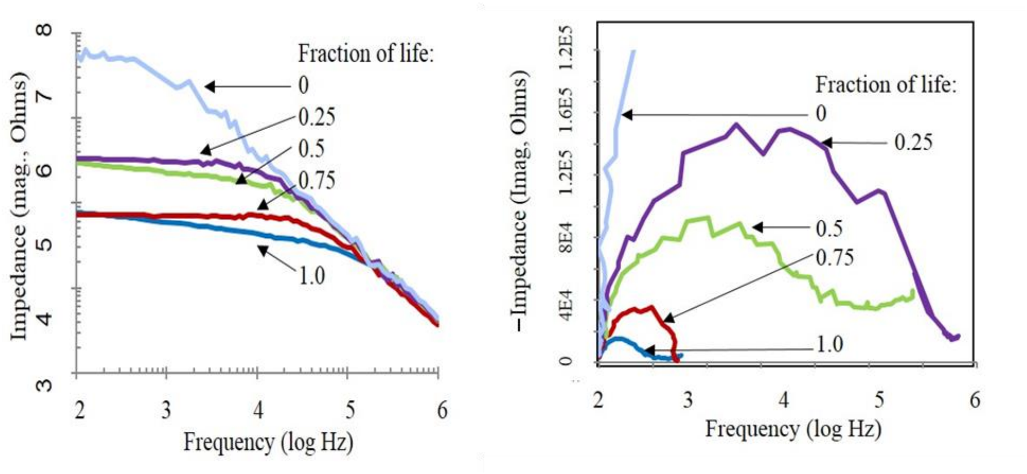

Figure 3.10 Observed Variation of Impedance with Frequency (left) and Nyquist Plots (right) showing variation of impedance with life in Fazzino's work. [17]

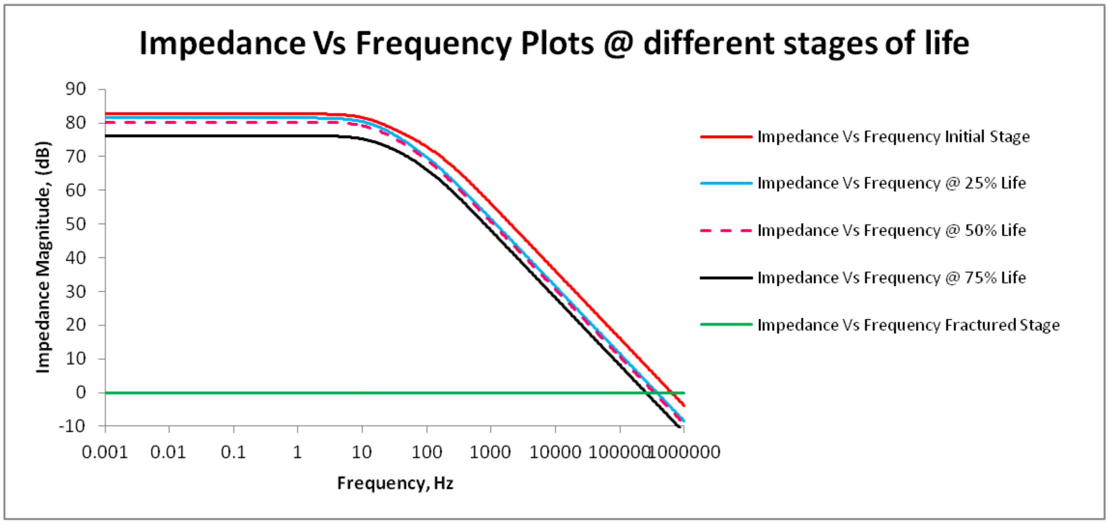

Figure 3.11 Variation of Di electric response with frequency at different stages of life

3.5.6 Nyquist Plot

By tabulating the real part of impedance, and imaginary part of impedance at different stages of life as shown in Table 3.4 , one can create a new representation of the change in electrical properties with increasing damage in the material. Creating a plot of tabulated values, one can observe that as damage increases the plot shifts to the left which indicates decreasing resistance as seen in Figure 3.12. Closely observing the plot at each stage of life the reactance increases at low frequency values, but as the frequency increases towards 1MHz the reactance approaches zero. These simulations are consistent with the previous observations of Fazzino, et al.[17] We will see that changes in the shape of these curves and the location of the intercepts are strong indicators of material state and sensitive to the final formation of a conductive ("fracture") path.

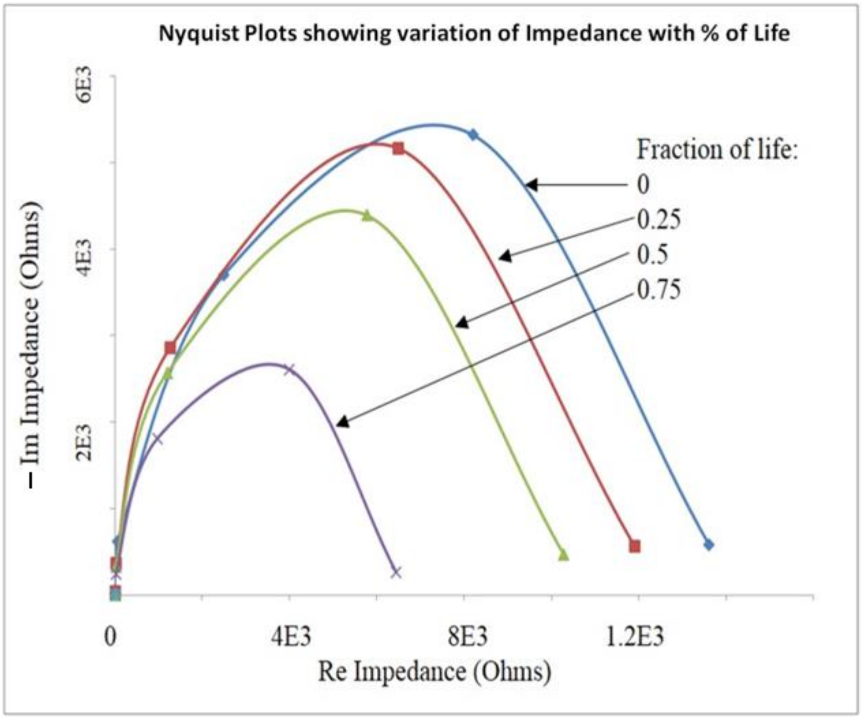

Figure 3.12 Nyquist plot showing the variation of impedance with % of life

Table 3.4: Tabulated values of Real and Imaginary part of Impedance at different frequencies for different stages of life

Frequency, Hz % of life	1		20		100		1E3		1E4		1E5		1E6	
	Re	- Im	Re	- Im	Re	- Im	Re	- Im	Re	- Im	Re	- Im	Re	- Im
Initial	1.36E+4	5.86E+2	8.1E+3	5.3E+3	2.5E+3	3.7E+3	5.96E+1	6.2E+2	6.1E-1	63.65	5.9E-3	6.27	6.1E-5	0.64
25	1.19E+4	5.62E+2	6.49E+3	5.16E+3	1.27E+3	2.86E+3	2.04E+1	3.69E+2	2.12E-1	38	2.06E-3	3.76	2.12E-5	0.38
50	1.03E+4	4.74E+2	5.76E+3	4.40E+3	1.20E+3	2.57E+3	1.84E+1	3.34E+2	1.90E-1	34	1.86E-3	3.4	1.90E-5	0.34
75	6.44E+3	2.64E+2	3.99E+3	2.61E+3	9.67E+2	1.81E+3	1.59E+1	2.49E+2	1.65E-1	25.5	1.60E-3	2.55	1.65E-5	0.26
Fractured	0	0	0	0	0	0	0	0	0	0	0	0	0	0

3.5.7 End of Life Prediction

Composite Materials, unlike metals, are capable of significant damage accumulation without loss of strength or stiffness, so it is difficult to measure something unique that can predict the end of life based on standard Non Destructive Testing (NDT) methodologies. However, using the methods of impedance spectroscopy based on the dielectric response of the material, as discussed above, one can determine end of life characteristics, as shown in the framework in Figure 1.1. At the initial state without damage, the response is similar to an insulator (frequency dependent) and at the fractured state it acts like a conductor (frequency independent). Using that concept and our model, we can identify the impedance peak value (e.g. in Figure 3.12) and the frequency at which it occurs at different stages of life and, tabulating those values as shown in Table 3.5, it is observed that although the frequency at which the peak value occurs remains constant up to 50% of life, when it reaches about 75% of life there is an abrupt increase in the frequency at which the maximum peak value of reactance is observed, as in Figure 3.13. We postulate that this inflection point can be used as an indicator of the ‘beginning of the end’ of life.

Table 3.5: Table showing variation of reactance peak frequency with % of life

% of Life	Reactance Peak frequency, Hz
Initial	20.7
25%	20.7
50%	20.7
75%	24.9
Fractured	NA

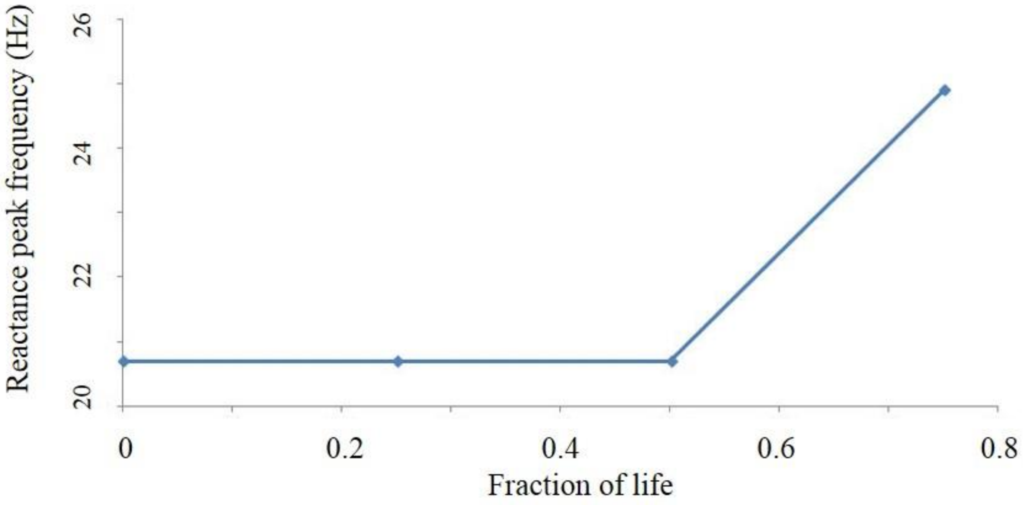

Figure 3.13 Variation of Reactance peak frequency with % of life

3.5.8 Heterogeneous Model

Although there have been traces of anisotropy in the current model, we have not yet discussed an actual composite, so a next goal is to introduce “real” heterogeneity in the model by proportionately varying the local property magnitudes (resistive and capacitive values in our case) of the elements in some systematic or random way. An example is shown in Figure 3.14. The analysis procedure remains the same, and a similar dielectric response was obtained with a slight variation in the local magnitudes using the heterogeneous model, as shown in Figures 3.15 & 3.16. Although “real” material variations have not yet been performed with this model, a sample heterogeneous circuit has been modeled and consistent dielectric response was demonstrated.

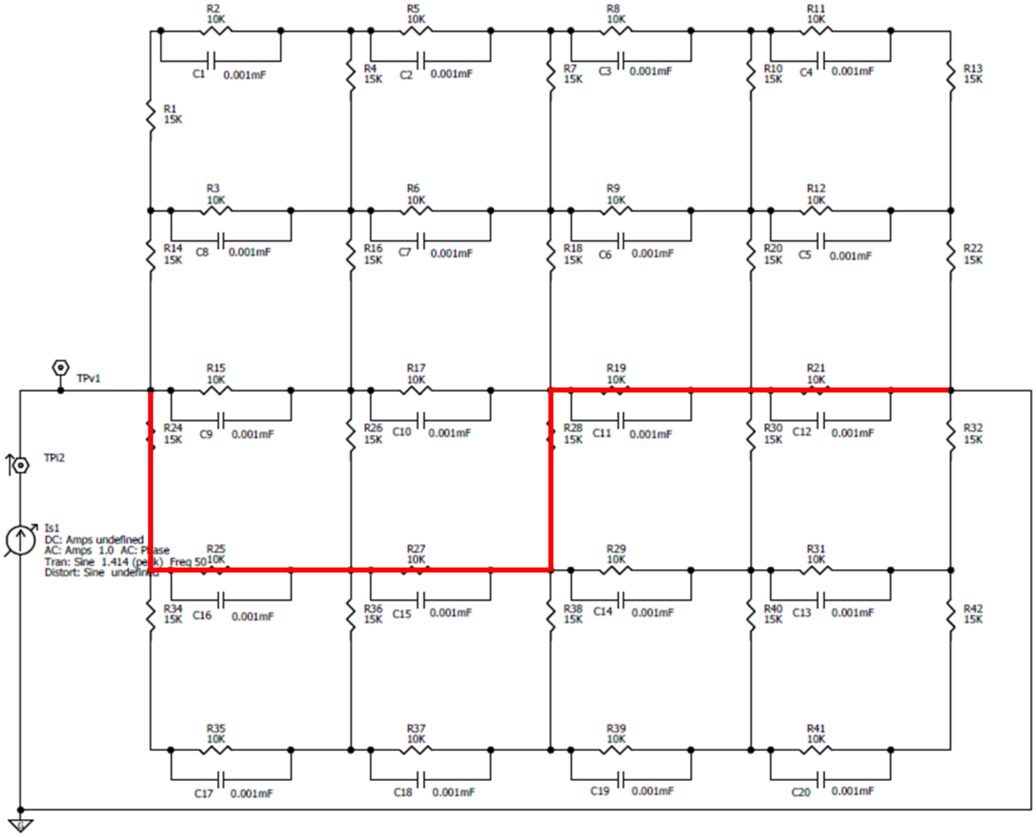

Figure 3.14 Model with heterogeneous elements with fracture path highlighted

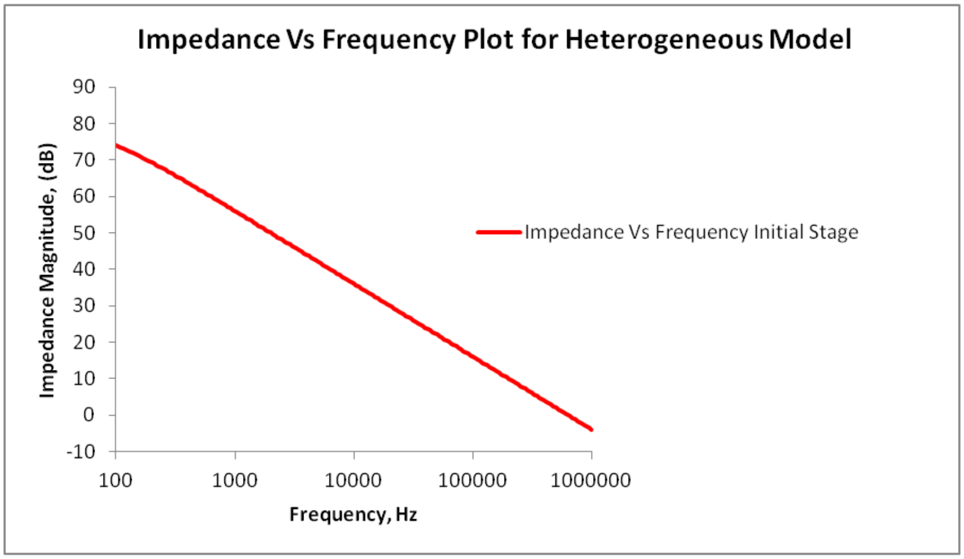

Figure 3.15 Frequency response of the heterogeneous model at Initial stage

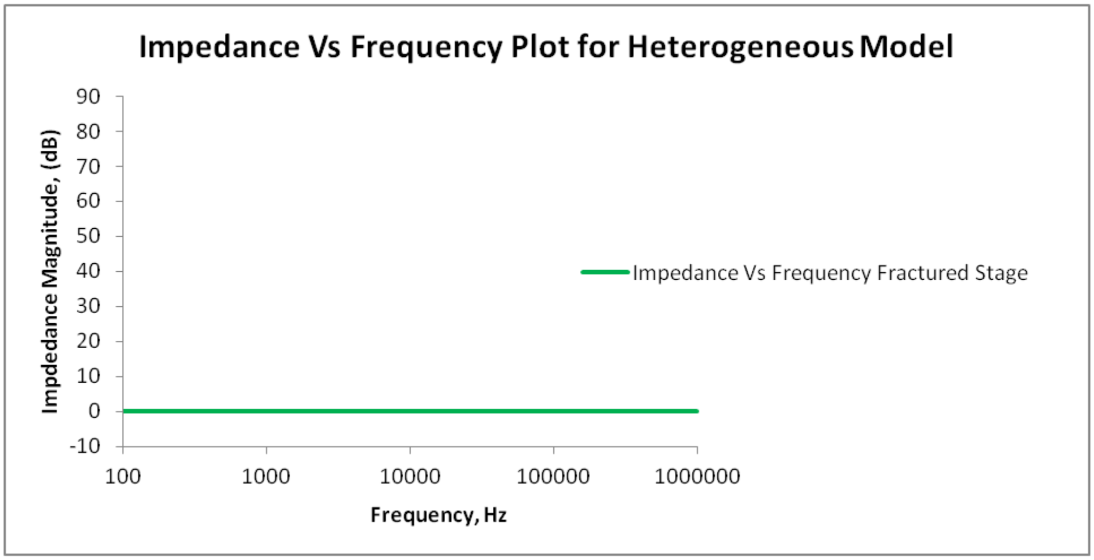

Figure 3.16 Frequency response of the heterogeneous model at Final stage

Similar to the prior anisotropic model, a plot between Effective Resistance and Number of Cracks was created using the tabulated values shown in Table 3.6. A similar significant change in the effective resistance was observed wherever a local interaction created a tertiary crack or fracture, as shown in Figure 3.17.

Table 3.6: Table showing variation of effective Resistance ‘R’ with No of cracks ‘N’

No. of Cracks ‘N’	Effective Resistance ‘R’ Ohms(Heterogeneous)
0	15578
1	14883
2	14303
3	13543
4	11125
5	5607.7
6	5510.5
7	5315.8
8	4745.5
9	0

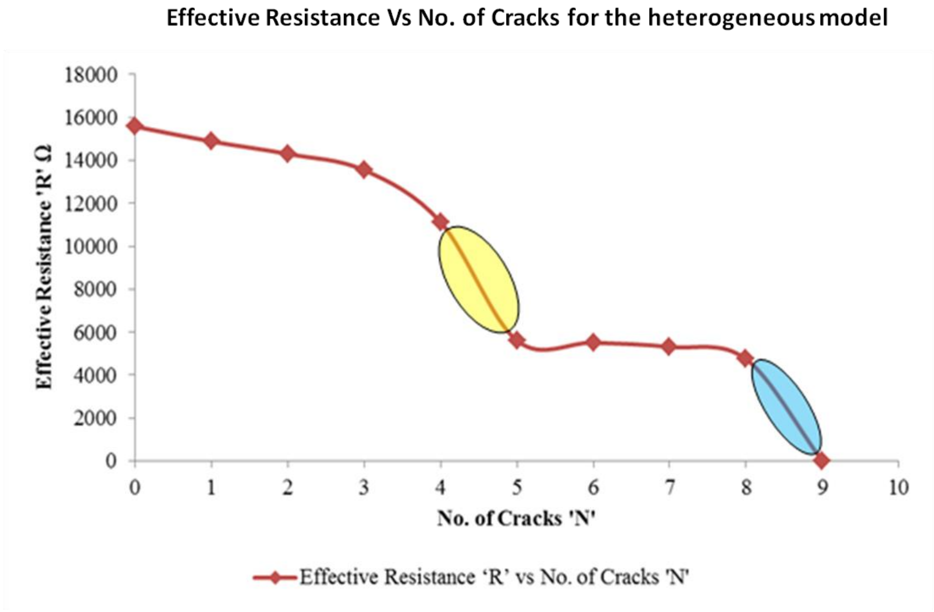

Figure 3.17 Plot showing variation of electrical compliance (Effective Resistance 'R') and no. of cracks 'N' for heterogeneous model

CHAPTER 4 2D MODELING AND ANALYSIS OF COMPOSITE MICROSTRUCTURE USING FEA

4.1 Hyper Elastic Material

We have seen that an analogue model can predict the onset of end of life, but this doesn’t represent a true composite material model. To simulate a ‘Real’ composite we define a microstructure of the ‘Real’ material model and perform structural analysis using FEA. In this process we load the structure with large strains to better understand the material behavior under these extreme conditions. To accomplish this we chose ‘Hyperelastic’ materials that have the capability to withstand these extreme loading conditions. Hyperelastic materials have properties of an ideal elastic material that cannot be defined by a linear elastic material, for these materials Stress Strain relationships are derived from Non-Linear elastic Strain Energy models such as Arruda-Boyce model, YEOH model, Mooney-Rivlin model etc,

4.2 YEOH Model

Non-Linear elastic material models are very useful for modeling elastomers (rubber like materials). These materials can undergo large reversible elastic deformations up to 500% strain. These materials can be characterized by stretch ratio (λ),

$$\lambda = L/L_0$$

Where L is the deformed length and L_0 is the undeformed length of the sample. Strain energy models are based on strain invariants which are functions of the stretch ratios in three directions, defined as

$$I_1 = \lambda_1^2 + \lambda_2^2 + \lambda_3^2$$

$$I_2 = \lambda_1^2\lambda_2^2 + \lambda_2^2\lambda_3^2 + \lambda_3^2\lambda_1^2$$

$$I_3 = \lambda_1^2\lambda_2^2\lambda_3^2$$

YEOH model has proved to satisfactorily model various deformation modes involving large strains and also has the added advantage of reduced requirements for material testing because of its dependence only on the first strain invariant I_1 [21] as defined in the equation below.

$$W = \sum_{i=1}^{n} C_{i0}(I_1 - 3)^i + \sum_{k=1}^{n} \frac{1}{d_k}(J - 1)^{2k}$$

Where W is the strain energy density function, C_{i0} and d_k are material constants obtained by curve fitting stress strain data, and for incompressible materials $I_3 = 1$, $J = 1$ and hence strain energy density function takes the form

$$W = \sum_{i=1}^{n} C_{i0}(I_1 - 3)^i$$

Silicone rubber is an elastomer that belong to this group of materials which serve our purpose for this research

4.3 Material Properties of Silicone Rubber

Silicone Rubber which is one of the most commonly used hyperelastic material has the capability to sustain larger strains up to 400%. YEOH strain energy model is used in this simulation using a commercial FEA package (ABAQUS). To analyze Hyperelastic materials using FEA, we need material constants of silicone rubber, which are $C_{10} = 0.235$ MPa, $C_{20} = -0.007$ MPa, $C_{30} = 0.0008$MPa, $d_1 = d_2 = d_3 = 0$[22]

4.4 2D Non-Linear Analysis using FEA

4. 4.1 Modeling

In the present model, we have Silicone Rubber (matrix) modeled as a sheet with Conductors inside it uniformly spaced from each other (for simplicity). In the model silicon rubber acts as the insulator (“matrix”) whereas steel (reinforcement) “fibers” act as the conductors within the insulator (like a 2-D model through the thickness of a fiber reinforced composite). Material properties of steel are E = 200 GPa, Poisson’s ratio = 0.33. ABAQUS supports only 2D non-linear analysis for Hyperelastic materials and hence we start with a 2D model of conductors inside an insulator as shown in Figure 4.1. The silicone rubber sheet is 20*20 cm in size and radius of steel fiber is 1.25 cm uniformly distributed with 4 cm from each other.

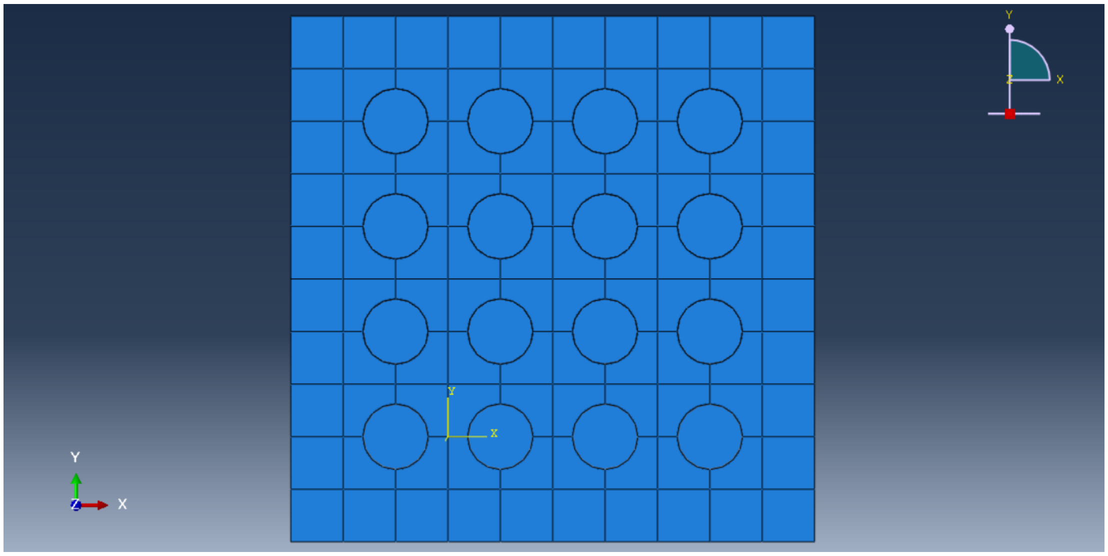

Figure 4.1 Silicone Rubber matrix with steel reinforced fibers

4.4.2 Meshing

The generated mesh consists of quadrilateral elements, CPS4R: A 4-node bilinear plane stress quadrilateral, reduced integration, hourglass control as shown in Figure 4.2. The total number of elements in the model = 2926, the total number of nodes = 3280. CPS4R is a plane stress quadrilateral element with 4 nodes as shown in Figure 4.2. Each node has three degrees of freedom two translation and one rotation degree of freedom.

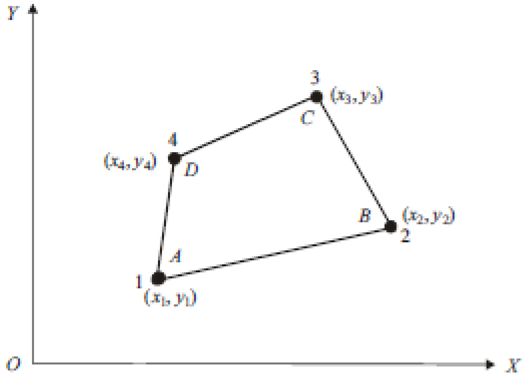

Figure 4.2 Plane stress quadrilateral element with four nodes

4.4.3 Displacement Continuity

Since rubber matrix and steel fibers are two different entities we need to create a constraint between them so that steel fibers remain connected throughout the analysis and also to ensure that forces and displacements are transmitted from one entity to other, for this purpose we create a displacement continuity with ‘tie’ constraint between the nodes of these two entities as shown in Figure 4.3.

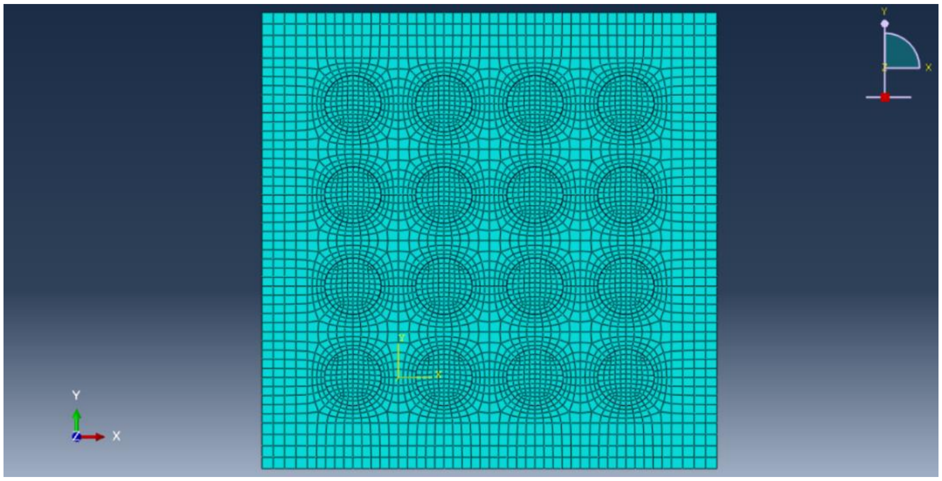

Figure 4.3 Final Mesh of the assembly with quadrilateral elements

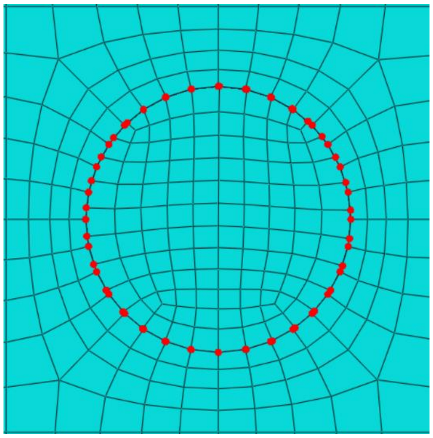

Figure 4.4 Displacement continuity between silicone rubber matrix and steel reinforced fibers

4.4.4 Boundary Conditions

The most important part of an analysis is to prescribe proper boundary conditions for the model so that solution converges without errors. Boundary conditions for the model are

1. Along the line passing through (0,0) and (0,20) $U_1 = 0$, constraint in X-direction
2. At X= 0, Y= 0 $U_2 = 0$, constraint in Y-direction as shown in Figure 4.4

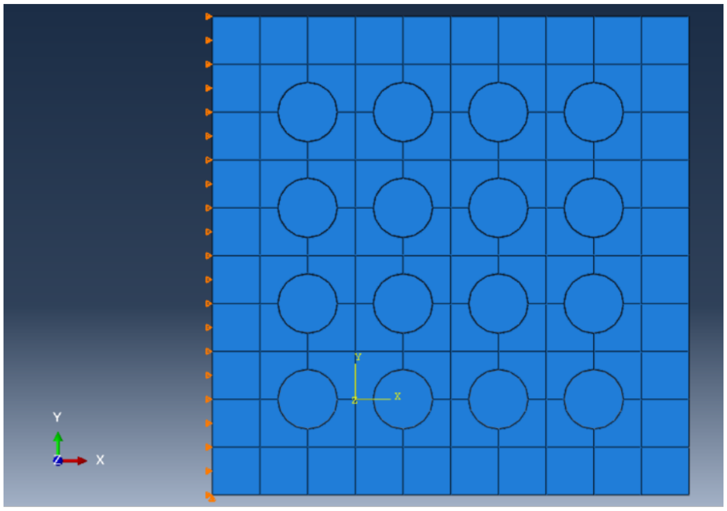

Figure 4.5 Model with prescribed boundary conditions

4.4.5 Tensile Loading

We load the model with a uniaxial displacement as shown in Figure 4.6 up to 133% Strain (Fracture) and the Von-Mises Stress plots are shown in Figures 4.7 to 4.12

.

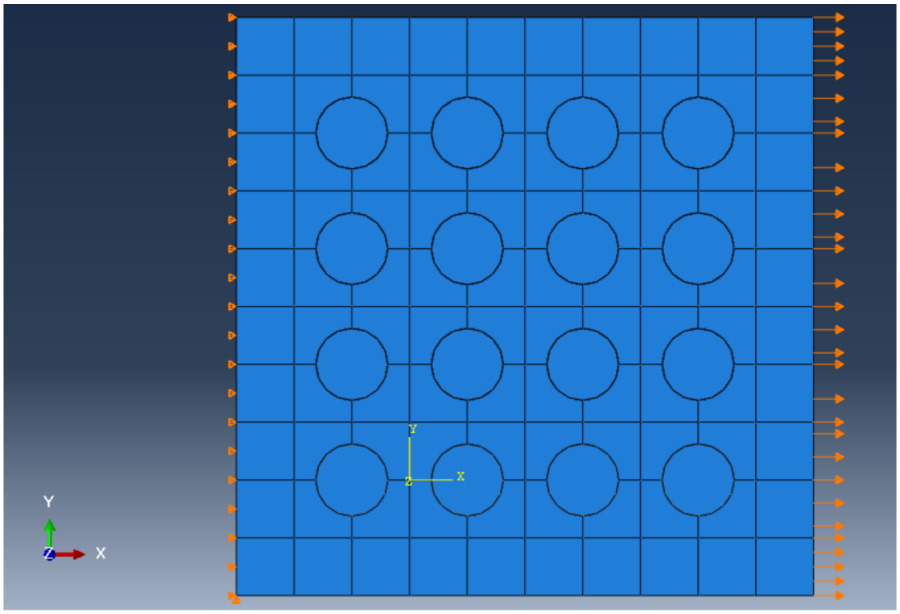

Figure 4.6 Model showing boundary conditions and tensile loading direction

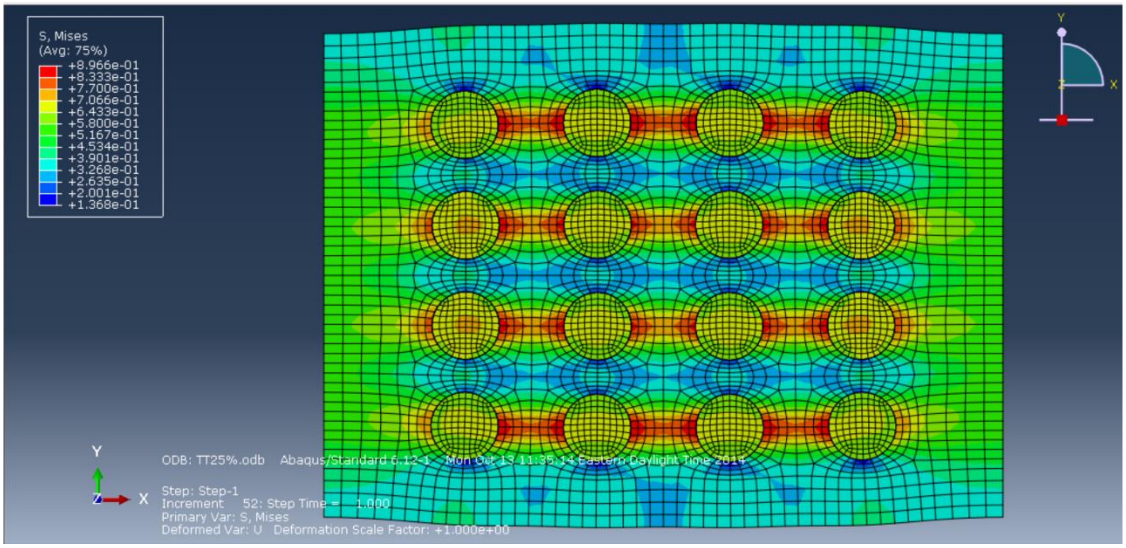

```
ODB: TT25%.odb    Abaqus/Standard 6.12-1    Mon Oct 13 11:35:14 Eastern Daylight Time 2014

Step: Step-1
Increment     52: Step Time =    1.000
Primary Var: S, Mises
Deformed Var: U   Deformation Scale Factor: +1.000e+00
```

Figure 4.7 Von Mises Stress plot on deformed contour for 25% Strain

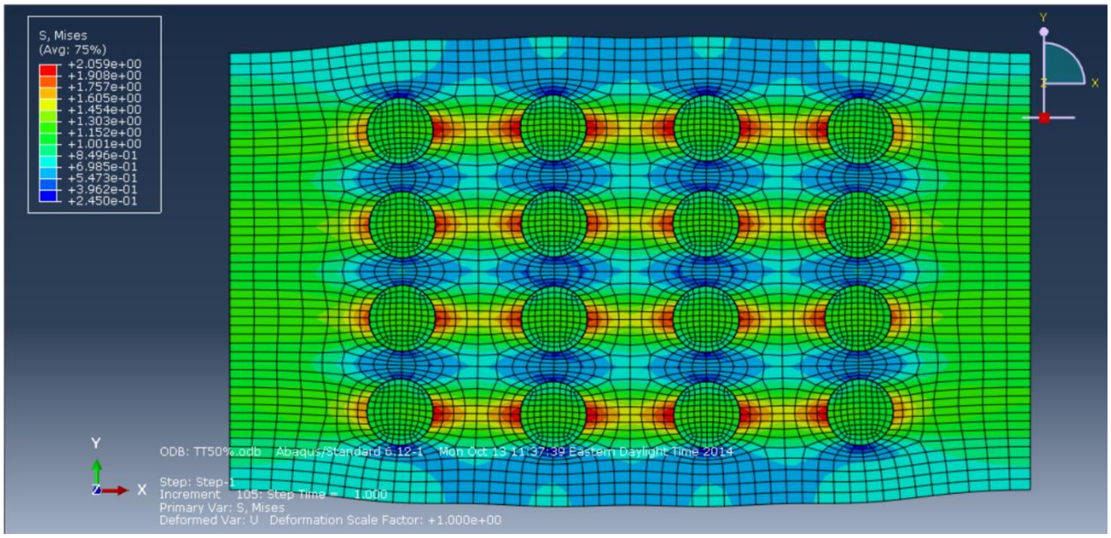

Figure 4.8 Von Mises Stress plot on deformed contour for 50% Strain

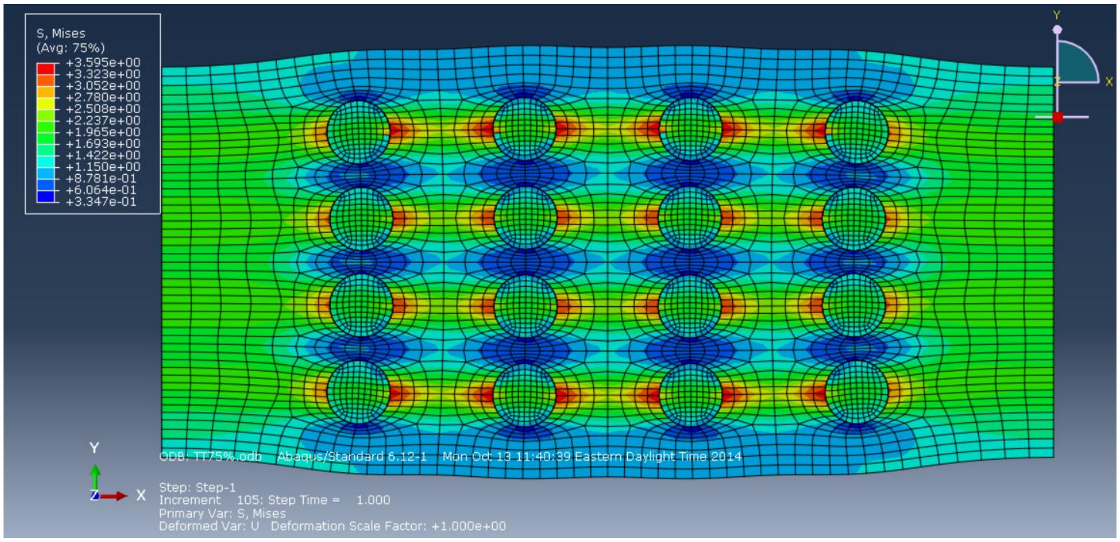

Figure 4.9 Von Mises Stress plot on deformed contour for 75% Strain

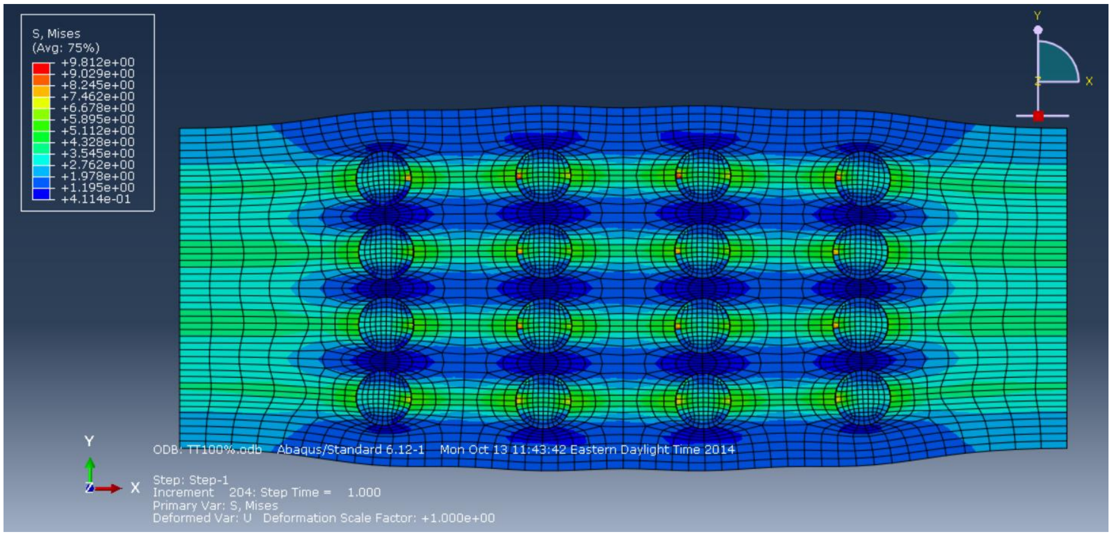

Figure 4.10 Von Mises Stress plot on deformed contour for 100% Strain

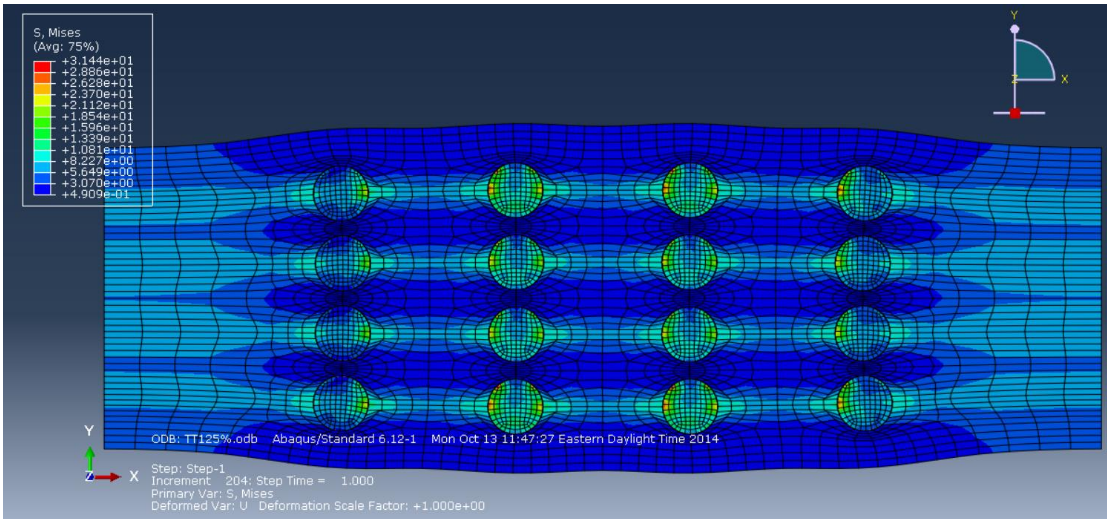

Figure 4.11 Von Mises Stress plot on deformed contour for 125% Strain

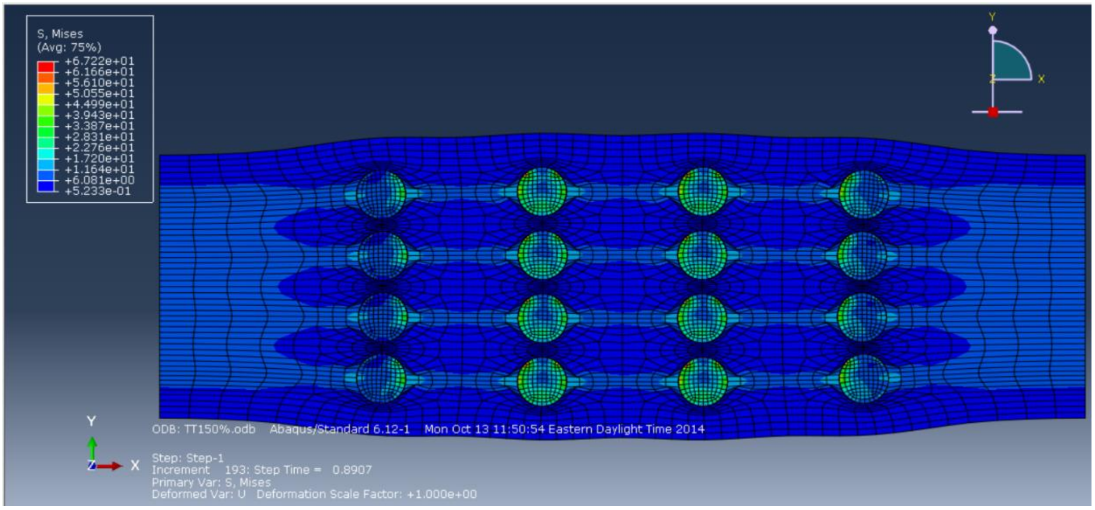

Figure 4.12 Von Mises Stress plot on deformed contour for 133% Strain

4.4.6 Compressive Loading

For this contrasting situation, we load the model with axial displacement as shown in Figure 4.13 up to 35% Strain (buckled) and the Von-Mises Stress plots are shown in Figures 4.14 to 4.20.

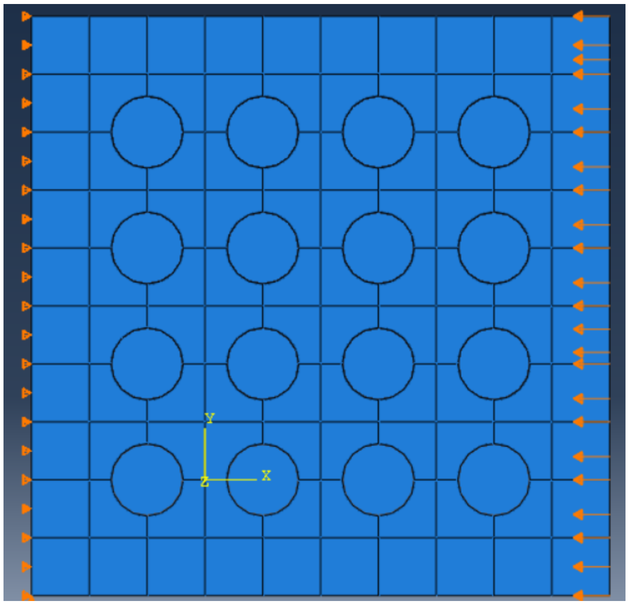

Figure 4.13 Model showing boundary conditions and compressive loading direction

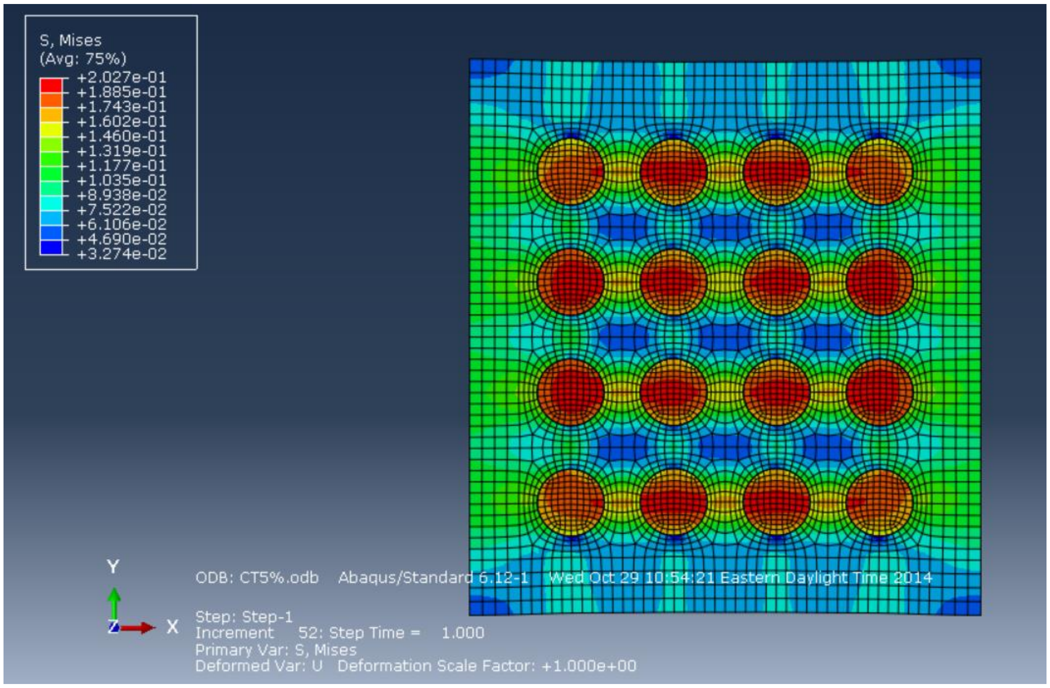

Figure 4.14 Von Mises Stress plot on deformed contour for 5% Strain

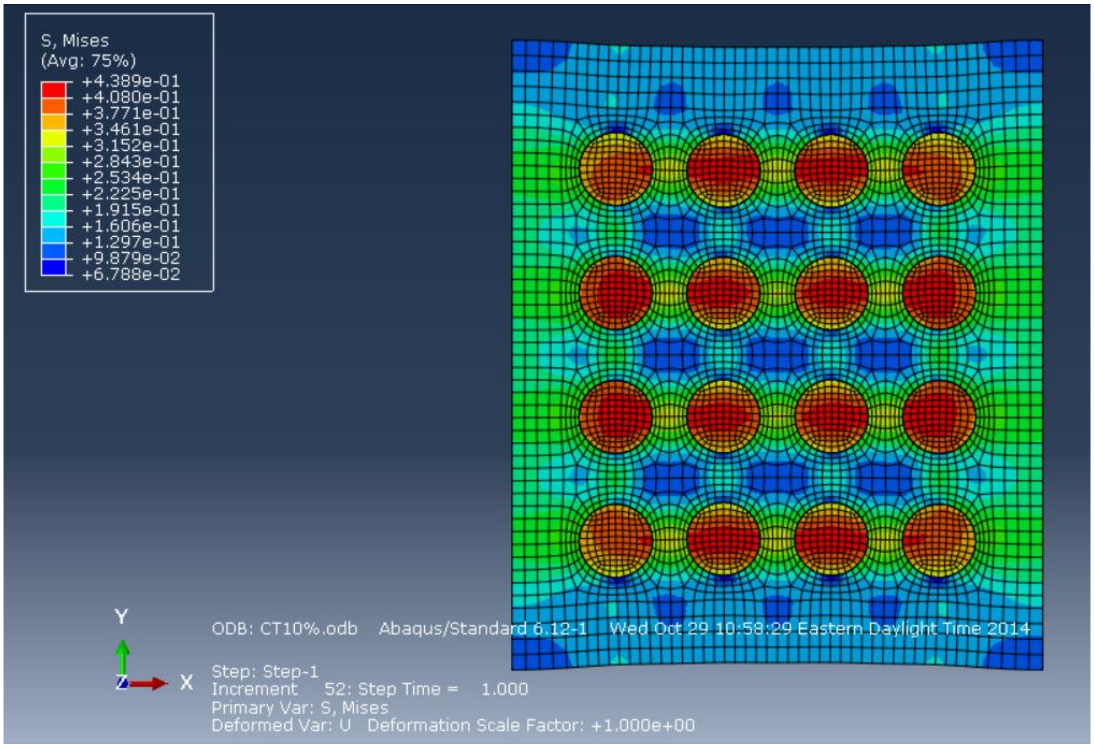

Figure 4.15 Von Mises Stress plot on deformed contour for 10% Strain

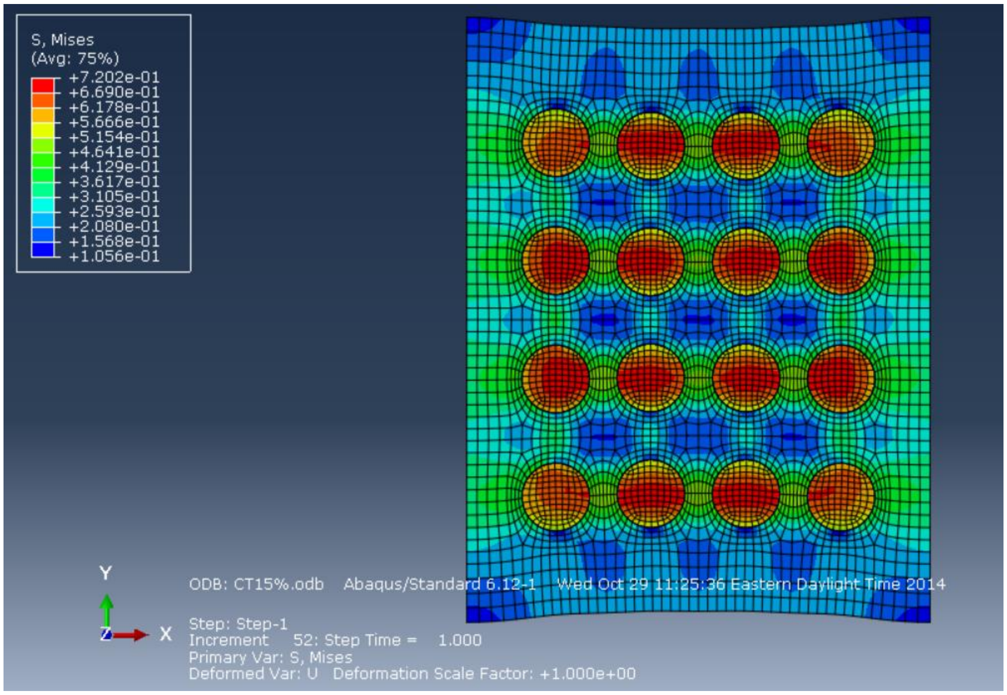

Figure 4.16 Von Mises Stress plot on deformed contour for 15% Strain

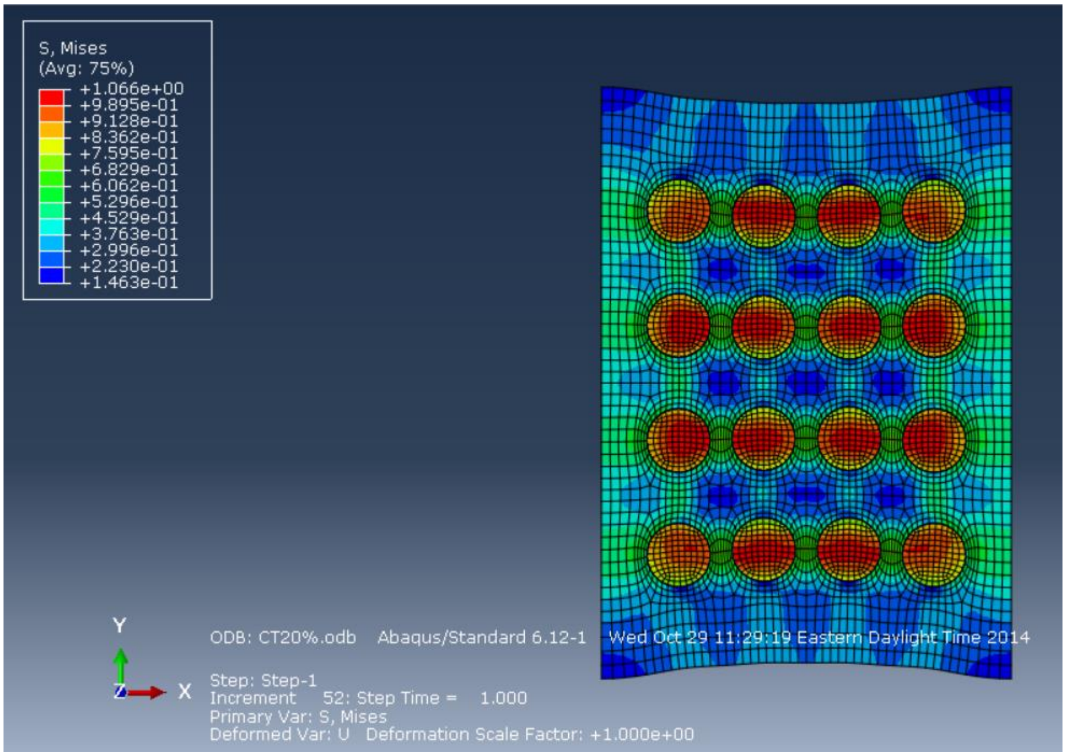

Figure 4.17 Von Mises Stress plot on deformed contour for 20% Strain

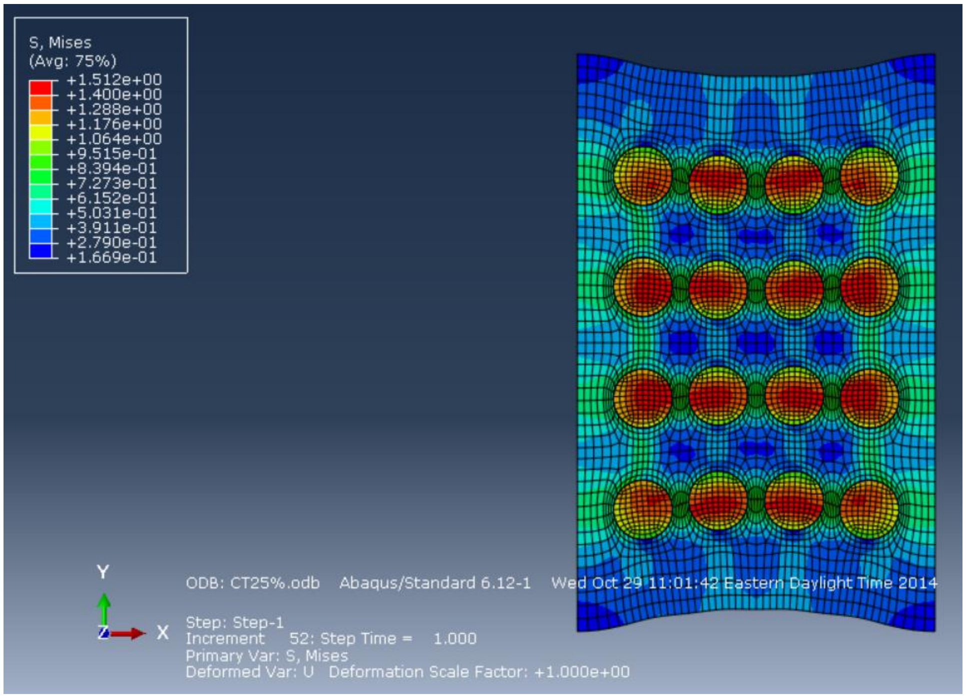

Figure 4.18 Von Mises Stress plot on deformed contour for 25% Strain

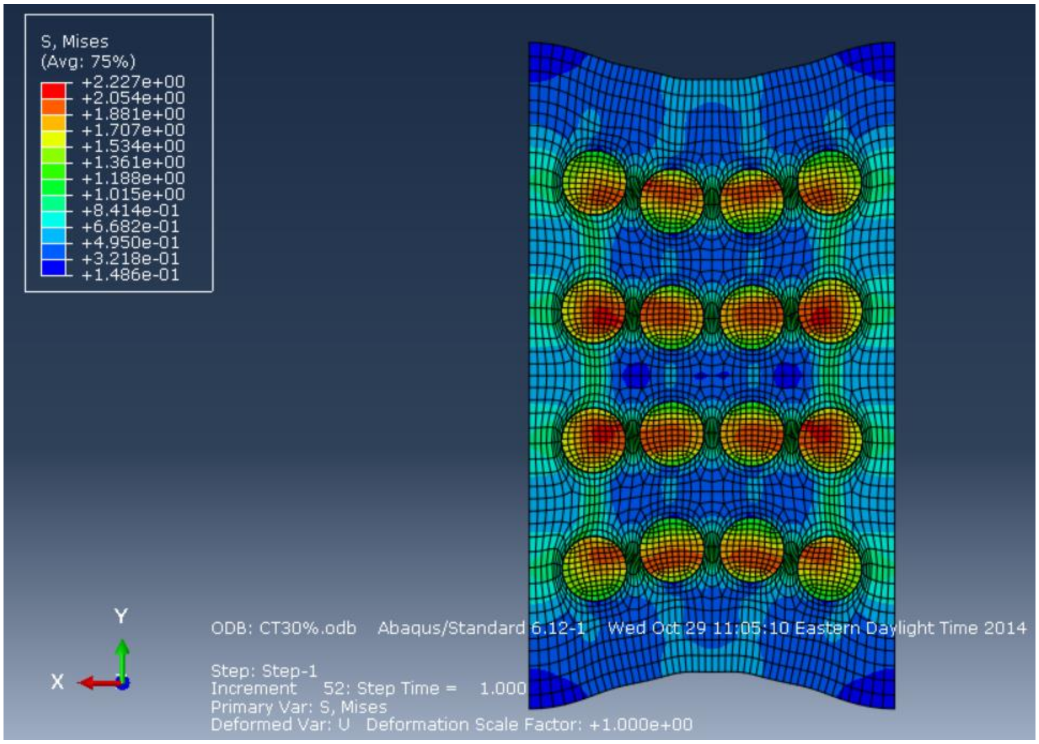

Figure 4.19 Von Mises Stress plot on deformed contour for 30% Strain

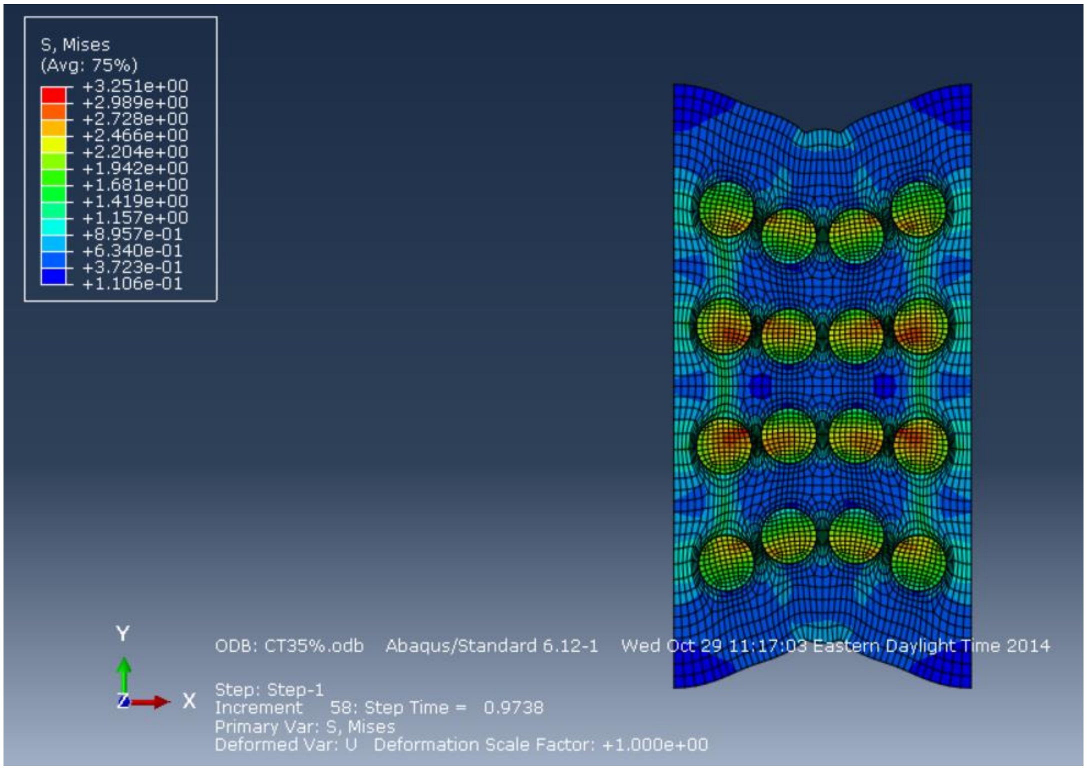

Figure 4.20 Von Mises Stress plot on deformed contour for 35% Strain

CHAPTER 5 DIELECTRIC STUDY OF THE COMPOSITE MICROSTRUCTURE BY MULTIPHYSICS SIMULATION

5.1 Dielectric Study using Maxwell's equations

We perform dielectric analysis of these deformed configurations using multiphysics simulation. To help us understand the material behavior, we solve for the Impedance and capacitance by application of Maxwell's equations. In the dielectric study we apply an AC signal (voltage or current) through which we can solve for Electric Field (E) by the relation

$$E = -\nabla V$$

The Electric field can then be subsequently related to current density J by

$$J = (\sigma + j\omega\varepsilon_0\varepsilon_r)E$$

Where σ is the electrical conductivity, ε_0 is the permittivity of air, ε_r is the permittivity or dielectric constant of the material. Current density J, helps us understand the charge distribution throughout the configuration with the help of continuity equation defined by

$$\nabla.(dsJ) = (dsQ)$$

Where ds is the shell element thickness. Charge displacement under the influence of electric field can be studied using the relation

$$D = \varepsilon_0 \varepsilon_r E$$

To measure the dielectric response we input dielectric constant and electrical conductivity of the materials. Material properties of steel are well defined in the literature, but for Silicone Rubber these details are available through experimental studies and were found out to be; dielectric constant (ε_r = 2.9) and electrical conductivity (σ = (3.1646E-12) S/m) [23]

5.2 3D Dielectric study of the 2D Model

To perform the dielectric study, we use the Electric Currents (EC) interface within AC/DC module of COMSOL multiphysics. The AC/DC module can model electric, magnetic, and electromagnetic fields in statics and low-frequency applications. The Electric Currents interface is used to model DC, AC, and transient electric current flow in conductive and capacitive media. We then import the deformed mesh into COMSOL using 3D Electric Currents interface, but the material model was defined in 2D during FEA (ABAQUS), to compensate this effect we use the Electric Currents Shell (ECS) interface which can solve 2D, 2D axisymmetric, and 3D geometries. ECS is used to model DC, AC, and transient electric current flow confined to conductive and capacitive thin current-conducting shells of fixed or varying thickness [24].

5.3 Importing Deformed Mesh for Multiphysics Simulation

To perform the dielectric study we import the deformed configurations as an orphan mesh (a mesh which doesn’t have an associated geometry) from FEA simulation. We import the orphan mesh as a *STL file, which can be imported into a multiphysics simulation software such as COMSOL. Through the imported mesh we assign the material properties and define boundary conditions for the analysis

5.3.1 Defining Boundary Conditions

After importing the mesh we assign material properties to entities in the model, and define BC's. We apply a 1 Volt AC signal across the edge perpendicular to loading direction as shown in Figure 5.1, so the top edge would be the source with 1 Volt and bottom would be connected to ground. Next we insulate the remaining two edges on the sides which is represented mathematically by the equation

$$n.J \ = 0$$

Where n is the vector normal to the surface, also since the matrix and fibers are two different entities, we assign a continuity boundary condition at the interface of these two constituent elements to make sure these two entities are connected and is defined by the equation

$$n.(J_1 - J_2) \ = 0$$

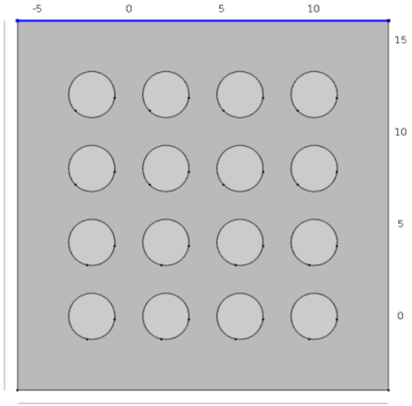

Figure 5.1 Model with 1 Volt signal applied perpendicular to loading direction

5.3.2 Dielectric study of the undeformed configuration

The undeformed configuration was imported and dielectric response was studied to determine the variation of the Electric Fields throughout the microstructure as shown in Figure 5.2.

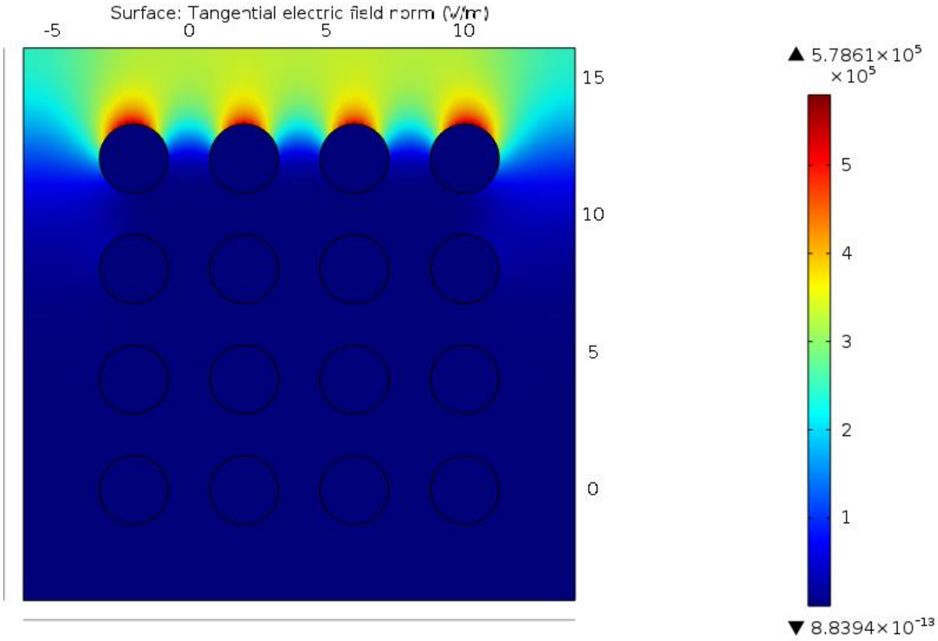

Figure 5.2 Variation of Electric Field in Undeformed model

5.3.3 Dielectric study of the model loaded in Tension

In Chapter 3, we have seen that as degradation (damage) of the material increases, we observed a variation in the dielectric response of the material. To verify this, the models loaded in tension during FEA simulation in chapter 4 are imported and variations in the dielectric response is studied for different mechanical load/strain cases as shown in Figures 5.3 to 5.14

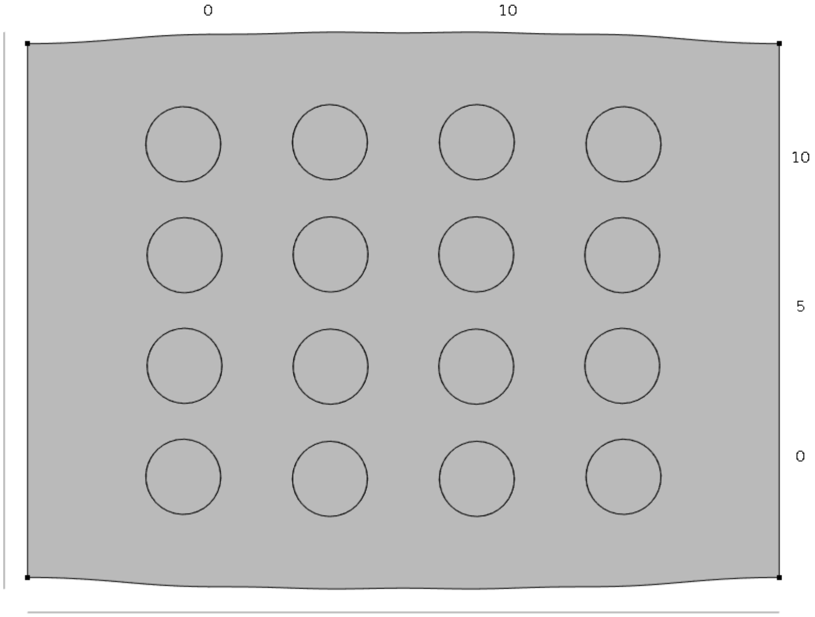

Figure 5.3 Model under 25% tension imported for dielectric study

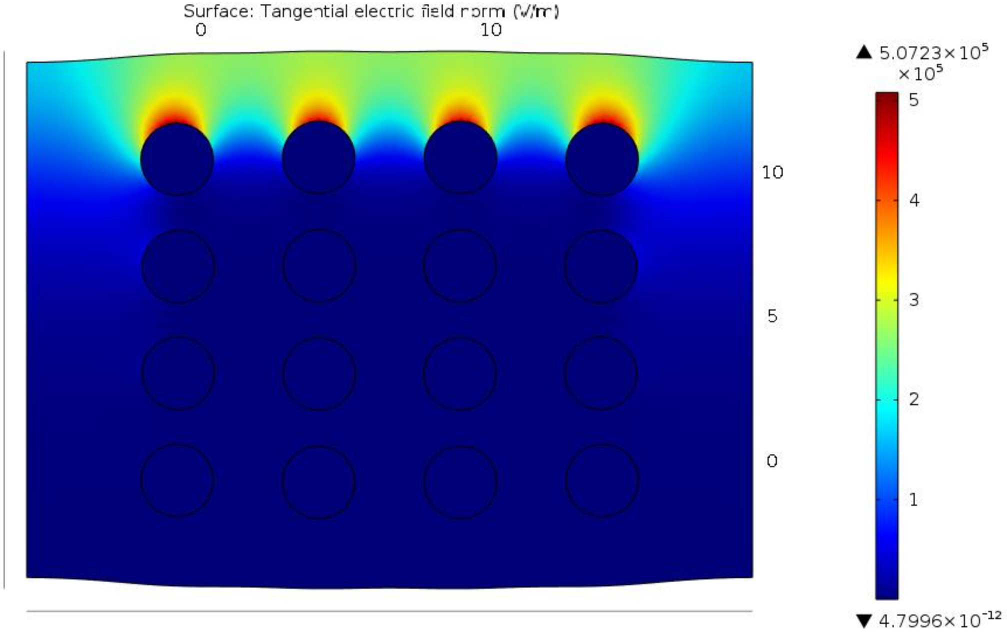

Figure 5.4 Electric Field variation in model under 25% Tension

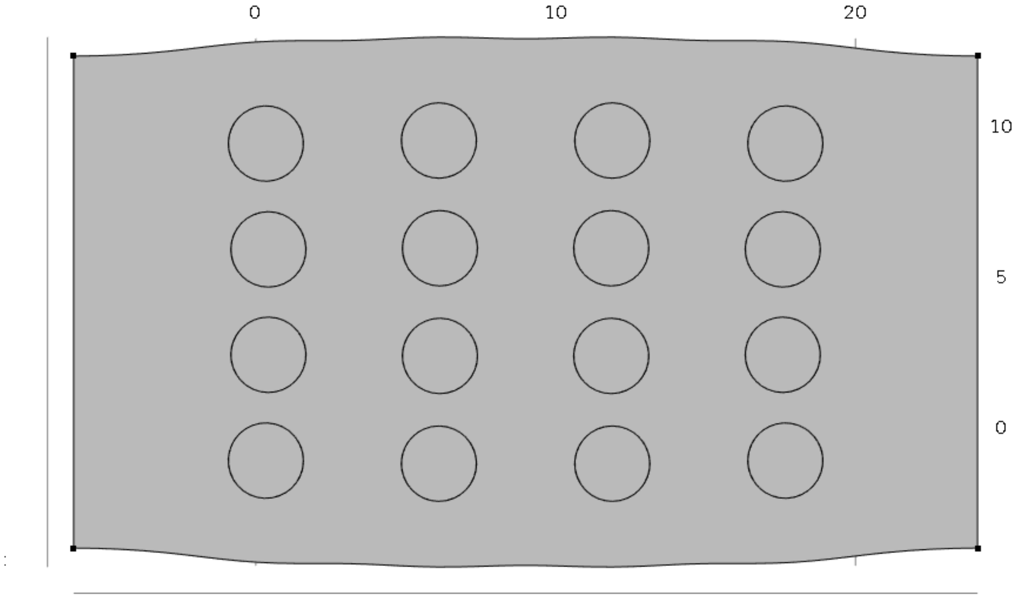

Figure 5.5 Model under 50% tension imported for dielectric study

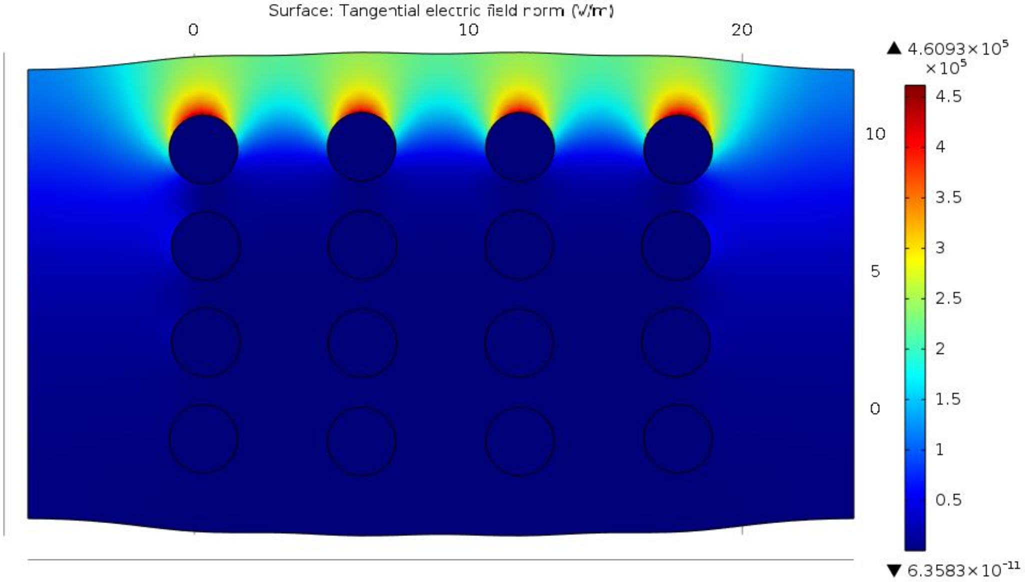

Figure 5.6 Electric Field variation in model under 50% Tension

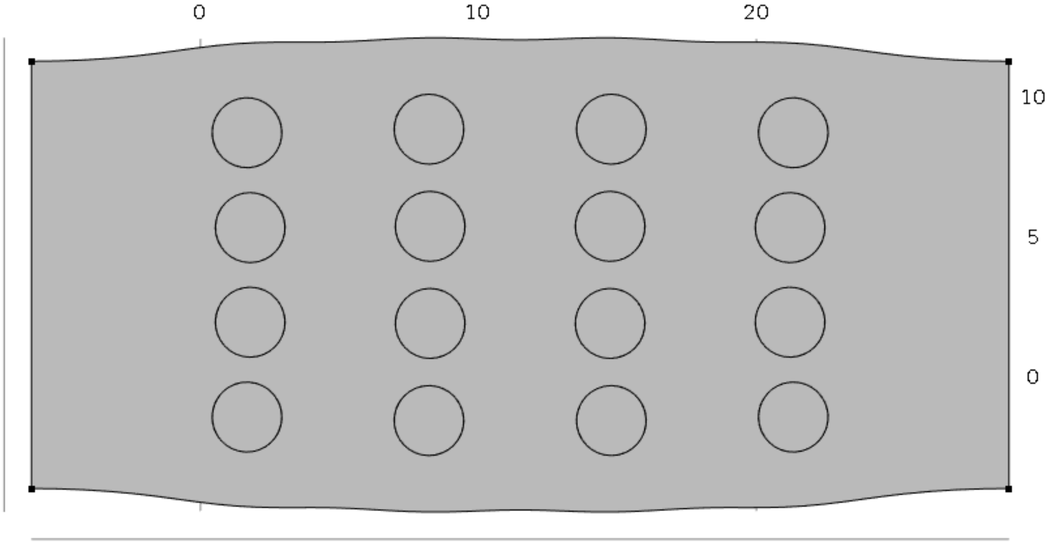

Figure 5.7 Model under 75% tension imported for dielectric study

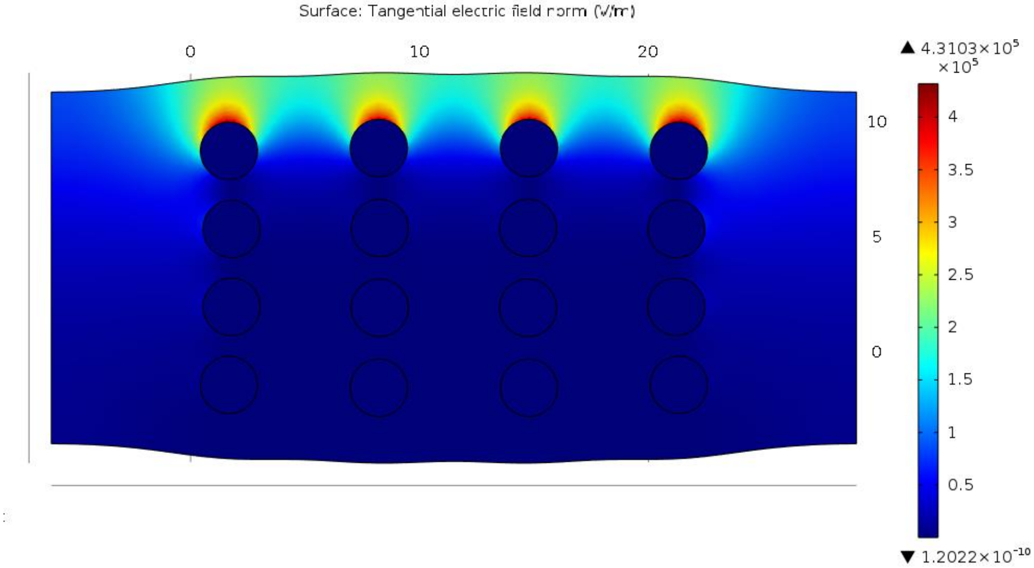

Figure 5.8 Electric Field variation in model under 75% Tension

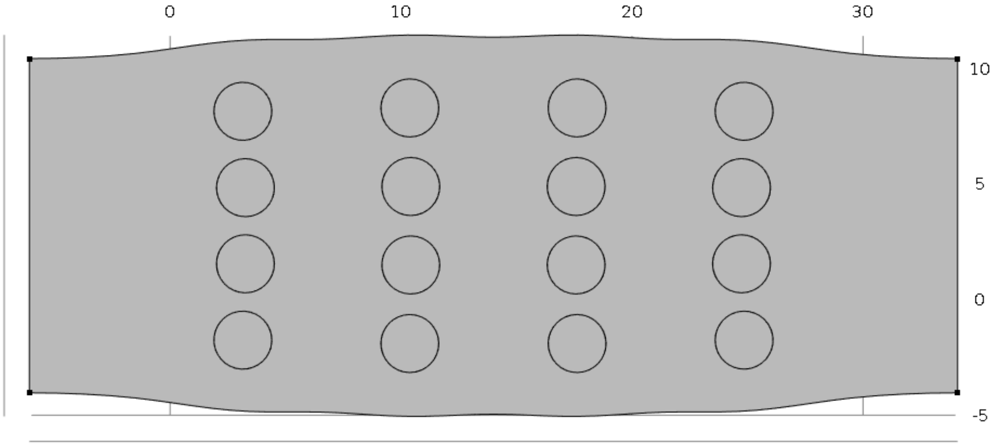

Figure 5.9 Model under 100% tension imported for dielectric study

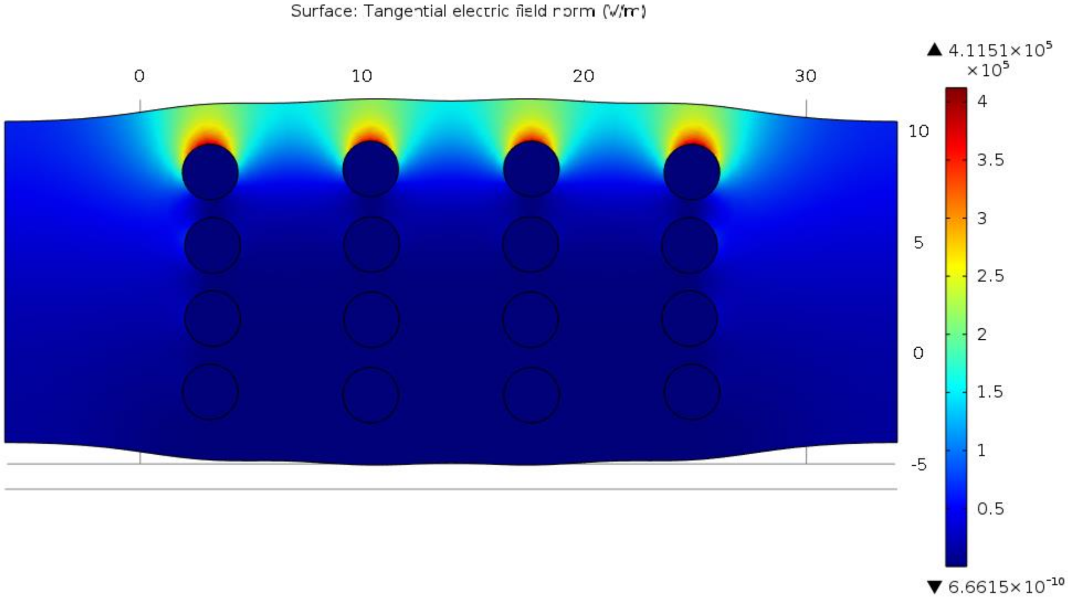

Figure 5.10 Electric Field variation in model under 100% Tension

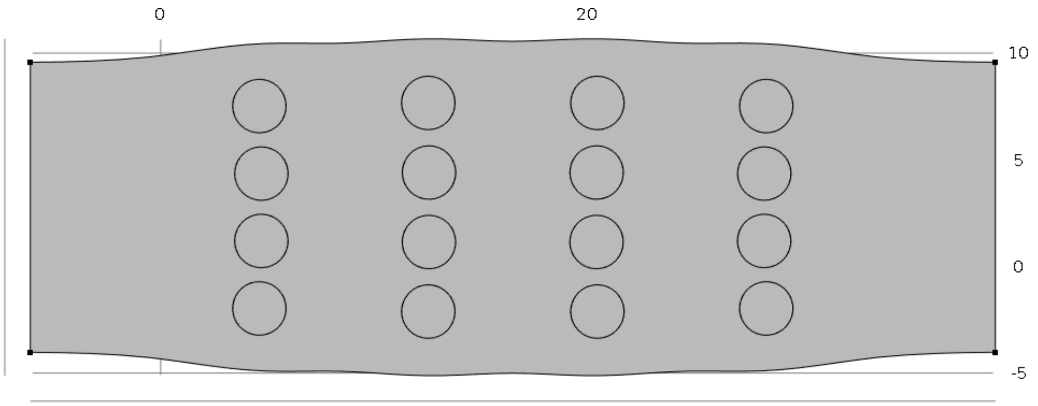

Figure 5.11 Model under 125% tension imported for dielectric study

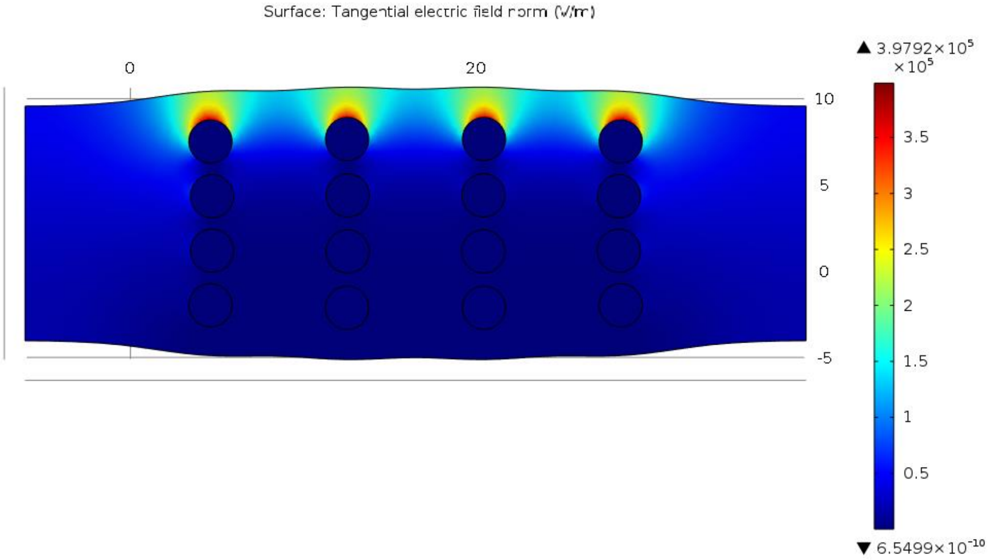

Figure 5.12 Electric Field variation in model under 125% Tension

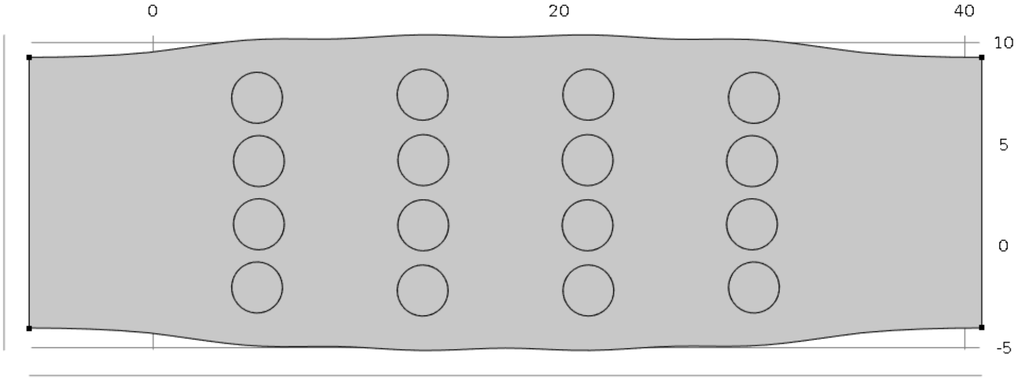

Figure 5.13 Model under 133% tension imported for dielectric study

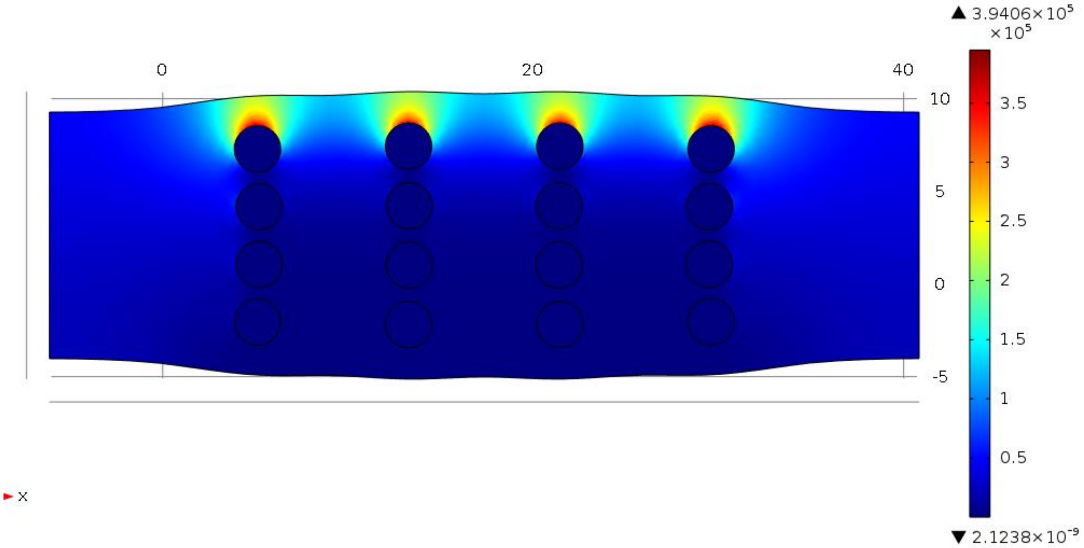

Figure 5.14 Electric Field variation in model under 133% Tension

5.3.4 Comparison of Dielectric response at various Tensile loads

As damage in the material increases, we observed a substantial variation in the dielectric response of the material in chapter 3, we observe a similar variation in the response during this multiphysics simulation. We see a net decrease of 60% in Normalized Impedance, Re (Z) of the model as shown in Figure 5.15. Normalized impedance in the model is calculated as

Normalized Re (Z) = (Re (Z) Deformed) / (Re (Z) Undeformed)

At the initial state, without damage the Normalized Re (Z) would be **1**. As damage increases we see the Normalized Re (Z) decreasing as shown in Figure 5.15

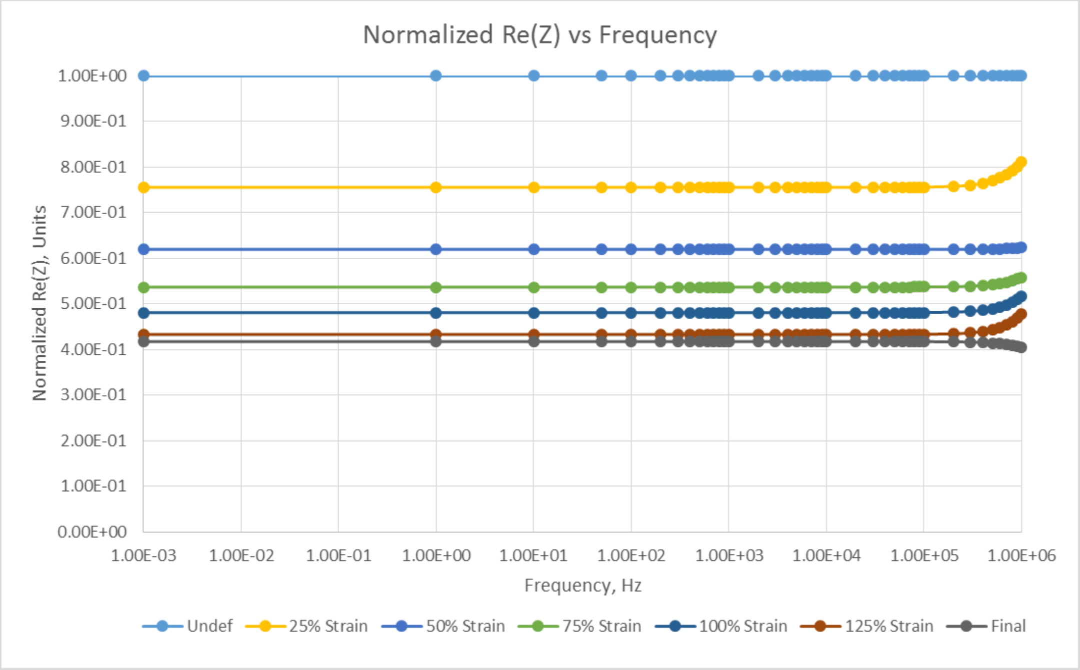

Figure 5.15 Normalized Re (Z) vs Frequency at different stages of life

Also when we study the variation in the Real part of Capacitance, Re (C), we observe some exciting variations. As damage increases, capacitance increases as the distance between the fibres in the lateral direction (direction of the electric field decreases). The variation in capacitance is plotted as shown in Figure 5.16. We can observe from this plot that the variation in capacitance increases initially than gradually decreases and just before failure we see a small increase followed by a sharp decrease as shown in Figure 5.16, which can be used as an inflation point to indicate failure.

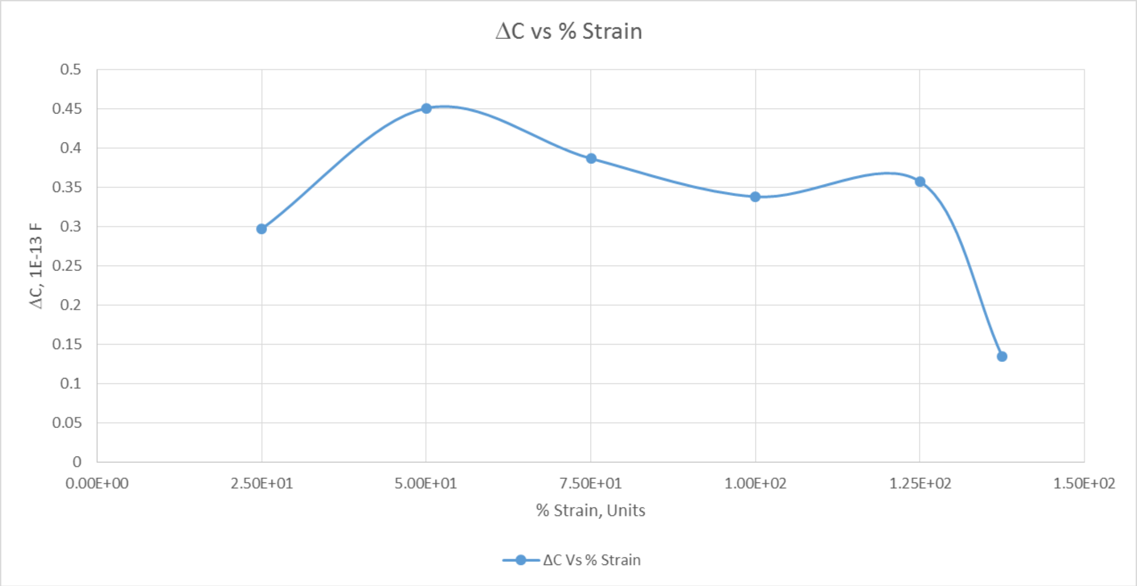

Figure 5.16 Change in Capacitance (ΔC) vs % tensile strain

5.3.5 Dielectric study of the models loaded in Compression

In Chapter 3, we have seen that as damage increases we observed a variation in the dielectric response of the material. To verify this, the models loaded in compression in chapter 4 during FEA simulation are imported and variation in dielectric response was studied at different mechanical load/strain cases as shown in Figures 5.17 to 5.30.

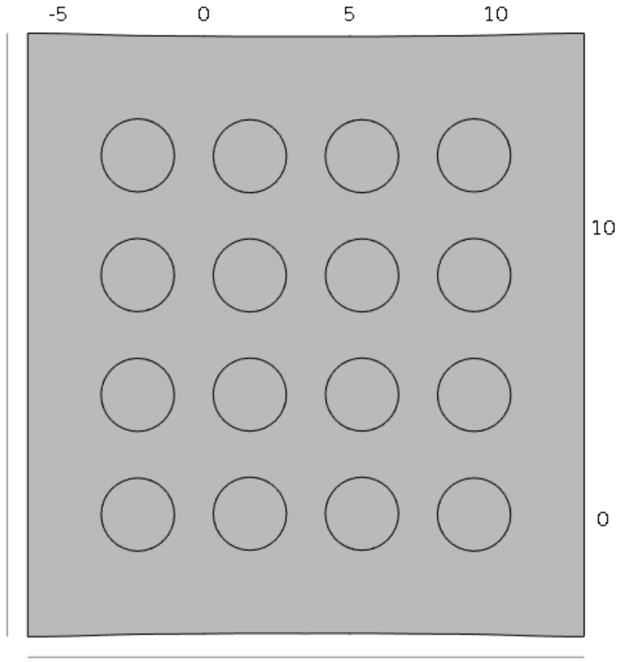

Figure 5.17 Model under 5% compression imported for dielectric study

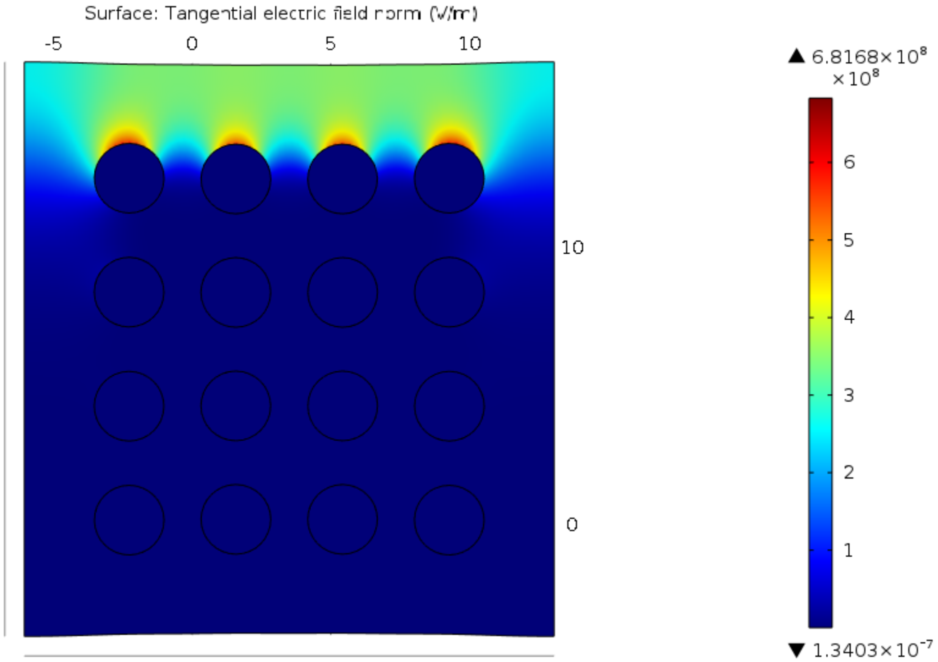

Figure 5.18 Electric Field variation in model under 5% Compression

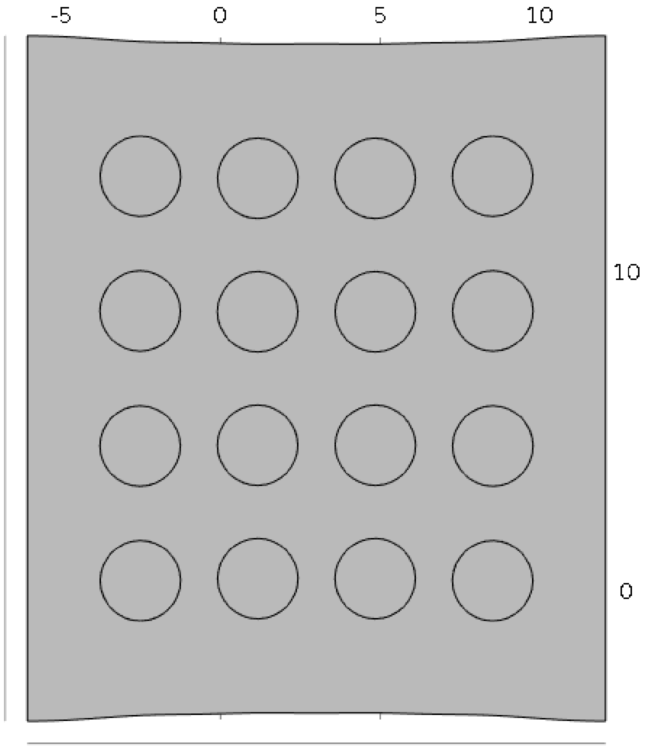

Figure 5.19 Model under 10% compression imported for dielectric study

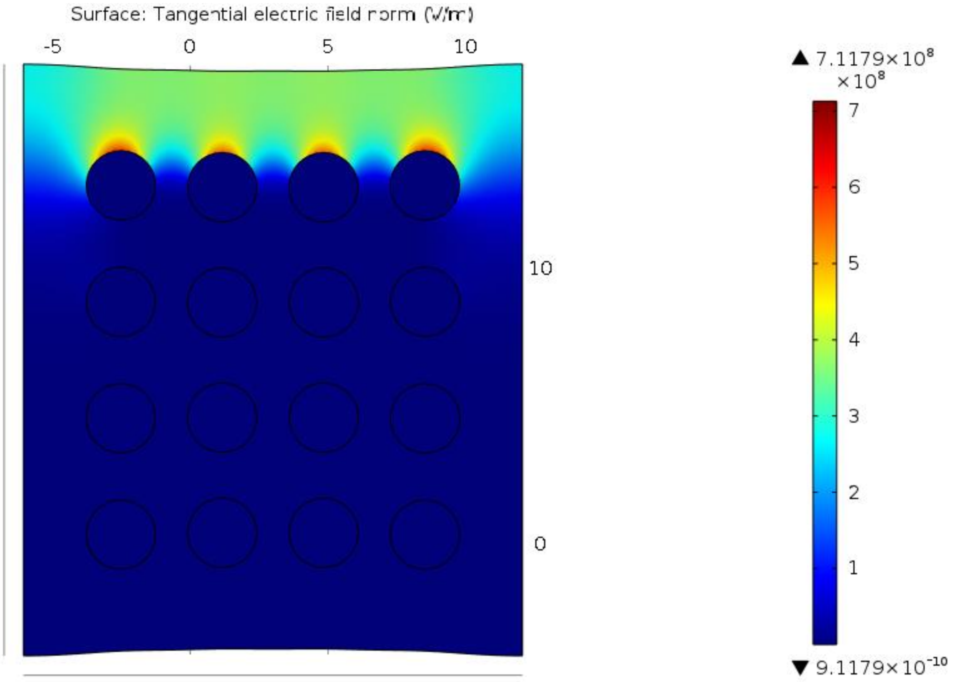

Figure 5.20 Electric Field variation in model under 10% Compression

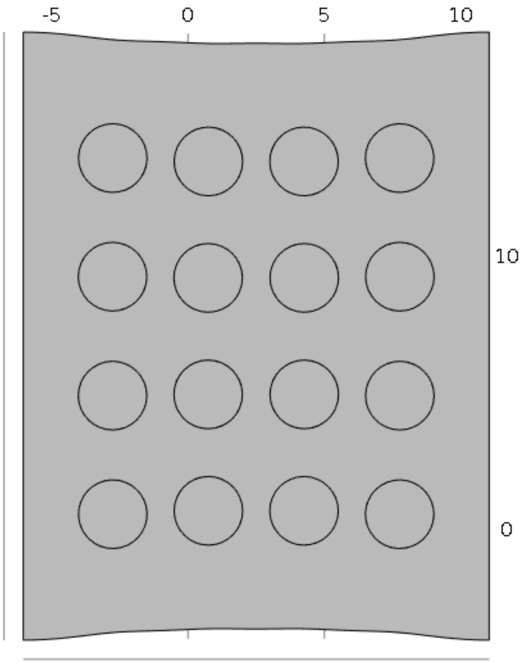

Figure 5.21 Model under 15% compression imported for dielectric study

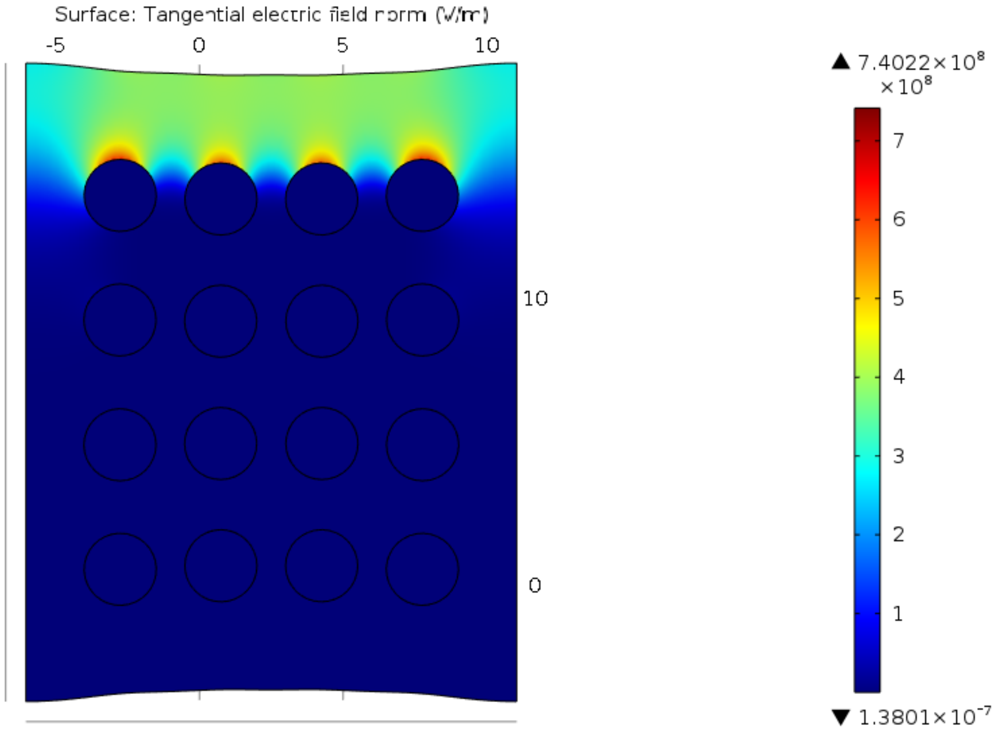

Figure 5.22 Electric Field variation in model under 15% Compression

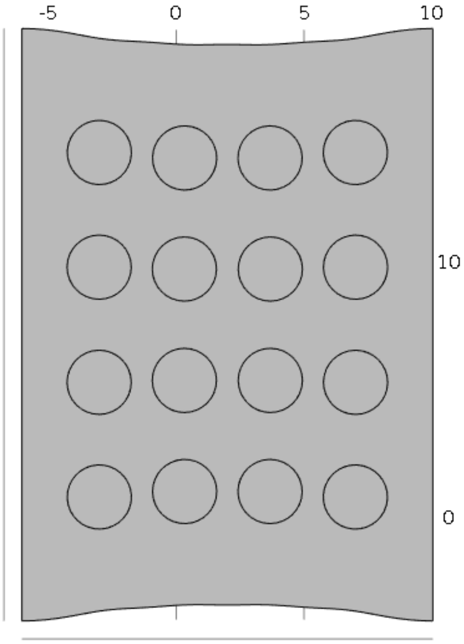

Figure 5.23 Model under 20% compression imported for dielectric study

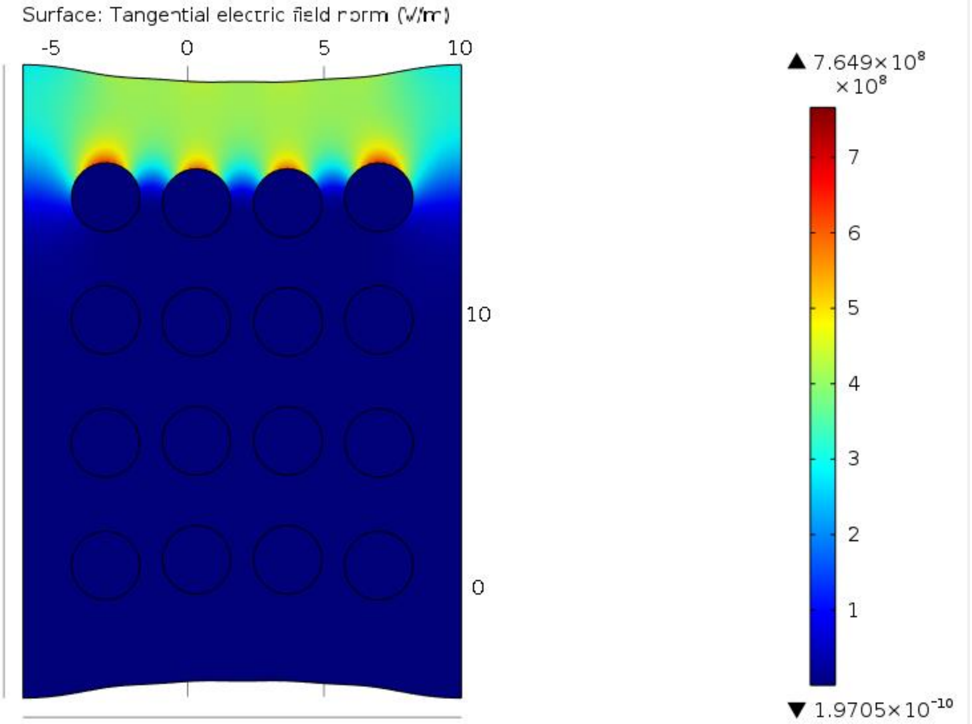

Figure 5.24 Electric Field variation in model under 20% Compression

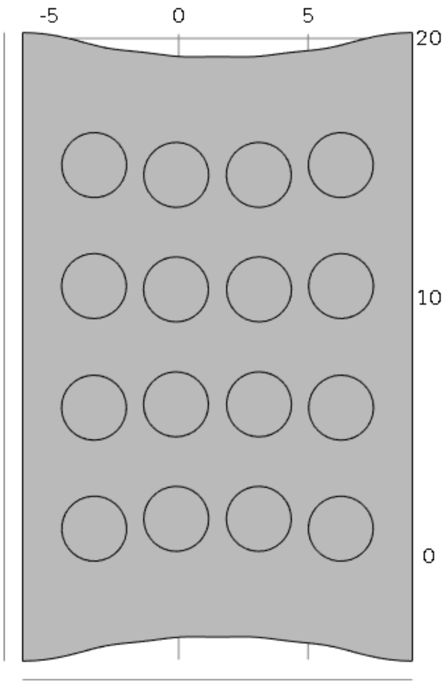

Figure 5.25 Model under 25% compression imported for dielectric study

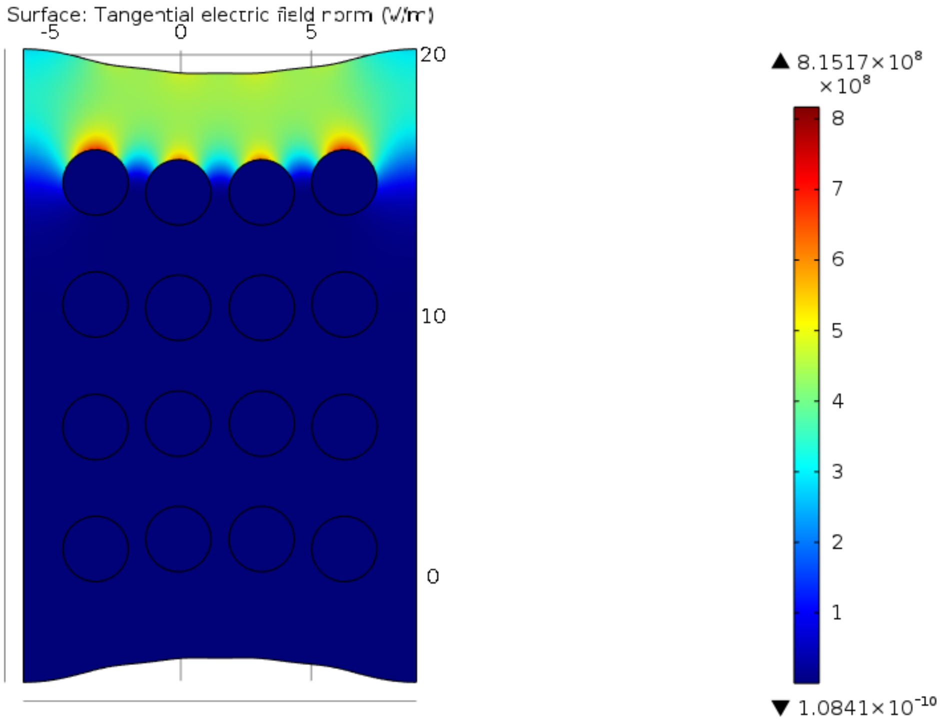

Figure 5.26 Electric Field variation in model under 25% Compression

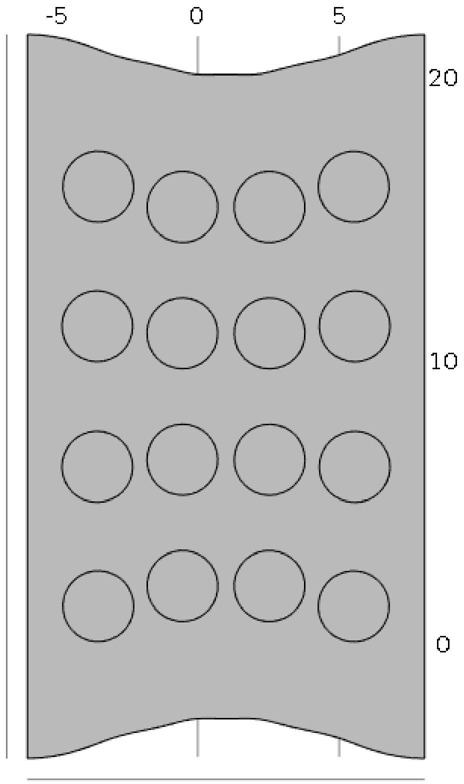

Figure 5.27 Model under 30% compression imported for dielectric study

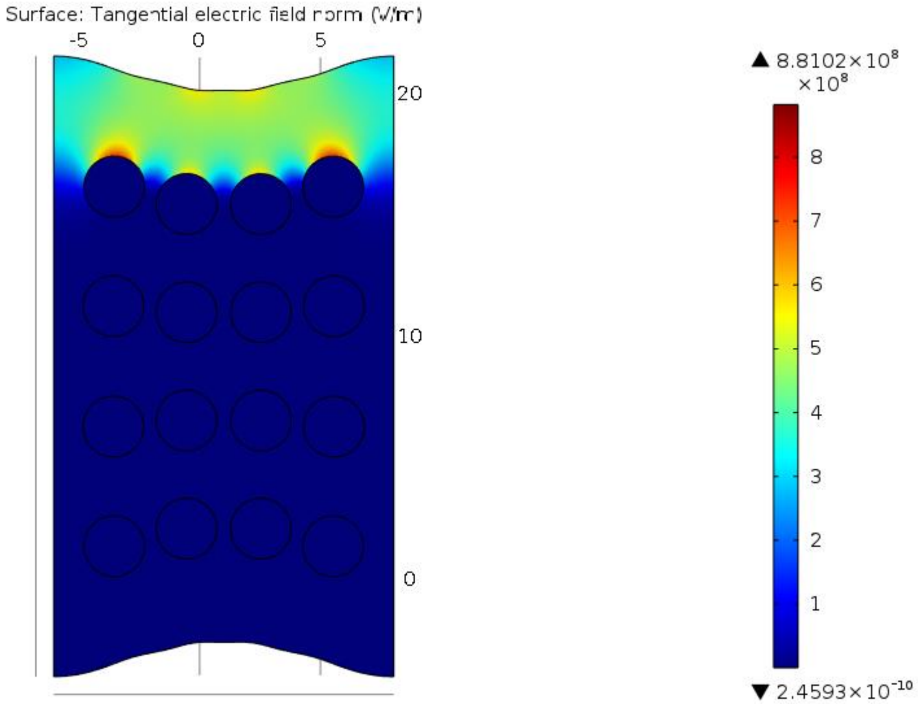

Figure 5.28 Electric Field variation in model under 30% Compression

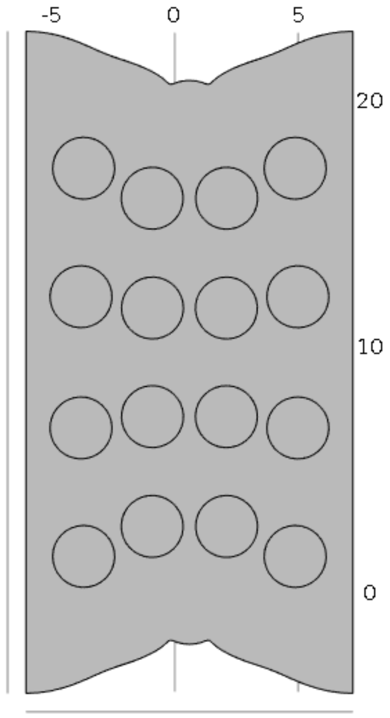

Figure 5.29 Model under 35% compression imported for dielectric study

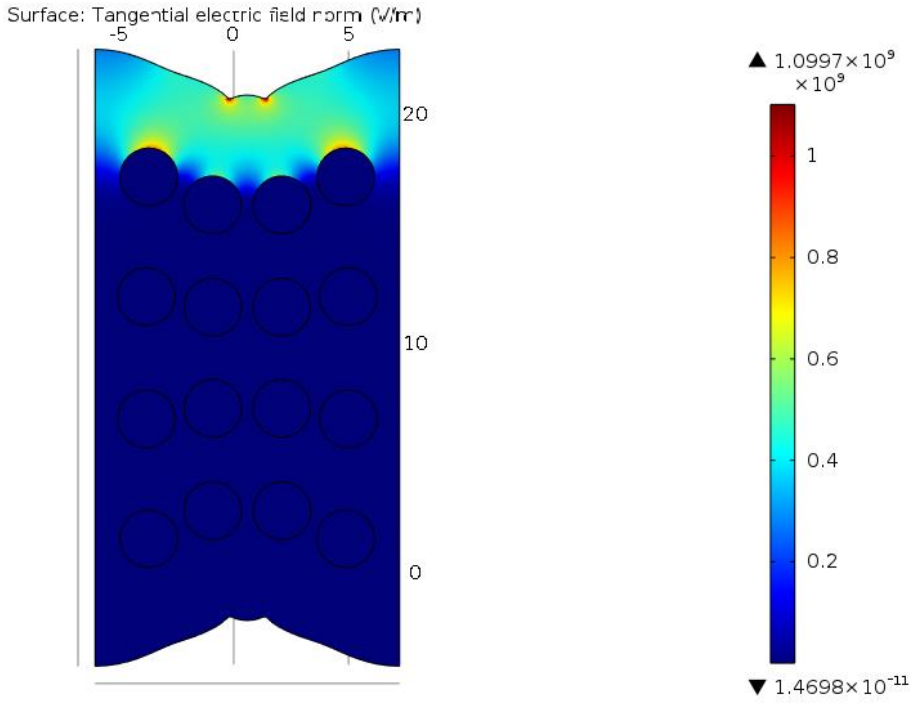

Figure 5.30 Electric Field variation in model under 35% Compression

5.3.6 Comparison of Dielectric study at various Compression loads

As damage in the material increases, we observed that impedance decreases during tensile loading, but in case of compression we observe that Impedance increases. We observed a net increase of 73% in Normalized Impedance, Re (Z) of the model as shown in Figure 5.31.

At the initial state, without damage the Normalized Re (Z) would be **1**. As damage increases we see the Normalized Re (Z) decreasing as shown in Figure 5.31.

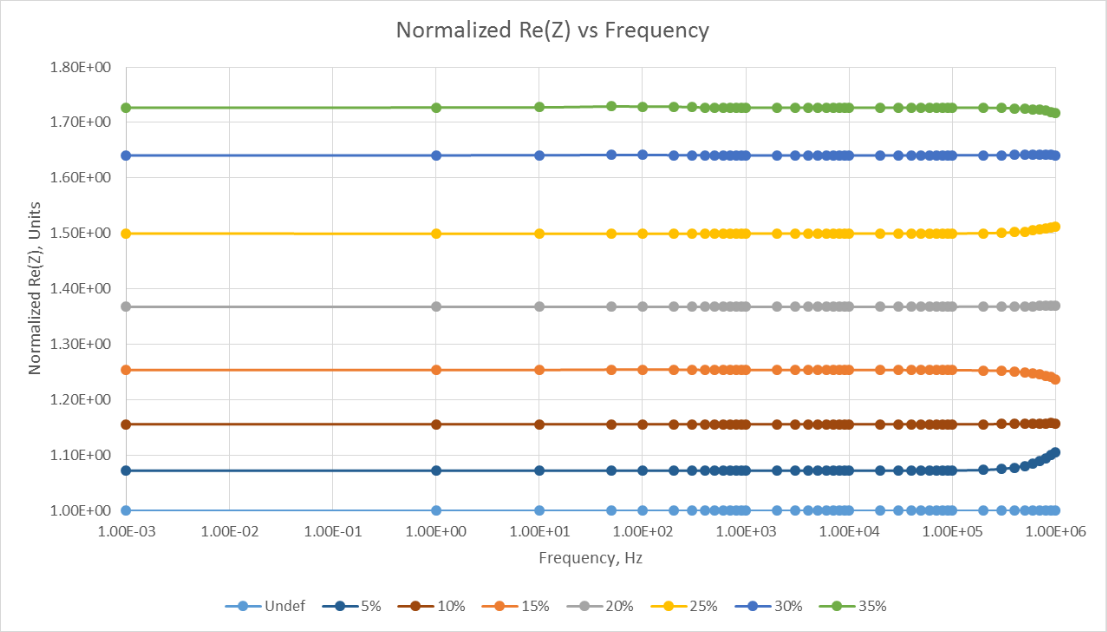

Figure 5.31 Normalized Re (Z) vs Frequency at different stages of life under compression

Also when we study the variation in Real part of Capacitance, Re (C) we observe a steady plot. As damage increases Capacitance decreases as the distance between the fibres in the lateral direction (direction of electric field increases). The variation in capacitance is plotted as shown in Figure 5.32. We can observe from this plot variation in capacitance decreases steadily.

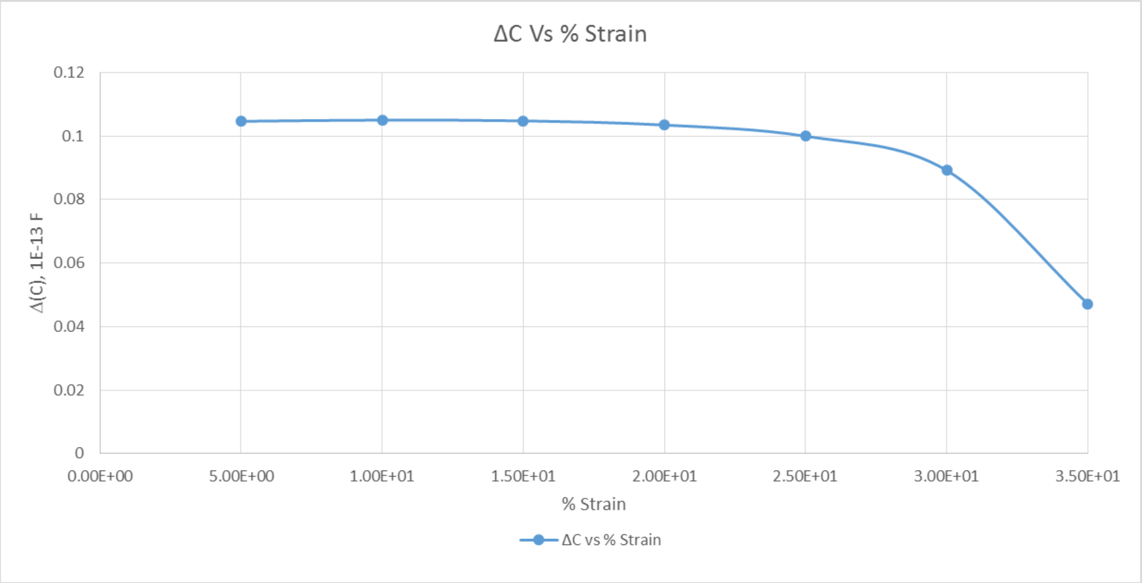

Figure 5.32 Change in Capacitance (ΔC) vs % Compressive strain

CHAPTER 6 THREE-PHASE MICROMECHANICS MODELING AND ANALYSIS USING FEA

6.1 Introducing third phase in to the model

In the above chapters we have noticed a variation in dielectric response as damage increases in the material. In real-time conditions, as material degrades we see moisture or other impurities settling in these cracks that can influence the response and performance of the material. In order to simulate this effect we introduced a third phase which represents moisture in this model.

6.2 Material Properties of the third phase

To analyze the three-phase model using FEA, we define moisture as a linear elastic material with Poisson's ratio ν = 0.5, since moisture (water) can be assumed as a liquid, where forces act equally in all directions. Taking ν = 0.5 would lead to singularity in the computation so we approximate it to 0.48. For an elastic material we need to define Young's Modulus (E) of the material. For moisture, we derive this value from the relation

$$\boldsymbol{E} = \boldsymbol{3} \times \boldsymbol{K} \times (\boldsymbol{1} - \boldsymbol{2\nu})$$

Where E is the Young's Modulus, K is the Bulk modulus and ν is the poisson's ratio. For moisture (water) K= 2.2E9 Pa, Hence from the relation we get E = 2.64E8 Pa.

6.3 2D nonlinear analysis of the three-phase model

6.3.1 Modeling Moisture as third phase

To model third phase, we create a ring of 1.25 cm radius around 1.23 cm fiber as shown in Figure 6.1. Then we assemble the model, mesh and assign displacement continuity as done in chapter 4. The final mesh assembly is shown in Figure 6.2.

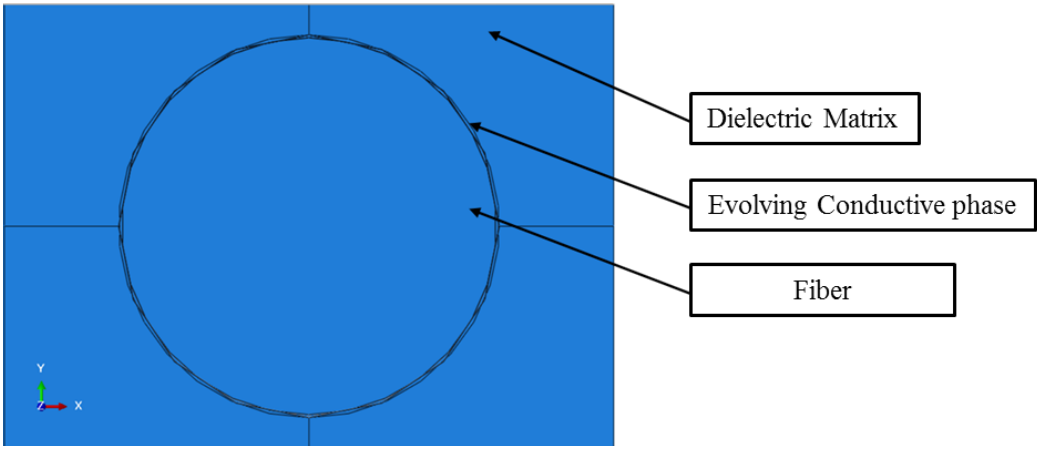

Figure 6.1 Three-phase model with ring of moisture surrounding steel reinforced fiber

The mesh consists of quadrilateral elements, CPS4R: A 4-node bilinear plane stress quadrilateral, reduced integration, hourglass control as shown in Figure 6.2. The total number of elements in the model = 5088, the total number of nodes = 6209.

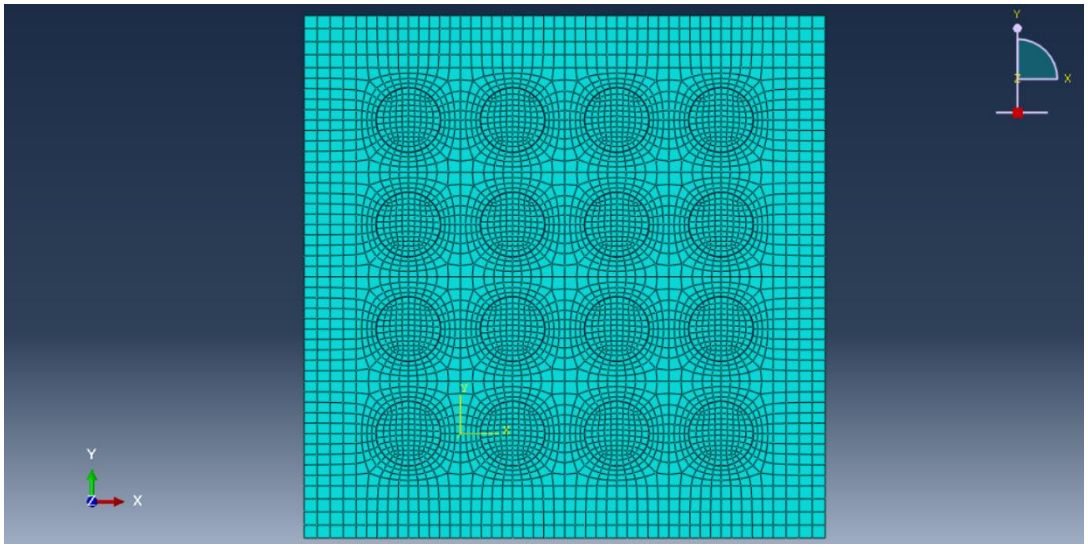

Figure 6.2 Final mesh of three-phase model with ring of moisture surrounding steel reinforced fibers

6.3.2 Model loaded in Tension

The Boundary conditions for the three-phase model remains the same as discussed in chapter 4. We deform the model by uni-axial displacement up to 133% Strain (Fracture) and the Von-Mises Stress plots are shown in Figures 6.3 to 6.8. It is observed that deformation patterns almost remain the same even with the inclusion of third phase

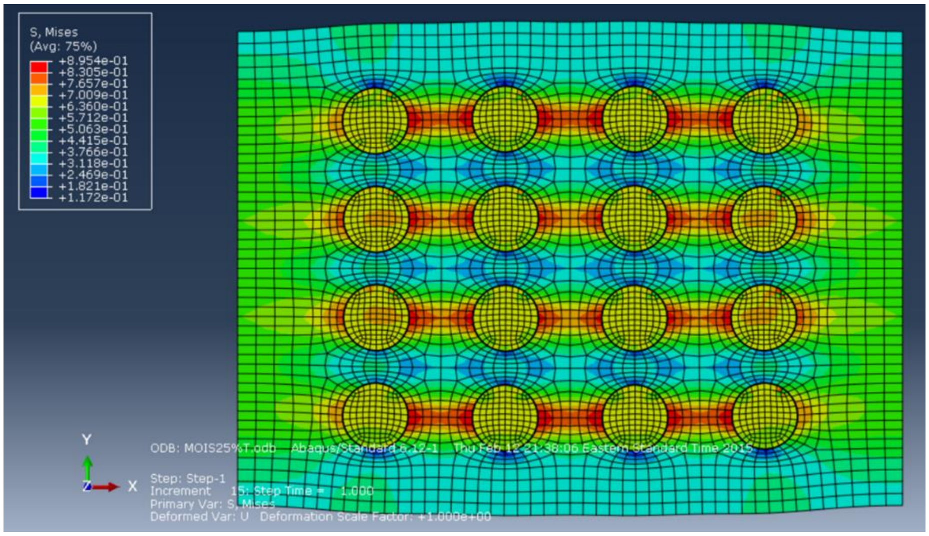

Figure 6.3 Von Mises Stress plot on deformed contour for 25% Strain

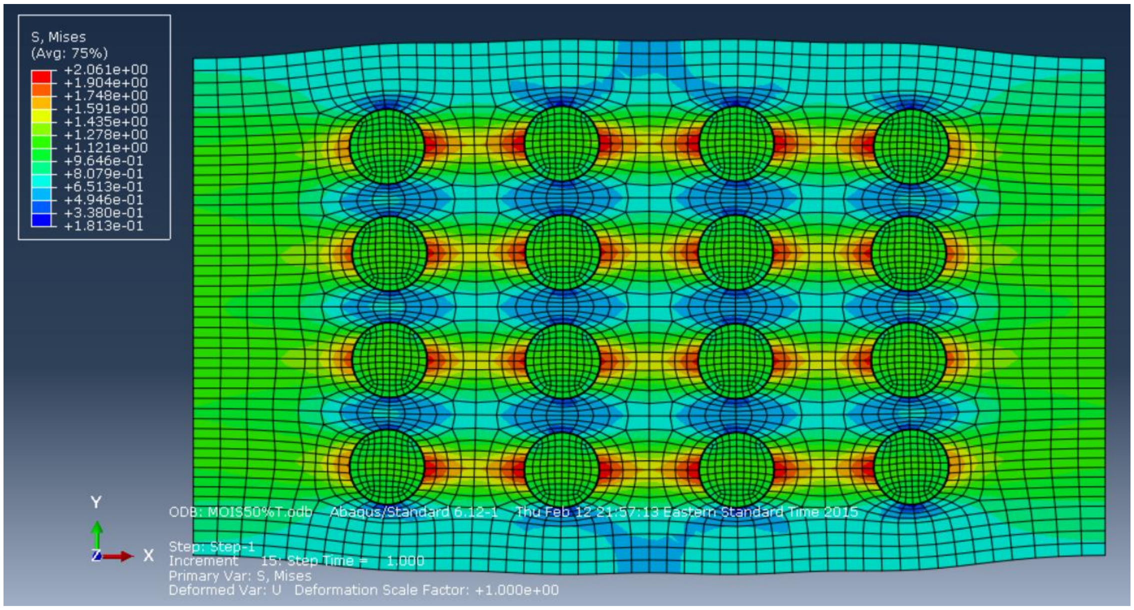

Figure 6.4 Von Mises Stress plot on deformed contour for 50% Strain

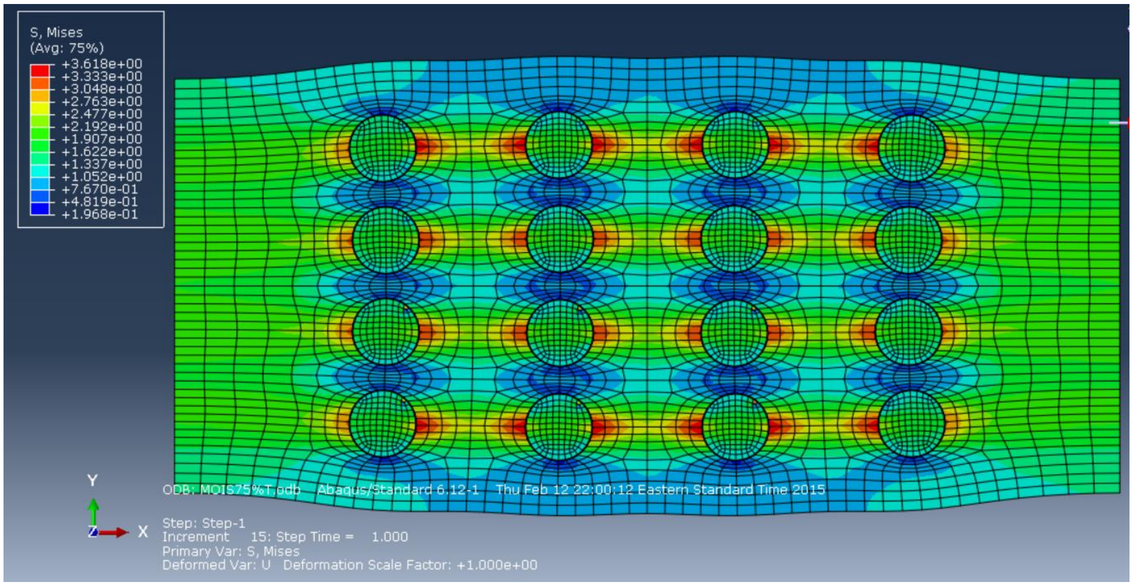

Figure 6.5 Von Mises Stress plot on deformed contour for 75% Strain

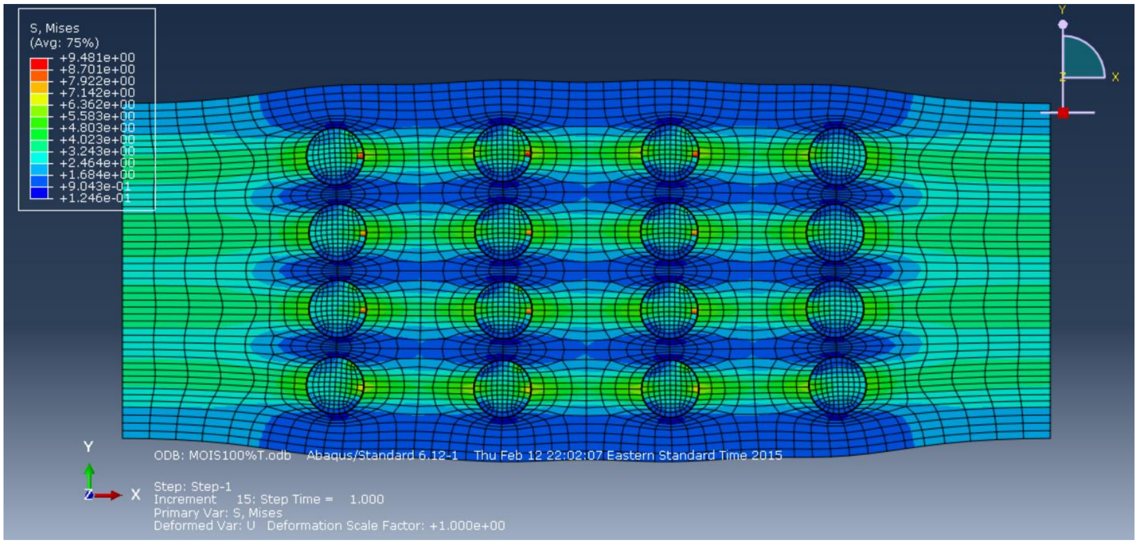

Figure 6.6 Von Mises Stress plot on deformed contour for 100% Strain

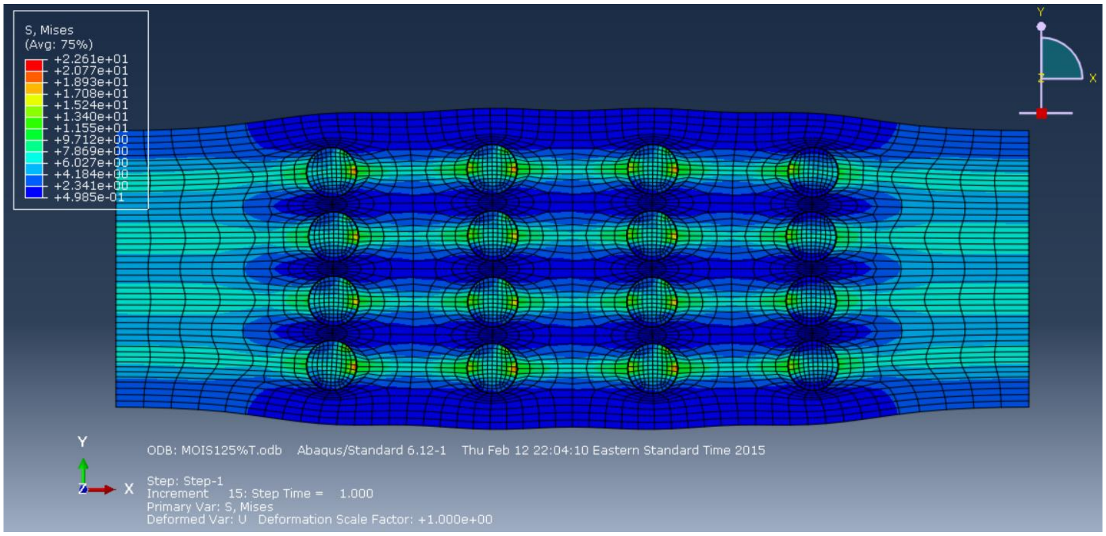

Figure 6.7 Von Mises Stress plot on deformed contour for 125% Strain

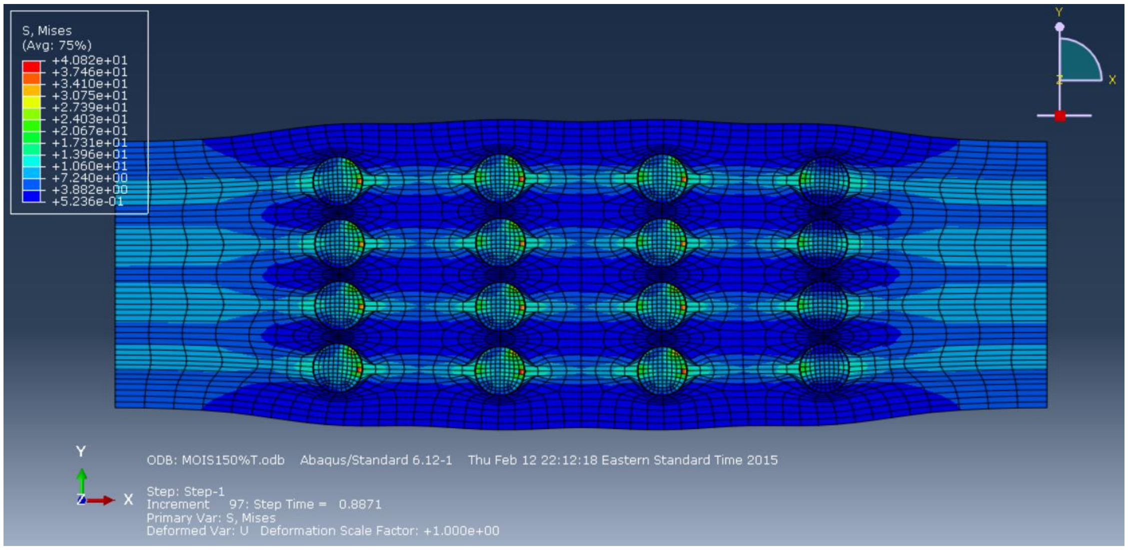

Figure 6.8 Von Mises Stress plot on deformed contour for 133% Strain

6.3.3 Model loaded in Compression

We deform the model by uni-axial displacement up to 35% Strain (buckling) and the Von-Mises Stress plots are shown in Figures 6.9 to 6.15. It is observed that deformation patterns almost remain the same even with the inclusion of third phase.

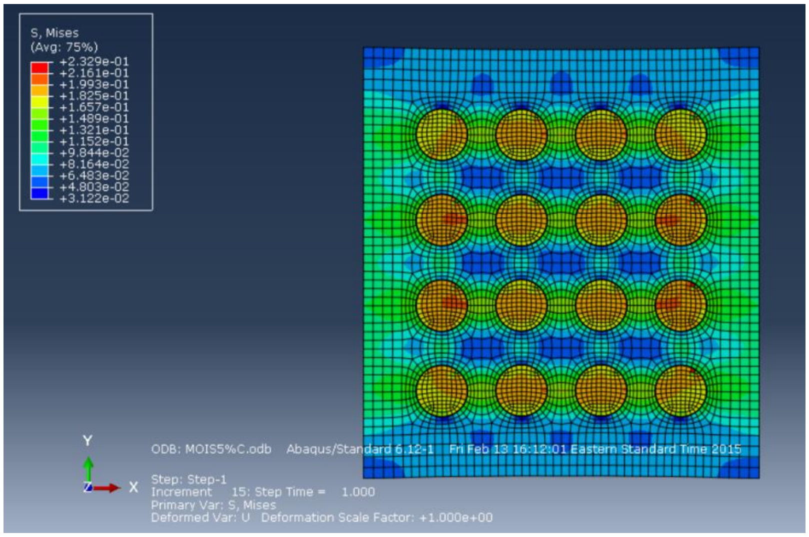

Figure 6.9 Von Mises Stress plot on deformed contour for 5% Compressive Strain

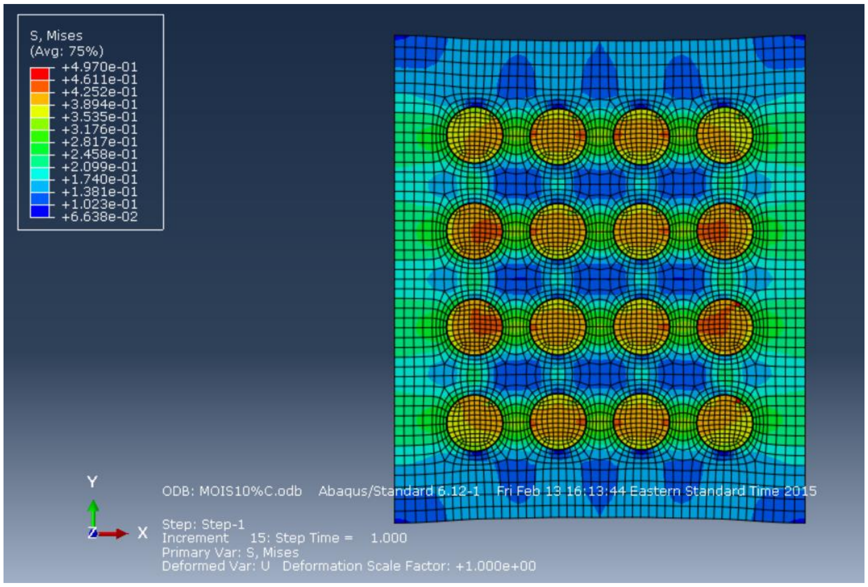

Figure 6.10 Von Mises Stress plot on deformed contour for 10% Compressive Strain

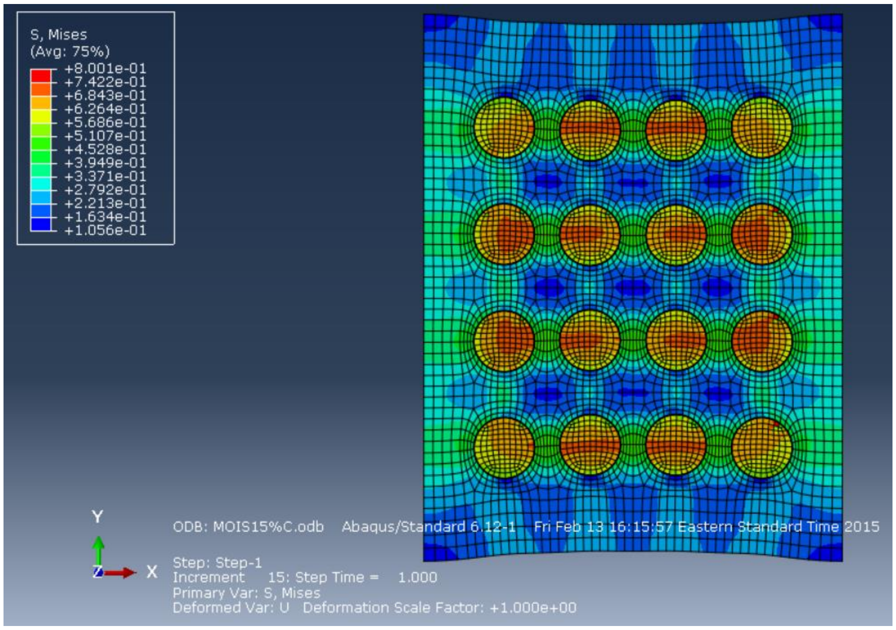

Figure 6.11 Von Mises Stress plot on deformed contour for 15% Compressive Strain

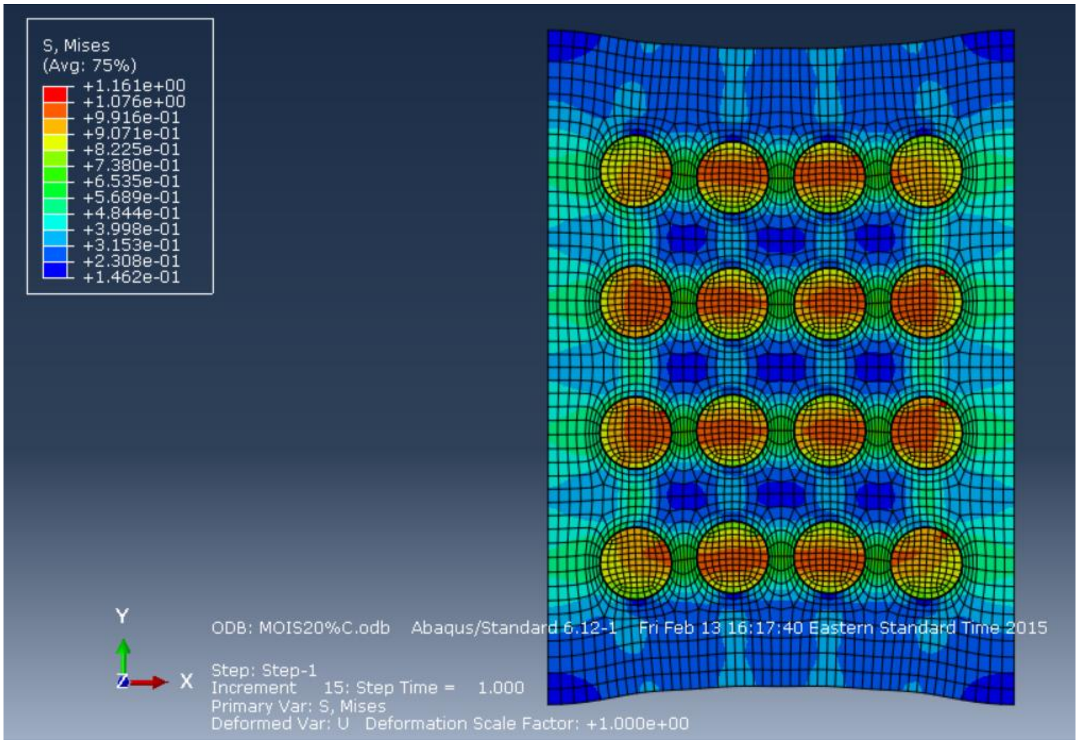

Figure 6.12 Von Mises Stress plot on deformed contour for 20% Compressive Strain

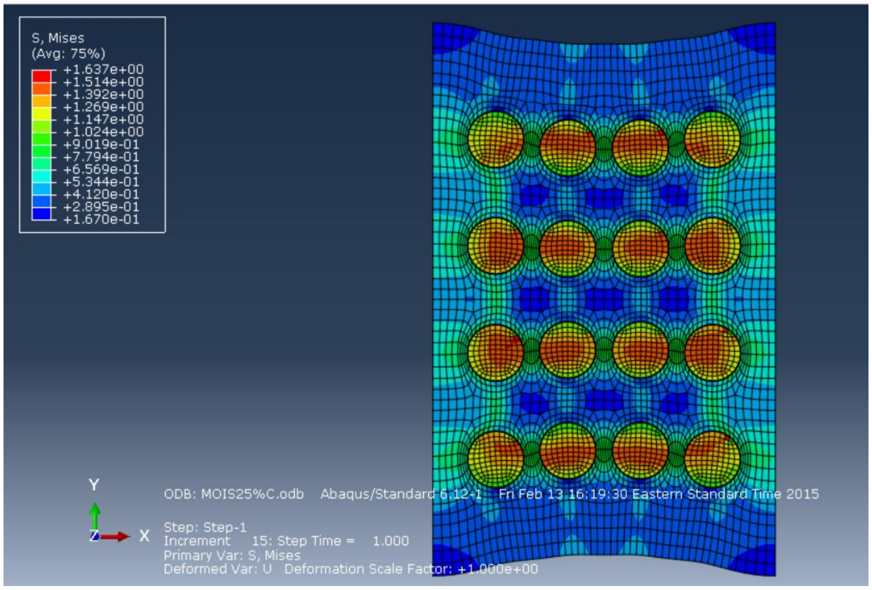

Figure 6.13 Von Mises Stress plot on deformed contour for 25% Compressive Strain

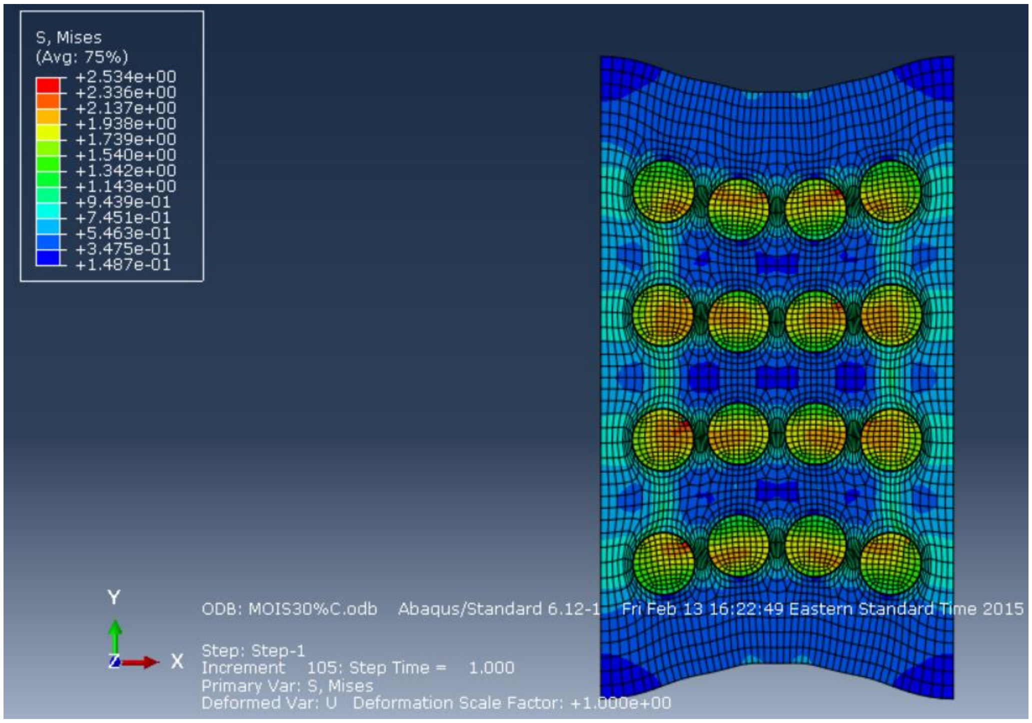

Figure 6.14 Von Mises Stress plot on deformed contour for 30% Compressive Strain

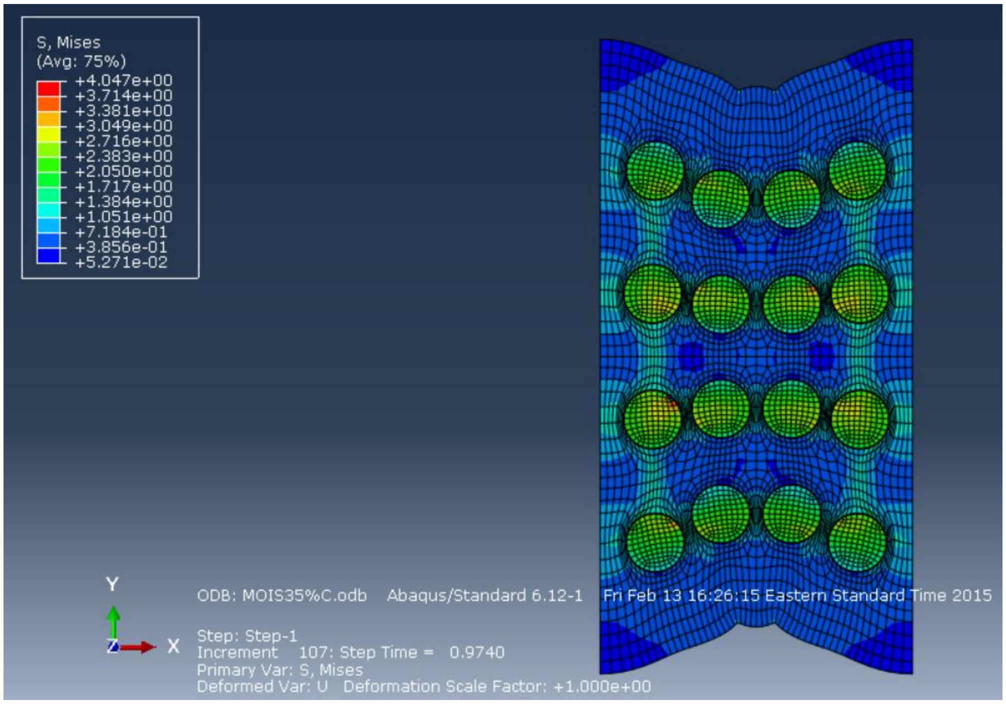

Figure 6.15 Von Mises Stress plot on deformed contour for 35% Compressive Strain

CHAPTER 7 DIELECTRIC STUDY OF THREE-PHASE MICROMECHANICS MODEL BY MULTIPHYSICS SIMULATION

7.1 Dielectric study of three-phase Micromechanics model loaded in tension

After importing the deformed mesh we assign material properties to entities in the model and define BC’s. For the third phase, moisture dielectric constant (ε) = 1 and electrical conductivity (σ) = 5E-4 S/m. Undeformed model is imported as shown in Figure 7.1 to understand variation of Electric Field throughout the model as shown in Figures 7.2 to 7.8.

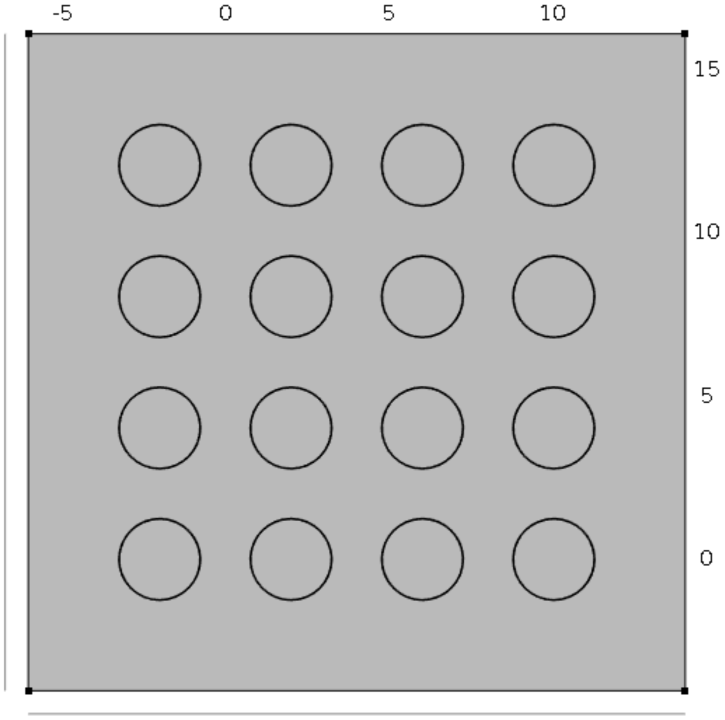

Figure 7.1 Undeformed Model imported for dielectric study

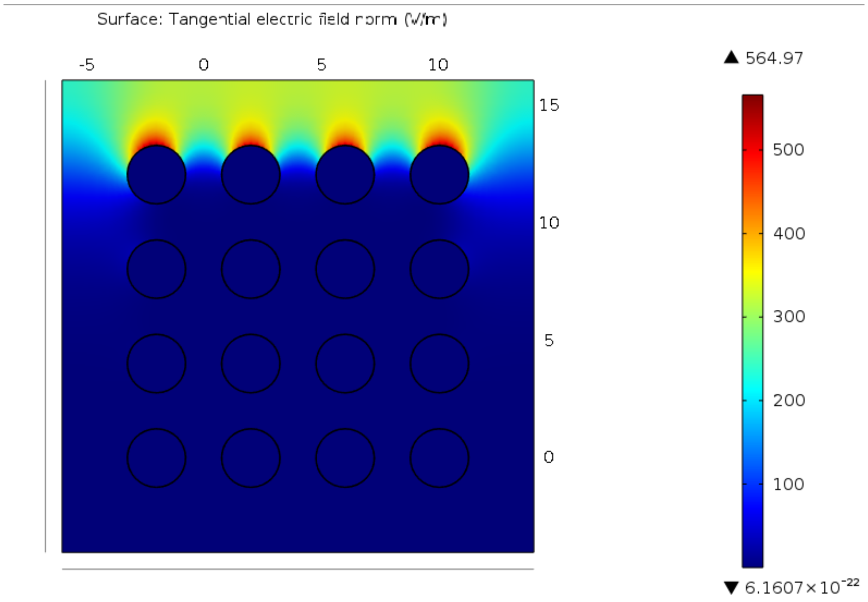

Figure 7.2 Variation of Electric Field in Undeformed model

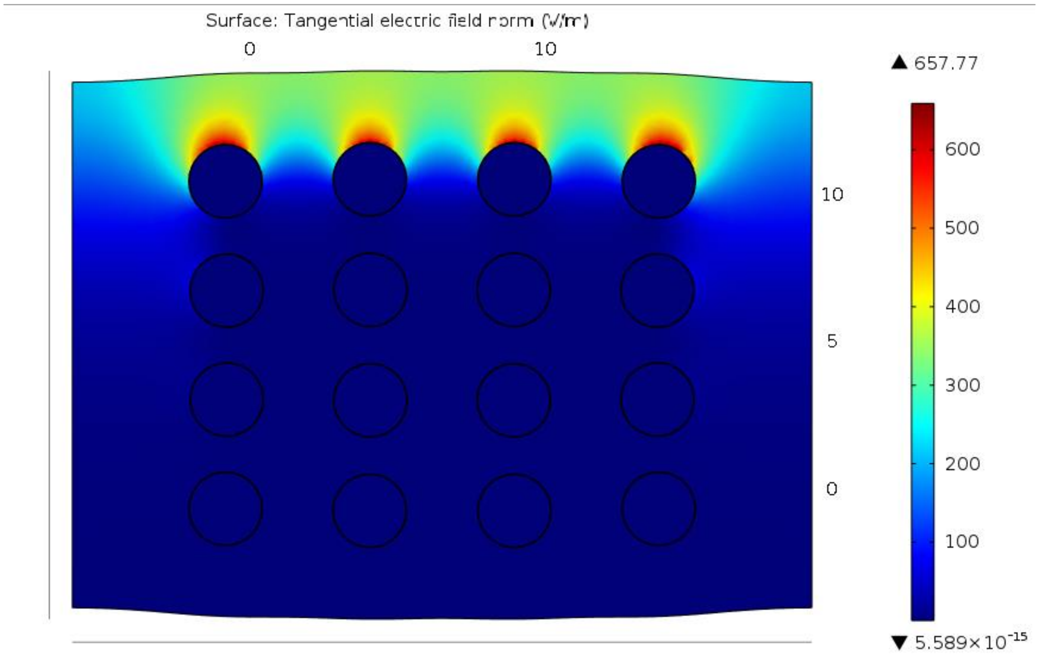

Figure 7.3 Variation of Electric Field in 25% tensile model

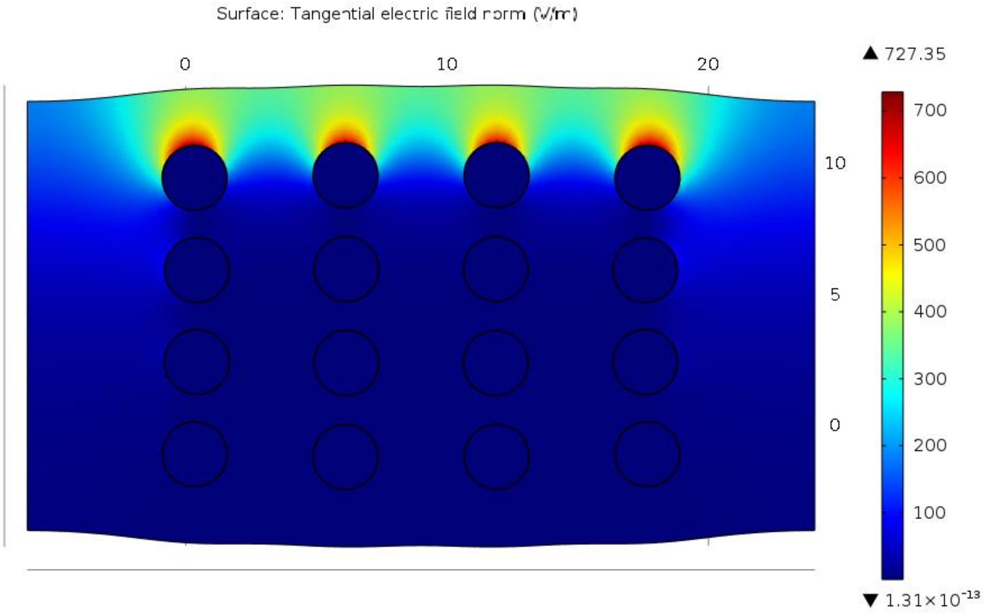

Figure 7.4 Variation of Electric Field in 50% tensile model

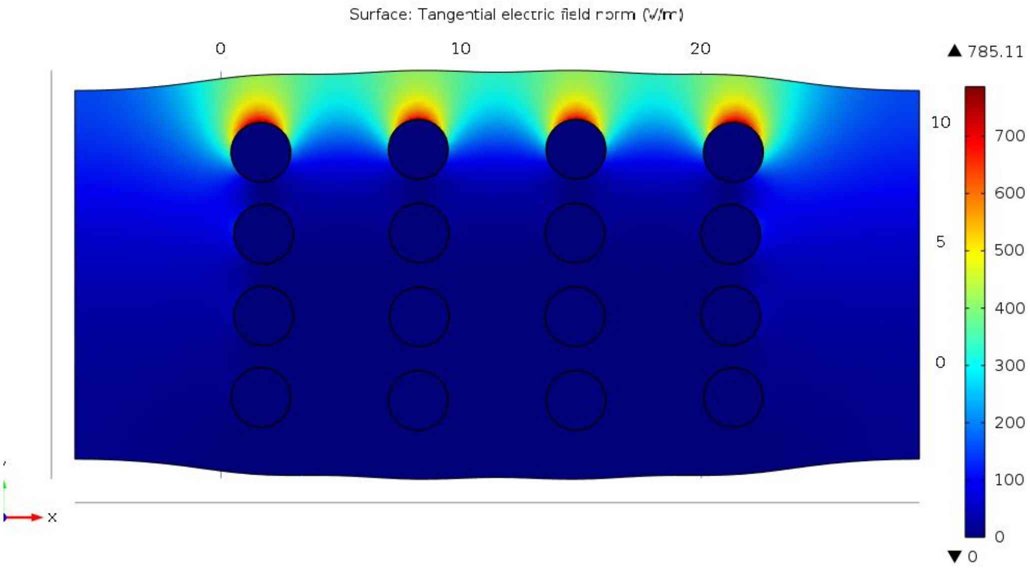

Figure 7.5 Variation of Electric Field in 75% tensile model

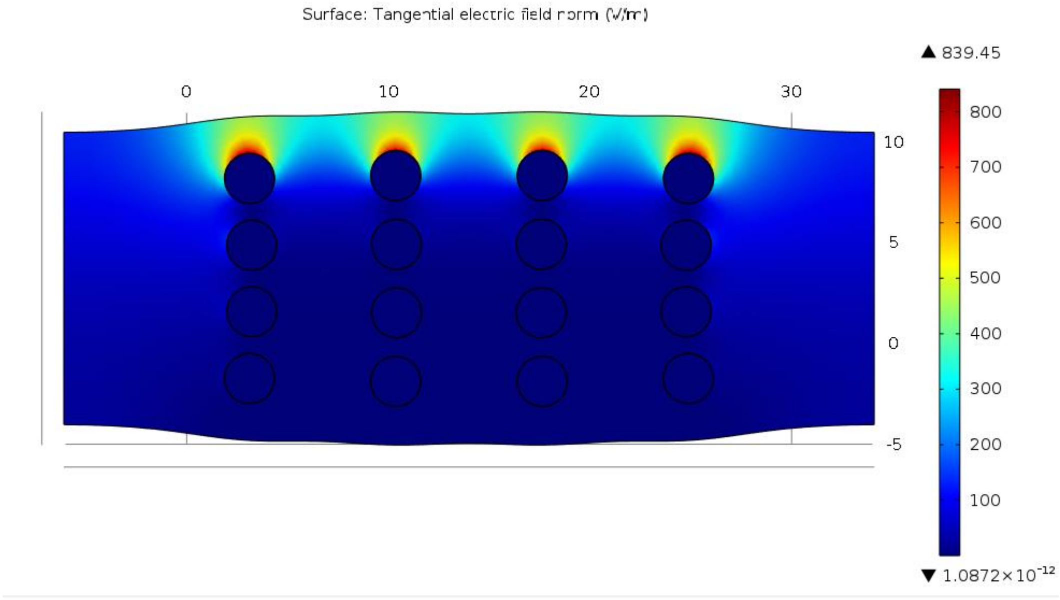

Figure 7.6 Variation of Electric Field in 100% tensile model

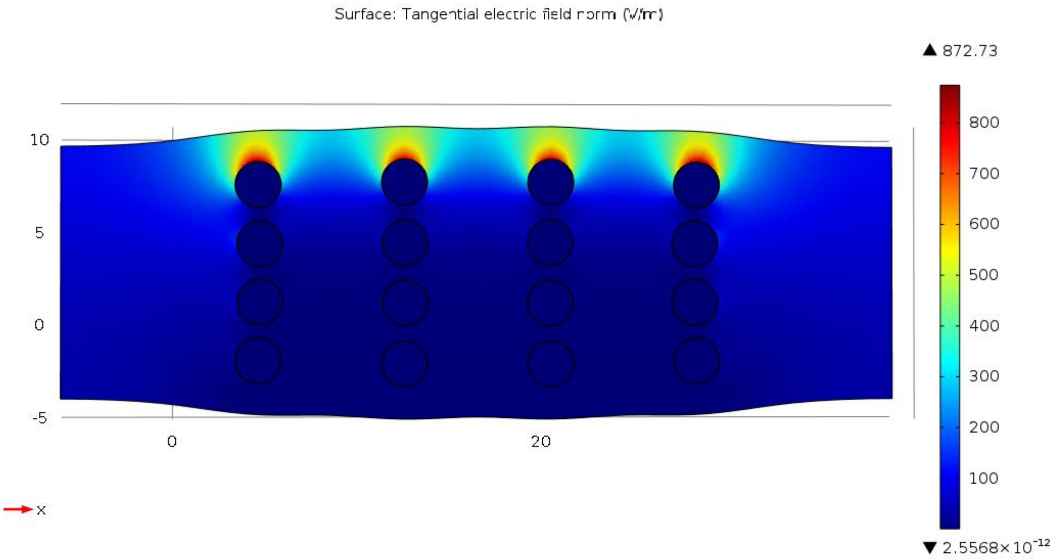

Figure 7.7 Variation of Electric Field in 125% tensile model

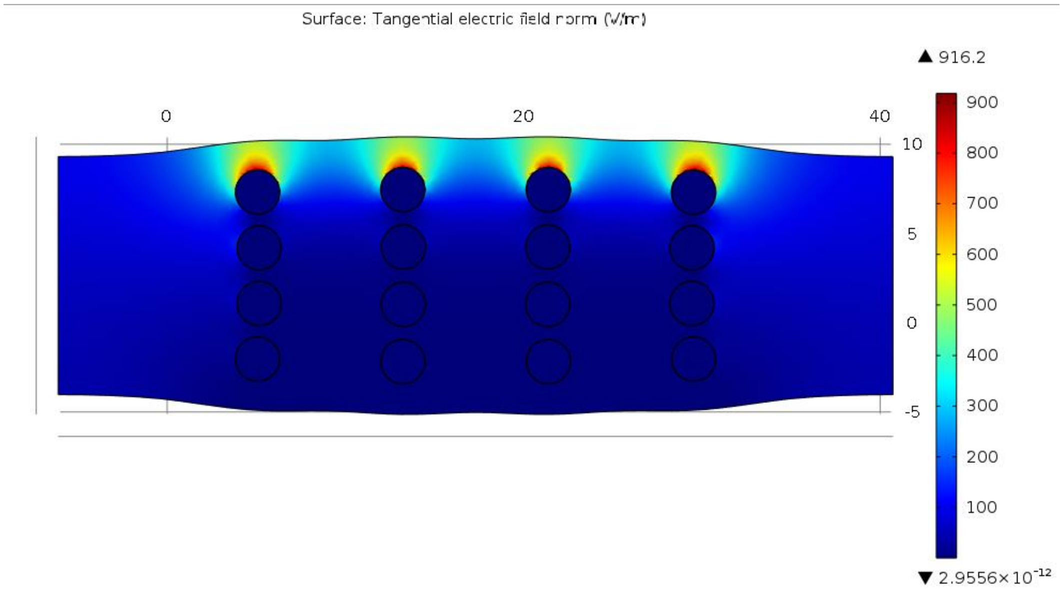

Figure 7.8 Variation of Electric Field in 133% tensile model

7.2 Comparison of Dielectric response at various Tensile loads

As damage in the material increases, we observed a change in the dielectric response of the material in chapter 5, and we observe a similar change in the response for this three-phase model. We see a net decrease of 60% in Normalized Impedance, Re (Z) of the model as shown in Figure 7.9.

At Initial state, without damage the Normalized Re (Z) would be **1**. As damage increases we see the Normalized Re (Z) decreasing as shown in Figure 7.9

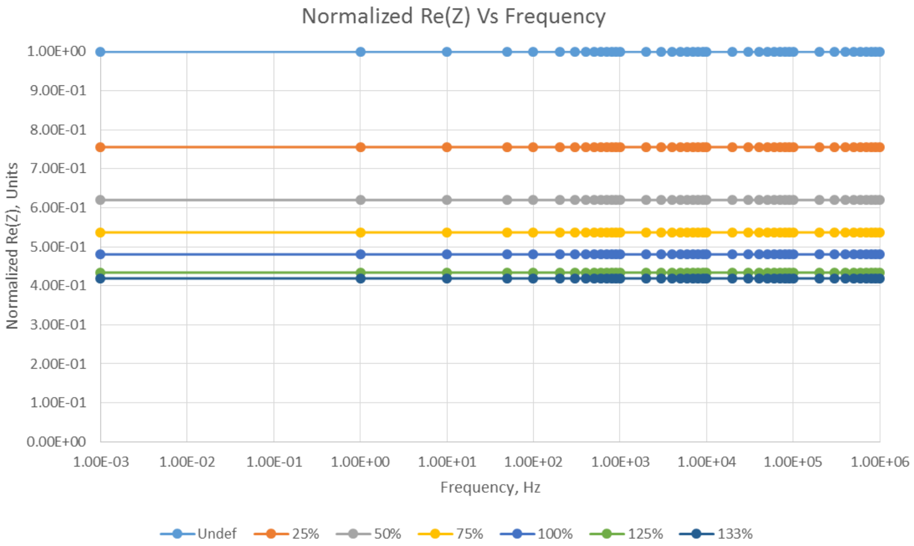

Figure 7.9 Variation of Normalized Impedance with % tensile strain for three-phase model

Also when we study the variation in Real part of Capacitance, Re (C) we observe similar variation as seen in two-phase model. As damage increases Capacitance increases as the distance between the fibres in the direction of electric field decreases. The variation in capacitance with damage is plotted as shown in Figure 7.10.

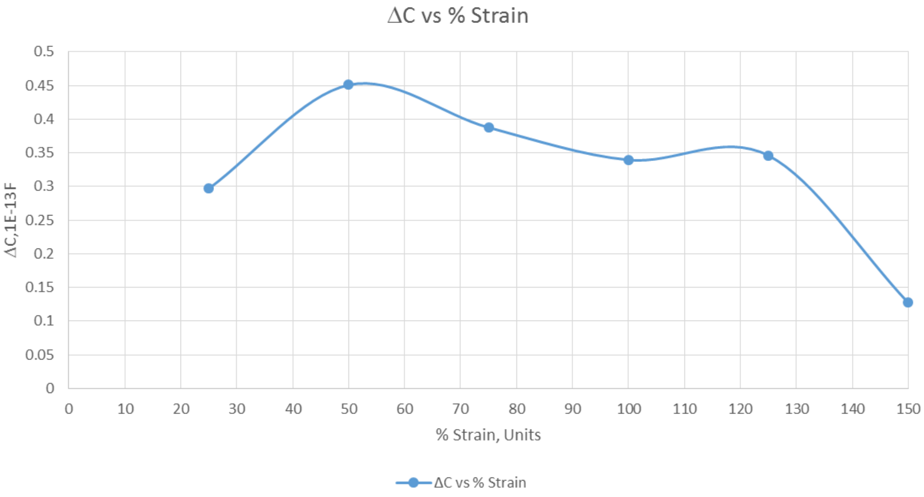

Figure 7.10 Change in capacitance ΔC vs % tensile strain for three-phase model

7.1.3 Dielectric study of three-phase Micromechanics model under compression

In Chapter 5, we have seen that as damage increases we see a difference in the dielectric response of the material. For the three-phase model we perform the dielectric study for the model loaded under compression by importing them and variation in dielectric response is studied at different load cases as shown in Figures 7.11 to 7.17

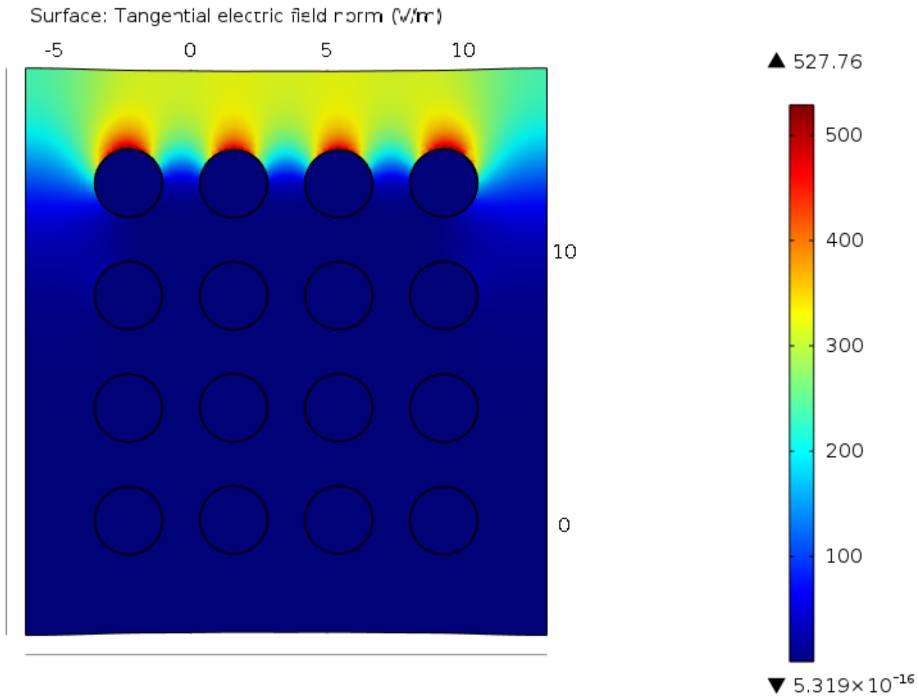

Figure 7.11 Variation of Electric Field in 5% Compression model

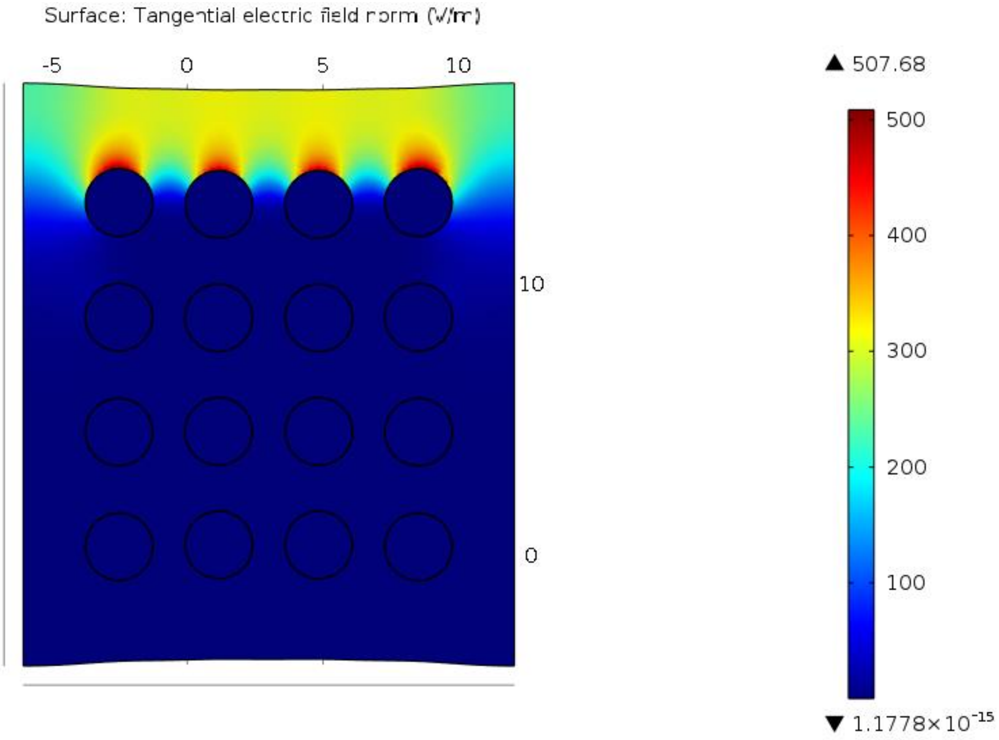

Figure 7.12 Variation of Electric Field in 10% Compression model

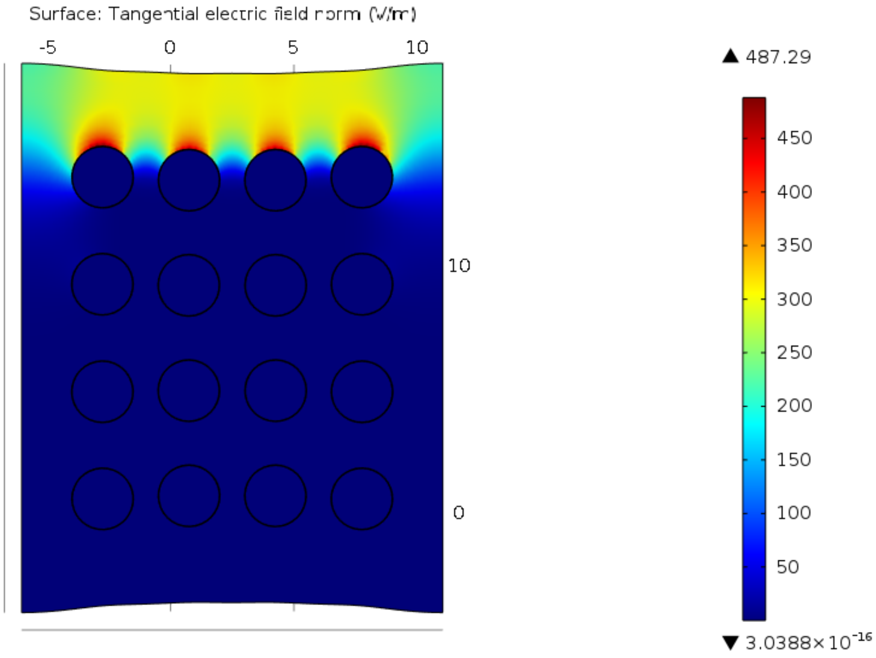

Figure 7.13 Variation of Electric Field in 15% Compression model

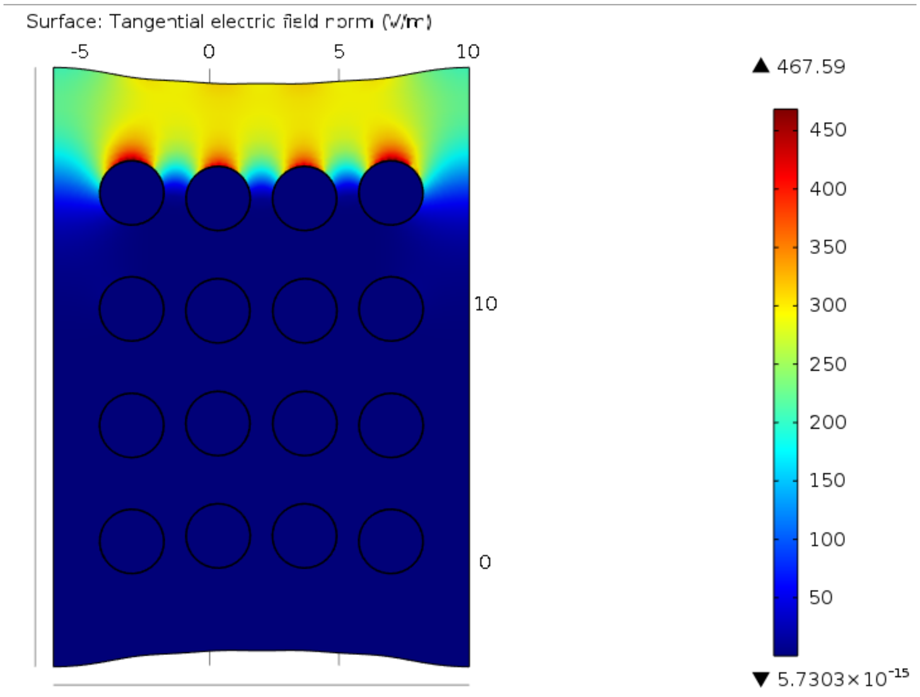

Figure 7.14 Variation of Electric Field in 20% Compression model

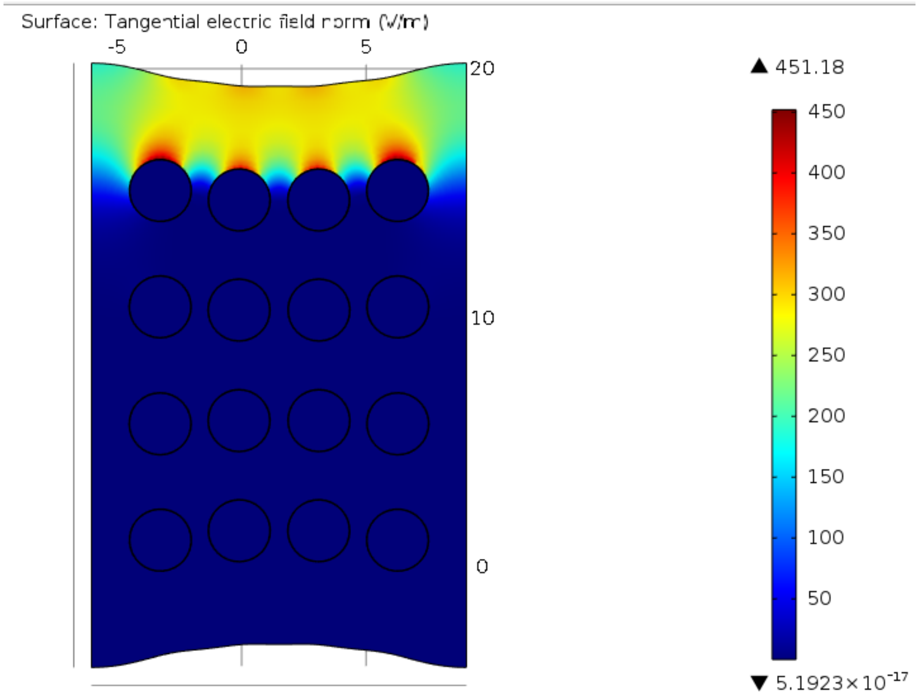

Figure 7.15 Variation of Electric Field in 25% Compression model

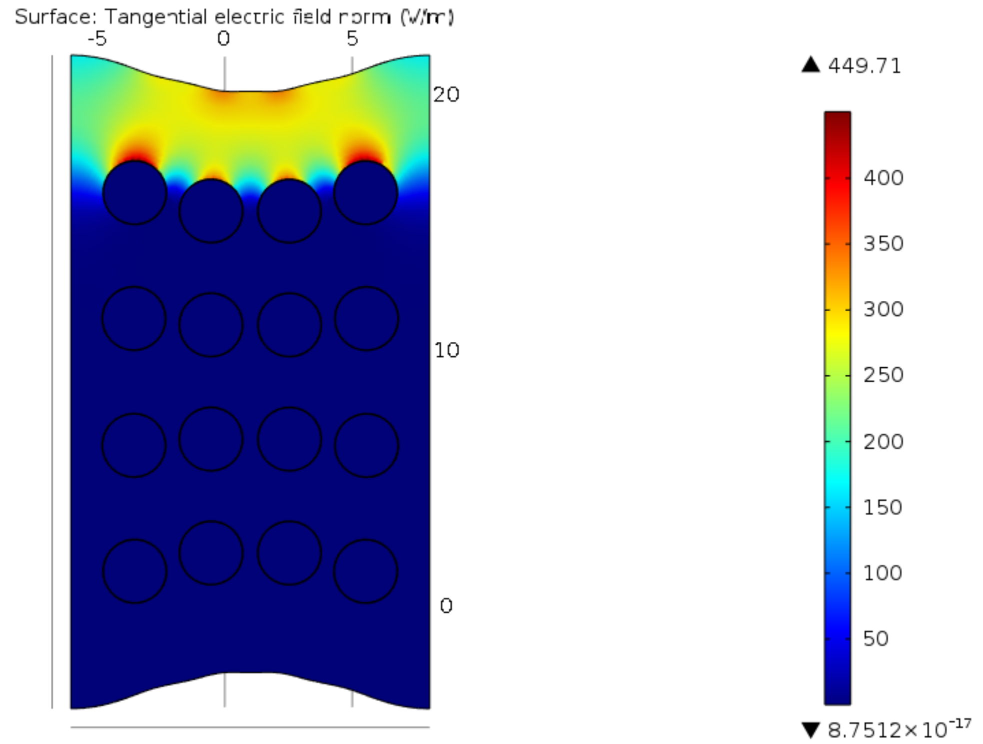

Figure 7.16 Variation of Electric Field in 30% Compression model

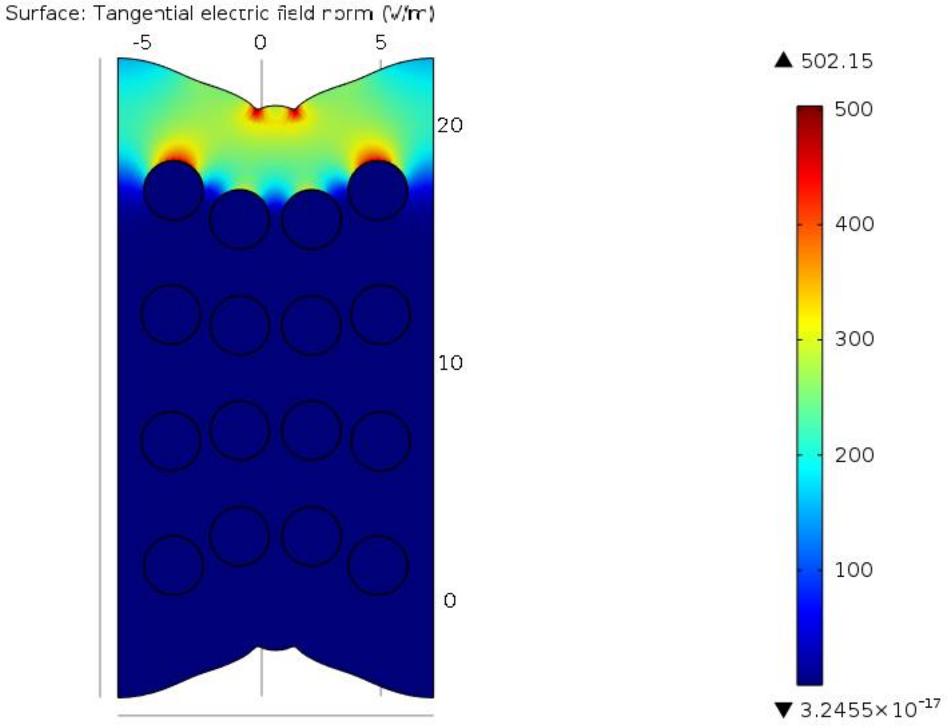

Figure 7.17 Variation of Electric Field in 35% Compression model

7.1.4 Comparison of Dielectric response at various compressive loads

As damage in the material increases, we observed a change in the dielectric response of the material in chapter 5, we observe a similar change in the response in this three-phase model. We see a net increase of 73% in Normalized Impedance, Re (Z) of the model as shown in Figure 7.18.

At the initial state, without damage the Normalized Re (Z) would be **1**. As damage increases we see the Normalized Re (Z) decreasing as shown in Figure 7.18

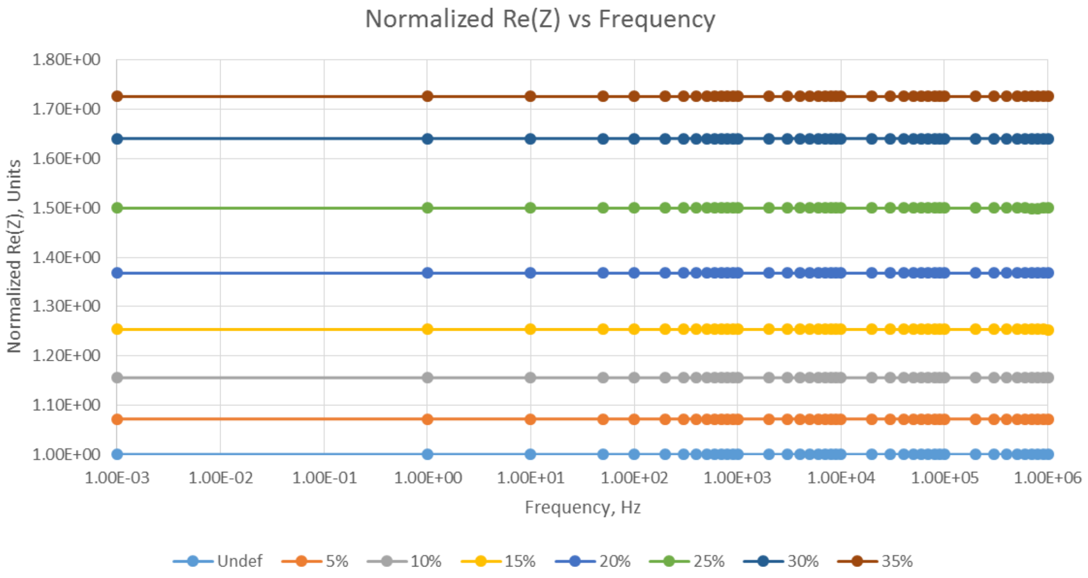

Figure 7.18 Variation of Normalized Impedance with % compressive strain for three phase model

Also when we study the variation in Real part of Capacitance, Re (C) we observe similar variation as seen in two phase model. As damage increases Capacitance decreases as the distance between the fibres in the direction of electric field increases. The variation in capacitance is plotted as shown in Figure 7.19.

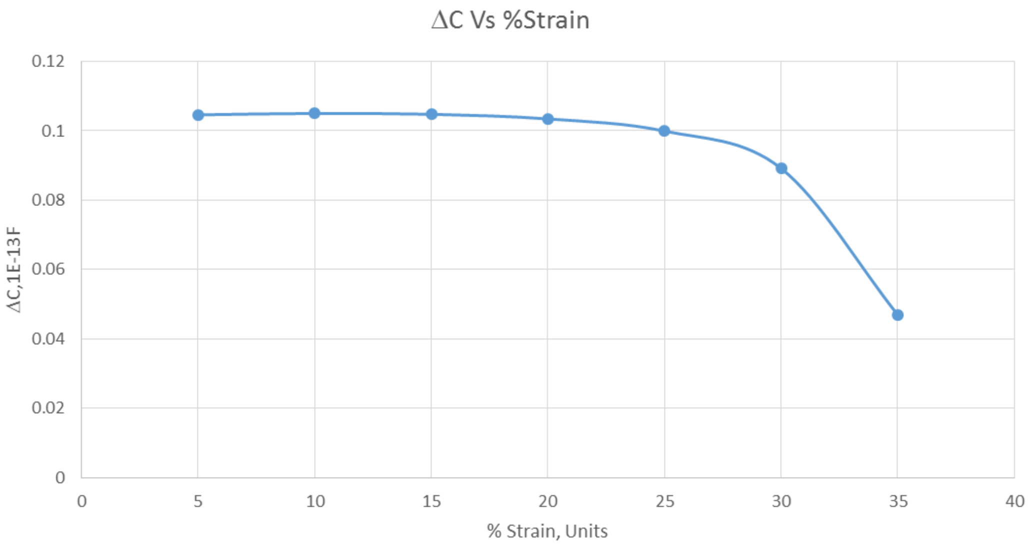

Figure 7.19 Change in capacitance ΔC vs % compressive strain for three phase model

CHAPTER 8 CONCLUSION AND CONTINUING WORK

We have shown that an alternating current analogue simulation of microcrack interaction and through-thickness fracture path development correctly predicts many of the features of the broadband dielectric spectroscopy (BBDS) measured response of continuous fiber composites loaded to failure in quasi-static and fatigue conditions. This multiphysics approach provides useful new insights into the nature of through-thickness damage and fracture plane development, while providing physical associations that are part of a foundation for the interpretation of broadband dielectric spectroscopy data for subsequent predictive theories.

We have also observed that the global compliance to applied AC electrical fields is closely related to the material compliance to mechanical stress fields during fracture path development. A key feature of that response was the observation of abrupt changes in multiphysics compliance (mechanical and electrical) that were identified with the onset of discrete fracture path instability and rupture. We also identified an inflection point in the frequency dependence of AC impedance that was an indicator of the 'beginning of the end of life.'

We have provided only a few first steps in simulating the multiphysics response associated with the development of discrete fracture paths in fibrous composites; much is yet to be done. However, on the basis of the present work, it would appear that the dielectric response through the thickness of continuous fiber reinforced composite materials seems to be uniquely sensitive to the details of microdamage accumulation and especially to “end of life” events such as the formation of contiguous incipient fracture paths, local micro-buckling and highly nonlinear deformation associated with shape change.

We have modeled composite specimens loaded with various tensile and compressive loads and observed various failure patterns, and studied dielectric response of the materials under those conditions. We have shown that in the two phase model, when loaded in tension we see a 60% decrease in the impedance and found some excitement in the change in capacitance, which if properly studied could be used to identify an inflection point that predicts onset of failure. When loaded in compression we have shown a 73% increase in impedance but the change in capacitance was rather in a steady rate. However in the three-phase micromechanics model we didn’t observe much difference from the two phase model, which is logical as the ring of moisture surrounding the conductor is not significant enough to effect the results in the simulation.

Next we wish to perform two phase and three-phase micromechanics model studies of a matrix material having higher conductivity than the fiber, which could respond differently under these loads and see if we could find variation in the dielectric response. As of now we have studied dielectric response with a field acting perpendicular to the loading direction, we also wish to perform the study with a field parallel to the loading direction to help us understand the material behavior under these variations.

However, the current study has clearly established that the dielectric response of a material through the thickness of a heterogeneous material is substantially and distinctly related to the development of deformations and defect development that are to be expected during the development of a fracture path. This is a step in the direction of understanding this essential but neglected element of the “end of life” events in fibrous composite materials.

REFERENCES

[1]. Majumdar P., Reifsnider K, "Study of Fracture Path Development and Remaining Life Utilizing Low-Frequency Electrical Response," Grant #NNX13AD43A-USC.

[2]. Gudmumdson P., and Zhang, W., Thermoelastic properties of microcracked composite laminates, *Mechanics of Composite Materials*, 29 #2, (1993) 107-114.

[3]. *Damage in Composite Materials*, ASTM STP 775, K. L. Reifsnider, Ed., *American Society for Testing and Materials* (1982) DOI: 10.1520/STP775-EB

[4]. Jamison, R.D., Schulte, K., Reifsnider, K., Stinchcomb, W., Characterization and Analysis of Damage Mechanisms in Tension-Tension Fatigue of Graphite/Epoxy Laminates, in Effects of Defects in Composite Materials, ASTM STP 836, ASTM (1984) 21-55

[5]. F.A.Firestone, A New analogy between Mechanical and Electrical Systems, *Journal of the Acoustical Society* , (Jan 1933) 250-267

[6]. Qian, H., Kucernak, A. R., Greenhalgh, E. S., Bismarck, A., & Shaffer, M. S.. Multifunctional structural supercapacitor composites based on carbon aerogel modified high performance carbon fiber fabric. *ACS applied materials & interfaces*, 5(13), 6113-6122 (2013).

[7]. Reifsnider, K. L.; Ed. *Damage in Composite Materials*. ASTM 775, American Society for Testing and Materials, Philadelphia 1982

[8]. Reifsnider, K.L., and Case, S. W., *Damage Tolerance and Durability of Material Systems*. New York: John Wiley and Sons (2002).

[9]. Highsmith, A. L., & Reifsnider, K. L. Stiffness-reduction mechanisms in composite laminates. *Damage in composite materials, ASTM STP*, *775*, 103-117(1982).

[10]. Nairn, J. A. Matrix microcracking in composites. *Polymer matrix composites*, *2*, 403-432 (2000).

[11]. Talreja, R. Transverse cracking and stiffness reduction in composite laminates. *Journal of composite materials*, *19*(4), 355-375 (1985).

[12]. Talreja, R., & Singh, C. V. *Damage and failure of composite materials*. Cambridge University Press (2012).

[13]. Varna, J., & Krasnikovs, A. Transverse cracks in cross-ply laminates 2. Stiffness degradation. *Mechanics of composite materials*, *34*(2), 153-170 (1998).

[14]. O'brien, T. K. Characterization of delamination onset and growth in a composite laminate. *Damage in composite materials, ASTM STP*, *775*(2), 140-167 (1982).

[15]. Stinchcomb, W. W., & Bakis, C. E. Fatigue behavior of composite laminates. *Fatigue of composite materials*, *4*, 105-180 (1990).

[16]. Reifsnider, K., and Case, S.W., *Durability and Damage Tolerance of Material Systems*, John Wiley & Sons (2002)

[17]. Fazzino, P., Reifsnider, K., Majumdar, P., “Impedance spectroscopy for progressive damage analysis in woven composites,” *Composites Science and Technology* 169 (2009) 2008-2014

[18]. Huang, M, Yang, J, Xiao, Z., Sun, J., and Peng, J., “Modeling the Dielectric Response in Heterogeneous Materials using 3D RC Networks,” *Modern Physics Letters B*, 23, No. 25 (2009) 3023‑3033

[19]. Chou, T-W., “Multifunctional Carbon Nanotube–Based Sensors for Damage Detection and Self Healing in Structural Composites,” contractors report, Grant No: FA9550-09-1-0218 (2009)

[20]. Reifsnider, K., Raihan, R. and Liu, Q., “Rational Durability Design of Heterogeneous Functional Materials: Some First Principles,” *Mechanics of Composite Materials*, 49#1 (2013) 31-54

[21]. A Comparative Study of Several Material Models for Prediction of Hyperelastic Properties: Application to Silicone-Rubber and Soft Tissues, P. A. L. S. Martins, R. M. Natal Jorge and A. J. M. Ferreira, *Strain (2006)* 42, 135–147

[22]. The Yeoh model applied to the modeling of large deformation contact/impact problems Christine Renaud, Jean-Michel Cros, Zhi-Qiang Feng, Bintang Yang, *International Journal of Impact Engineering 36 (2009)* 659–666

[23]. Electrical properties of Silicone Rubber Retrieved from:

http://www.azom.com/properties.aspx?ArticleID=920

[24]. COMSOL Multiphysics© Reference Guide, Version 4.3a (2012).